

Unitarization Models For Vector Boson Scattering at the LHC

Zur Erlangung des akademischen Grades eines
DOKTORS DER NATURWISSENSCHAFTEN
von der Fakultät für Physik des
Karlsruher Instituts für Technologie (KIT)

genehmigte

DISSERTATION

von

M. Sc. Genessis M. Perez Rivera
Aus Mérida (Venezuela)

Tag der mündlichen Prüfung: 26. Januar 2018

Referent: Prof. Dr. Dieter Zeppenfeld
Korreferent: Prof. Dr. Margarete Mühlleitner

Abstract

Effective Field Theories (EFT) can be used to quantify deviations from the Standard Model in a model independent way: keeping the symmetries and local gauge invariance. It is possible then to write new physics as an extension of the Standard Model in an Effective Lagrangian including higher dimensional operators composed of the already known fields.

In general, it is of interest to study the EFT for electroweak precision tests, as they are among the most sensitive searches to constrain new physics. Therefore, precise knowledge of the Triple Gauge Couplings and Quartic Gauge Couplings is desirable, as new physics effects could manifest in their final states.

Once the higher dimensional operators are included in the Effective Lagrangian, the amplitudes have terms that grow proportional to the energy, hence the cross section falls off more slowly than expected and it points to a unitarity violation of the S matrix: this implies that the Effective Field Theory is used beyond its validity region and it leads to a non-physical cross section, an idea that has been used previously to indicate the scale of new physics. This unitarity problem needs to be solved, as nature guarantees unitarity conservation.

The unitarity bounds are calculated from the partial wave analysis of the on-shell $2 \rightarrow 2$ scattering amplitudes and a unitarization scheme needs to be used to reconstruct the off-shell amplitudes. In this work, a T-matrix unitarization scheme is described for Vector Boson Scattering at the LHC and implemented in VBFNLO, a parton level Monte Carlo for processes with electroweak bosons.

Zusammenfassung

Effektive Feldtheorien (EFT) können verwendet werden, um Abweichungen vom Standardmodell modellunabhängig zu quantifizieren: die Symmetrien und die lokale Eichinvarianz bleiben erhalten. Es ist dann möglich, neue Physik als Erweiterung des Standardmodells als eine Effektiven Lagrange-Dichte zu schreiben, einschließlich höherdimensionaler Operatoren, die sich aus den bereits bekannten Feldern zusammensetzen.

Im Allgemeinen ist es von Interesse, die EFT für elektroschwache Präzisionstests zu studieren, da sie zu den sensitivsten Suchen gehören, um neue Physik einzuschränken. Daher ist eine genaue Kenntnis der trilinearen und quartischen Eichkopplungen wünschenswert, da sich neue physikalische Effekte in ihren Endzuständen manifestieren könnten.

Sobald die höherdimensionalen Operatoren in der Effektiven Lagrange-Dichte enthalten sind, haben die Amplituden Terme, die proportional zur Energie wachsen. Daher fällt der Wirkungsquerschnitt langsamer ab als erwartet, und es deutet auf eine Unitaritätsverletzung der S -Matrix hin. Dies impliziert, dass die Effektive Feldtheorie über ihren Validitätsbereich hinaus verwendet wird und führt zu einem nicht-physikalischen Wirkungsquerschnitt, eine Idee, die zuvor verwendet wurde, um den Gültigkeitsbereich der neuen Physik anzugeben. Dieses Problem der Unitaritätsverletzung muss gelöst werden, da die Natur die Unitarität der Streumatrix garantiert.

Die Unitaritätsgrenzen werden aus der Partialwellen Analyse der $2 \rightarrow 2$ Streuamplituden berechnet und ein Unitarisierungsschema muss verwendet werden, um die Off-Shell-Amplituden zu rekonstruieren. In dieser Arbeit wird ein T-Matrix Unitarisierungsschema für Vector Boson Streuung am LHC beschrieben und in VBFNLO, einem Parton Level Monte Carlo für Prozesse mit elektroschwachen Bosonen, implementiert.

Contents

| | |
|-----------------------------------------------------------------|------------|
| Abstract | i |
| Zusammenfassung | iii |
| Introduction | 1 |
| Part I: Theoretical Foundations | 5 |
| 1 The Standard Model as an Effective Field Theory | 7 |
| 1.1 The Standard Model of particle physics | 7 |
| 1.1.1 Symmetries and interactions | 7 |
| 1.1.2 The elementary particles | 9 |
| 1.1.3 Lorentz transformations | 10 |
| 1.1.4 The elements of the Standard Model Lagrangian | 12 |
| 1.1.4.1 The Higgs mechanism | 13 |
| 1.2 Beyond the Standard Model: Effective Field Theory | 14 |
| 1.2.1 Building an SM bottom-up EFT | 16 |
| 1.2.2 Anomalous couplings in the electroweak sector | 17 |
| 1.3 Dim-8 operators for VBS | 18 |
| 2 Vector Boson Scattering | 21 |
| 2.1 Particle scattering inside the colliders | 21 |
| 2.1.1 The S -matrix | 22 |
| 2.1.2 Detector jargon | 23 |
| 2.1.3 Vector Boson Scattering at the LHC | 24 |
| 2.2 VBFNLO | 25 |
| 2.2.1 Structure of VBFNLO | 25 |
| 2.2.1.1 Calculation of the amplitudes | 27 |
| Part II: Unitarization in Monte Carlo Generators | 29 |
| 3 Restoring Unitarity for On-shell Scattering | 31 |
| 3.1 The Unitarity Bounds | 31 |
| 3.1.1 The Partial Wave decomposition | 33 |
| 3.2 AQC's Unitarity Violation | 34 |
| 3.3 The K matrix and T -matrix | 37 |
| 3.4 Linear T -matrix on-shell unitarization | 37 |

| | |
|--------------------------------------------------------------------------|------------|
| 4 Restoring Unitarity for Off-shell processes | 39 |
| 4.1 Previous Unitarization Efforts | 39 |
| 4.1.1 Form Factor unitarization | 41 |
| 4.1.2 K -matrix unitarization | 41 |
| 4.2 Off-shell Anomalous Quartic Couplings in VBFNLO | 42 |
| 4.3 On-Shell and Off-Shell polarization vectors | 43 |
| 4.4 On-Shell/Off-Shell Matching | 46 |
| 4.4.1 Polarization Vector Matching | 48 |
| 4.4.2 Calculating the New Amplitude | 49 |
| 4.4.2.1 From q_i^μ to k_i^μ | 50 |
| 4.5 Numerical T-matrix unitarization for off-shell processes | 56 |
| 4.5.1 Partial Wave Decomposition for off-shell processes | 57 |
| 4.5.2 From On-shell to Off-shell T-matrix | 57 |
| 4.5.3 Testing the unitary condition: a non-symmetric amplitude | 60 |
| 4.6 Off-shell T-matrix for VBS | 62 |
| 5 Limits for Anomalous Couplings at 13 TeV collisions | 69 |
| 5.1 Electroweak production of same-sing W boson pairs | 69 |
| 5.1.1 QGCs Unitary Bound | 70 |
| 5.1.2 EFT with unitarization: coupling limits | 71 |
| 5.1.3 More Observables | 75 |
| Summary | 79 |
| A Feynman Rules | 81 |
| B VBFNLO and Éboli convention | 84 |
| C Wigner \mathcal{D}-function | 85 |
| D Factorization methods | 86 |
| E Eigenvalues calculation in VBFNLO | 89 |
| F VBFNLO implementation | 92 |
| Bibliography | 95 |
| Acknowledgements | 101 |

“Would you tell me, please, which way I ought to go from here?”

“That depends a good deal on where you want to get to”, said the Cat.

“I don’t much care where -” said Alice.

“Then it doesn’t matter which way you go”, said the Cat.

“- so long as I get somewhere”, Alice added as an explanation.

“Oh, you’re sure to do that”, said the Cat, “if you only walk long enough”.

Alice’s Adventures in Wonderland, Lewis Carroll.

Introduction

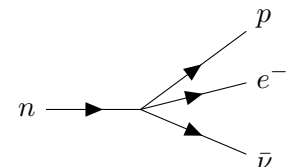
The Standard Model (SM) of particles is a complete and successful theory in physics able to describe the fundamental particles and their interactions. Nevertheless, it cannot explain all the phenomena of the universe and many open questions remain to be answered, leading to the search for a greater description of nature.

It is not the lack of new models that makes this search a complicated task. On the contrary, many possible scenarios Beyond the SM (BSM) are being studied and published, which implies (from an experimental point of view) a huge need of resources to obtain and analyze data from the different experiments in the search of new physics.

Where should one look to find new physics if the parameter region is so extensive? And, if new physics is accessible within the energy available in the experiments, e.g. at the LHC, which theory would it correspond to?

A favorable choice in this sea of options are the so called Effective Field Theories (EFT), a generalized model to extend the SM without reference to the underlying theory. Examples through time are existent, with results that have been a good approximation of the complete model.

For example, consider the β -decay process described by Enrico Fermi originally in 1933 [1, 2]: the neutron decay did not agree with the known interactions at the time and yet, experiments could measure a neutron decaying into a proton, an electron and missing energy, as shown in the relation (1),

$$n \rightarrow pe^- \bar{\nu}_e \quad (1)$$
A Feynman diagram illustrating the beta decay process. A single horizontal line on the left is labeled 'n' (neutron) with an arrow pointing to the right. This line enters a vertex from which three lines emerge to the right. The top line is labeled 'p' (proton) with an arrow pointing to the right. The middle line is labeled 'e⁻' (electron) with an arrow pointing to the right. The bottom line is labeled 'ν̄' (anti-neutrino) with an arrow pointing to the right.

Fermi considered the following idea: take a four-point interaction vertex and define a “current”, which explains the transition from one particle to another. For instance, a baryon current for the neutron going to the proton and a fermion current connecting the

neutrino and the electron, as shown in the figure (1). The interaction point is explained then as constant coupling, named G_F .

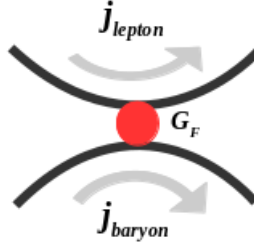


FIGURE 1: Fermi theory for the β decay.

The corresponding matrix element can be written effectively as the product of the two “currents”,

$$M = G_F j_{\text{lepton}} \cdot j_{\text{baryon}} , \quad (2)$$

the currents can be written using an operator \mathcal{O} corresponding to the transition, for example,

$$j_{\text{lepton}} \propto \bar{\Psi}_e \mathcal{O} \Psi_\nu . \quad (3)$$

Therefore, the matrix element for the β -decay can be rewritten as,

$$M \propto G_F (\bar{\Psi}_p \mathcal{O} \Psi_n) (\bar{\Psi}_e \mathcal{O} \Psi_\nu) . \quad (4)$$

Despite the paper and the idea were originally rejected, this is the genesis of the weak interactions. *A posteriori*, a more complete theory took over, with the effective coupling being replaced by a new particle as mediator (the W boson), as shown in the figure (2).

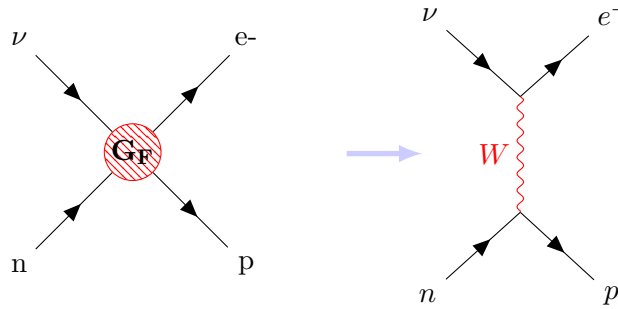


FIGURE 2: Inclusion of the W boson as a mediator of the interaction for the β -decay.

The EFT will introduce higher dimensional operators using the already known SM fields and an effective coupling (anomalous coupling) to describe possible scenarios beyond the

SM. This approach is useful, for instance, for a better understanding of the dynamical nature of the spontaneous electroweak symmetry breaking, where one could introduce anomalous interactions between the electroweak field strength tensors, as the electroweak sector is among the most sensitive observables to constrain new physics.

Regardless of the EFT advantages, the inclusion of anomalous couplings for new interactions also introduces unitarity violating effects when the model is used beyond the limits of applicability, leading to non-physical cross sections. As nature will guarantee unitarity conservation, it is necessary to restore it without inserting *ad-hoc* elements that will dilute the generality of the model.

For this purpose, one could either apply a cut-off and truncate any process out of the EFT validity region, or modify the scattering amplitudes to guarantee they remain below the unitarity bound. Nevertheless, as nothing has been observed in the experiments within the validity region so far, it is necessary to extend this range and ensure that the searches are not done in a non-valid parameter region.

The goal is to investigate unitarity models for dimension-8 bosonic operators in quasi-elastic vector boson scattering at proton-proton collisions with two jets,

$$pp \rightarrow (V \rightarrow ff)(V \rightarrow ff) + jj .$$

The first part of this work explains basic concepts: in Chapter 1 the SM as an EFT is introduced and the operators of interest for vector boson scattering processes are explained; then, in Chapter 2 the Monte Carlo program VBFNLO is introduced, as numerical calculations become more convenient than analytic phase-space integration to achieve the desired accuracy in the predictions of SM and new physics models.

The second part of this work addresses the unitarization problem: Chapter 3 explains the unitarity bounds for $2 \rightarrow 2$ scattering and introduces the T-matrix linear unitarization model; then, in Chapter 4 off-shell processes ($2 \rightarrow 6$ scattering) are introduced, explaining the challenges that needed to be overcome to obtain a suitable unitarization scheme.

Finally, Chapter 5 gives an example on how the unitarization can expand the validity regions to search for new physics, using the current experimental limits on the anomalous couplings.

Throughout this work the natural units were used, with the speed of light c and the reduced Planck constant \hbar set equal to 1.

PART I:

Theoretical Foundations

CHAPTER 1

The Standard Model as an Effective Field Theory

1.1 The Standard Model of particle physics

Since ancient times, the macroscopic matter was theorized as a cluster of components in an empty space and not divisible into smaller pieces. For example, the ancient Greek word “atomos” ($\hat{\alpha}\tau\omicron\mu\omicron\nu$) [3] translates as an adjective to define something indivisible, uncut.

Albeit it is true that the atom did not remain as the smallest component of nature, the universe is indeed composed of elementary particles interacting with each other and described by the SM.

The SM is a fully mathematical theory that identifies the fundamental elements of the Universe, describes the forces they feel and how do they behave given these forces.

1.1.1 Symmetries and interactions

The gravitational and electromagnetic interactions have played an important role in the history of science for a long time: the electromagnetic interactions describe the behavior between electrically-charged particles, while gravitational interactions are existent between all the particles, particularly playing an important role in the macroscopic world [2]. However, many experimental phenomenoma found from 1900 onward would not have a satisfactory explanation if only these two interactions existed [4].

Since a nucleus containing several protons holds together despite their electrical repulsion, another force (attractive) stronger than electromagnetism must occur. In 1935 Yukawa postulated the existence of pions [2] as mediators of this *strong interaction*. Although the pions were discovered, a more fundamental explanation arose, resulting in the Quantum Chromodynamic (QCD) theory.

In addition, a different interaction was necessary to explain phenomena such as the process of hydrogen fusion in stars or the radioactive decay of subatomic particles. The *weak interactions* made possible to explain these unstable particle decays, but it was not until 1973 [2] when the first observation of a weak neutral current was observed at CERN. This discovery confirmed not only the existence of the weak interactions, but that weak and electromagnetic interactions are two different aspects of the same force. The unification of the weak and electromagnetic interactions into one underlying force by Glashow, Weinberg and Salam [5–7], has been one of the milestones in particle physics from the last years.

The SM is a quantum gauge field theory with a Lagrangian invariant under some symmetry transformations (or local phase transformations), which describes the particles and their interactions.

These symmetries are important not only to derive and simplify the equations that describe a physical system but, as the Nöther’s theorem reveals, due the correspondence between symmetries and conserved quantities. In other words, “if there is a symmetry, there is a conserved quantity; and vice versa, if there is a conserved quantity observed, there should be an associated symmetry” [4]. For example, internal symmetries have associated “charges”, while spatial translation symmetries are related to momentum conservation.

The SM¹, is based on three internal symmetries, $SU(3)_C \times SU(2)_L \times U(1)_Y$:

- The $U(1)_Y$ group is related to the *electromagnetic interactions* and it guarantees a phase invariance. There is only one $U(1)$ generator denoted as Y , the hypercharge. The gauge field B_μ transforms under spatial rotations in the usual way an ordinary derivative ∂_μ does.
- The $SU(2)_L$ group is related to the *weak interactions*, and it assures a non-Abelian phase invariance (electroweak invariance). The $SU(2)$ group requires three generators I_j , with $j = 1,2,3$ (the weak isospin). The three associated gauge fields are named W_μ^j .
- The $SU(3)_C$ group is related to the *strong interactions*. It guarantees an additional, independent, non-Abelian phase invariance. There are eight generators of the $SU(3)$ group, T_a with $a=1,2,3\dots 8$. The associated gauge fields are G_μ^a .

¹The gravitational interaction is not a relevant topic of discussion in this work.

1.1.2 The elementary particles

In quantum field theory (QFT), the quantum fields have associated particles. They can be classified into two categories: the **matter particles** (fermions) and, the **interaction particles** (gauge bosons), which constitute the fundamental building blocks out of which everything else in nature is formed.

- **The fermions:**

The quarks and leptons are the particles of which all matter is composed (thereby their name as “matter particles”). There are six *flavors* of quarks and six of leptons, which are observed to be either electroweak SU(2) singlets (right-handed chirality) or parts of electroweak doublets (left-handed chirality).

The lepton flavor doublets (L_L^i) and lepton singlets (l_R^i) are grouped into three generations, $i = 1, 2, 3$, as shown in table (1.1). The doublet includes the electron (e), the muon (μ) and the tau (τ) and their respective neutrinos ($\nu_{e,\mu,\tau}$).

The quarks are carrying the color charge necessary for the strong interaction. They are named (for historical reasons): up (u), down (d), strange (s), charmed (c), bottom (b) and top (t), and are also grouped into three generations, Q_L^i and u_R^i, d_R^i , as shown in the table (1.1).

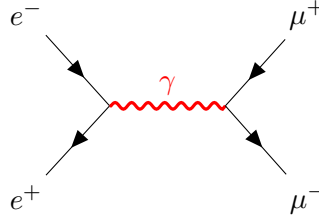
In general, the stable matter is built from the first generation of quarks and leptons (lightest ones), while the heavier generations decay into them.

| | Leptons | Quarks |
|----------------|--------------------------------------------------------------------------|--------------------------------------------------------------|
| 1st Generation | $L_L^1 = \begin{pmatrix} e_L^- \\ \nu_{eL} \end{pmatrix}; e_R^-$ | $Q_L^1 = \begin{pmatrix} u_L \\ d_L \end{pmatrix}; u_R, d_R$ |
| 2nd Generation | $L_L^2 = \begin{pmatrix} \mu_L^- \\ \nu_{\mu L} \end{pmatrix}; \mu_R$ | $Q_L^2 = \begin{pmatrix} c_L \\ s_L \end{pmatrix}; c_R, s_R$ |
| 3rd Generation | $L_L^3 = \begin{pmatrix} \tau_L^- \\ \nu_{\tau L} \end{pmatrix}; \tau_R$ | $Q_L^3 = \begin{pmatrix} t_L \\ b_L \end{pmatrix}; t_R, b_R$ |

TABLE 1.1: Fermion singlets (u_R^i, d_R^i, l_R^i) and doublets (Q_L^i, L_L^i), with $i = 1, 2, 3$ in correspondence with each generation.

- **Gauge bosons:**

The gauge bosons are the mediators of the interactions between the matter and anti-matter particles. When two particles interact, they exchange quanta of energy (a bosonic field), as shown in the example diagram (1.1), which will be then reabsorbed within a given probability.

FIGURE 1.1: Example of a bosonic field exchange (γ) between matter particles.

The gluon field strength tensor $G_{\mu\nu}^a$ can be written as [8],

$$G_{\mu\nu}^a = \partial_\mu G_\nu^a - \partial_\nu G_\mu^a + g_s f^{abc} G_\mu^b G_\nu^c . \quad (1.1)$$

The $SU(2)$ field strength tensor $W_{\mu\nu}^j$ is defined as

$$W_{\mu\nu}^j = \partial_\mu W_\nu^j - \partial_\nu W_\mu^j + g \epsilon^{jkm} W_\mu^k W_\nu^m . \quad (1.2)$$

Finally, the $U(1)$ field strength tensor $B_{\mu\nu}$ can be written as,

$$B_{\mu\nu} = \partial_\mu B_\nu - \partial_\nu B_\mu . \quad (1.3)$$

- **The Higgs boson:**

To generate massive gauge bosons W^\pm , Z keeping the photon massless and the gauge invariance, a new field needs to be introduced. Therefore, for a consistent theory including the particle masses and interactions, another particle with spin $J=0$ (a complex scalar) is needed: the Higgs boson (as it will be explained in (1.1.4.1)).

1.1.3 Lorentz transformations

In an inertial system S , an event \mathbf{P} in a space-time system of coordinates is characterized by three coordinates specifying the space point \bar{x} and a time parameter t : $\mathbf{P} = (t, x, y, z)$. If another inertial system S' is considered, the same event will be specified by $\mathbf{P}' = (t', x', y', z')$.

If the systems of coordinates are moving relative to each other with a velocity \bar{v} (assuming Cartesian coordinates $\bar{v} = (v_x, v_y, v_z)$), and the origins O and O' from each frame coincide at $t = t' = 0$, then, the transformation from \mathbf{P} to \mathbf{P}' (as explained in [9]) is

given by the Lorentz transformation matrix L

$$L = \begin{pmatrix} \gamma & -\gamma\beta_x & -\gamma\beta_y & -\gamma\beta_z \\ -\gamma\beta_x & 1 + \frac{(\gamma-1)\beta_x^2}{\beta^2} & \frac{(\gamma-1)\beta_x\beta_y}{\beta^2} & \frac{(\gamma-1)\beta_x\beta_z}{\beta^2} \\ -\gamma\beta_y & \frac{(\gamma-1)\beta_x\beta_y}{\beta^2} & 1 + \frac{(\gamma-1)\beta_y^2}{\beta^2} & \frac{(\gamma-1)\beta_y\beta_z}{\beta^2} \\ -\gamma\beta_z & \frac{(\gamma-1)\beta_x\beta_z}{\beta^2} & \frac{(\gamma-1)\beta_y\beta_z}{\beta^2} & 1 + \frac{(\gamma-1)\beta_z^2}{\beta^2} \end{pmatrix} \quad (1.4)$$

where $\bar{\beta}^2$ and γ are defined as,

$$\bar{\beta} = \frac{\bar{p}}{E}, \quad \gamma = \frac{1}{(1 - |\bar{\beta}^2|)^{\frac{1}{2}}}.$$

Any fundamental equation of physics must have the same form in every inertial system. In other words, the fundamental equations must be form-invariant or *covariant* under Lorentz transformations.

For this work, it is necessary to define a new transformation matrix, $T_{RL} = R \cdot L$, where R refers to the rotation matrix around a specific axis³.

For example, to rotate a $2 \rightarrow 2$ scattering ($12 \rightarrow 34$), aligning the incoming particles to the z-axis as shown in the figure (1.2), one could define the following vectors:

$$\hat{n}_1 = \frac{\vec{p}'_1}{|\vec{p}'_1|}, \quad \hat{n}_3 = \frac{\vec{p}'_3}{|\vec{p}'_3|}, \quad (1.5)$$

and redefine new unitary vectors as

$$\hat{e}_3 = \hat{n}_1, \quad \hat{e}_1 = \frac{\hat{n}_3 - \hat{n}_3(\hat{n}_1 \cdot \hat{n}_3)}{|\hat{n}_3 - \hat{n}_3(\hat{n}_1 \cdot \hat{n}_3)|}, \quad \hat{e}_2 = \hat{e}_3 \times \hat{e}_1. \quad (1.6)$$

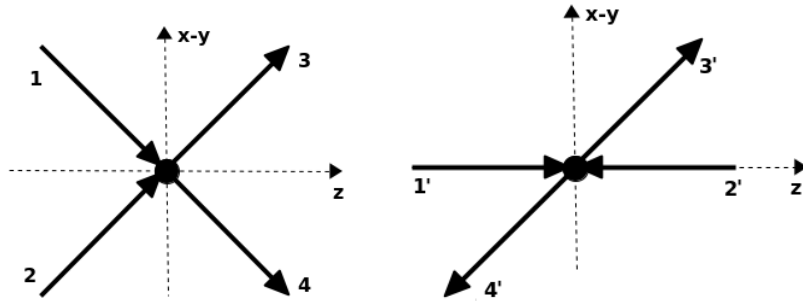


FIGURE 1.2: $2 \rightarrow 2$ scattering rotation, aligning the incoming particles to the z-axis (from left to right figure).

² (E, \bar{p}) and (E', \bar{p}') are the total momentum-energy of the system in the inertial frames S and S' .

³For a deeper explanation see [10].

The rotation matrix is defined as

$$R = \begin{pmatrix} 1 & 0 & 0 & 0 \\ 0 & \hat{e}_{1x} & \hat{e}_{1y} & \hat{e}_{1z} \\ 0 & \hat{e}_{2x} & \hat{e}_{2y} & \hat{e}_{2z} \\ 0 & \hat{e}_{3x} & \hat{e}_{3y} & \hat{e}_{3z} \end{pmatrix}. \quad (1.7)$$

Any quantity invariant under Lorentz transformations should also be invariant under the transformation matrix T_{RL} .

1.1.4 The elements of the Standard Model Lagrangian

To guarantee that the SM Lagrangian is invariant under local gauge transformations, one needs to define a covariant derivative as

$$D_\mu = \partial_\mu - ig_s T_a G_\mu^a - ig I_j W_\mu^j - ig' \frac{1}{2} Y B_\mu \quad (1.8)$$

with g_s the $SU(3)$ coupling, g the $SU(2)$ coupling and g' the $U(1)$ coupling.

| Field | Fermions | | | | | Gauge Bosons | | |
|------------|------------------------------|---------------|------------------------------|----------------|----------------|--------------|------------|---------|
| | $L_L^i(e_L^i, \nu_L^i)$ | l_R^i | $Q_L^i(u_L, d_L)$ | u_R^i | d_R^i | G_μ^a | W_μ^j | B_μ |
| $Q[e]$ | 0; -1 | -1 | $+\frac{2}{3}; -\frac{1}{3}$ | $+\frac{2}{3}$ | $-\frac{1}{3}$ | 0 | $\pm 1, 0$ | 0 |
| I_3 | $+\frac{1}{2}; -\frac{1}{2}$ | 0 | $+\frac{1}{2}; -\frac{1}{2}$ | 0 | 0 | 0 | $\pm 1, 0$ | 0 |
| Y | $-\frac{1}{2}$ | -1 | $\frac{1}{6}$ | $\frac{2}{3}$ | $-\frac{1}{3}$ | 0 | 0 | 0 |
| Dim | $\frac{3}{2}$ | $\frac{3}{2}$ | $\frac{3}{2}$ | $\frac{3}{2}$ | $\frac{3}{2}$ | 1 | 1 | 1 |

TABLE 1.2: Overview of the Standard Model content and some of the quantum numbers: Q electric charge, I_3 the weak isospin third component, Y the weak hypercharge and the related dimension, dim.

The SM Lagrangian is written in terms of the elementary fields shown in table (1.2),

$$\begin{aligned} \mathcal{L}_{\text{SM}} = & \left[-\frac{1}{4} G_{\mu\nu}^a G^{\mu\nu} - \frac{1}{4} W_{\mu\nu}^j W^{j\mu\nu} - \frac{1}{4} B_{\mu\nu} B^{\mu\nu} \right] && \leftarrow \text{gauge sector} \quad (1.9) \\ & + i \sum_{\mathbf{f}^i} \bar{\mathbf{f}}^i \gamma^\mu D_\mu \mathbf{f}^i; \quad \mathbf{f}^i = Q_L^i, u_R^i, d_R^i, L_L^i, l_R^i \quad (i = 1, 2, 3) && \leftarrow \text{fermions} \end{aligned}$$

The dimension (or mass dimension) in table (1.2) refers to the measure of any quantity in units of energy to some power d : [quantity dimension = (units of energy) d] = d . For example, $[m] = [p^\mu] = 1$ while $[x^\mu] = -1$.

The action defined as,

$$S = \int d^4x \mathcal{L}(x), \quad (1.10)$$

is dimensionless, $[S] = 0$. Therefore, in QFT the Lagrangian dimension is $[\mathcal{L}] = 4$; this implies that every term in the SM Lagrangian is dimension 4. For example, $[B_{\mu\nu}B^{\mu\nu}] = 4$, thus $[B_{\mu\nu}] = 2$, $[\partial_\mu] = 1$ and $[B_\mu] = 1$.

1.1.4.1 The Higgs mechanism

Until this moment, all possible ingredients for the SM Lagrangian have been described, as well as their interactions. Yet, there is not a term in the Lagrangian that will explain the mass of any of the particles.

To include a mechanism that gives masses to the particles without violating gauge invariance, it is also necessary to introduce the electroweak symmetry breaking (EWSB), a original mechanism proposed originally by Brout-Englert-Higgs [11, 12].

A more detailed explanation of this mechanism can be found in [13], but the main idea is to introduce an $SU(2)$ doublet of scalar fields with at least 3 degrees of freedom,

$$\Phi = \begin{pmatrix} \phi^+ \\ \phi^0 \end{pmatrix} = \begin{pmatrix} \phi_1 + i\phi_2 \\ \phi_3 + i\phi_4 \end{pmatrix}, \quad (1.11)$$

and with hypercharge $Y_\phi = 1$. The corresponding $SU(2)$ -invariant Lagrangian is,

$$\mathcal{L}_{\text{Higgs}} = (D_\mu \Phi)^\dagger (D^\mu \Phi) + \mu^2 \Phi^\dagger \Phi - \lambda (\Phi^\dagger \Phi)^2. \quad (1.12)$$

To generate the gauge boson masses, it is necessary that $\mu^2 < 0$. Then, in the ground state, the field Φ develops a vacuum expectation value (vev) and the symmetry breaks spontaneously,

$$\langle \Phi \rangle_0 = \langle 0 | \Phi | 0 \rangle = \begin{pmatrix} 0 \\ \left(\frac{v}{\sqrt{2}}\right) \end{pmatrix} \quad v = \left(\frac{-\mu^2}{\lambda}\right)^{\frac{1}{2}}. \quad (1.13)$$

Expanding the scalar field around the vev, equation (1.11) is rewritten as,

$$\Phi = \begin{pmatrix} \phi_1 + i\phi_2 \\ \frac{1}{\sqrt{2}}(v + H) + i\phi_4 \end{pmatrix},$$

with H being the Higgs field. When the unitary gauge is used, only the Higgs field survives

$$\Phi = \begin{pmatrix} 0 \\ \frac{1}{\sqrt{2}}(v + H) \end{pmatrix}. \quad (1.14)$$

The values of μ^2 and λ are not predicted by the SM but obtained from measurements; however, as shown in equation (1.13), μ and λ are not independent and it is sufficient to do precision measurements only for one of them.

Expanding the kinetic term from the Lagrangian (1.12), using the expression (1.14), it is possible to obtain the following expression:

$$(D^\mu\Phi)^\dagger(D^\mu\Phi) = \frac{1}{2}(\partial^\mu H)(\partial_\mu H) + \frac{1}{8}g^2(v+H)^2(W^{1\mu} - iW^{2\mu})(W_\mu^1 + iW_\mu^2) \quad (1.15)$$

$$+ \frac{1}{8}(v+H)^2(gW^{3\mu} - g'B^\mu)(gW_\mu^3 - g'B_\mu) .$$

Introducing a linear combination of the gauge fields W^1 , W^2 , W^3 and B

$$W_\mu^\pm = \frac{1}{\sqrt{2}}(W_\mu^1 \mp iW_\mu^2) , \quad (1.16)$$

$$Z_\mu = c_w W_\mu^3 - s_w B_\mu , \quad (1.17)$$

$$A_\mu = s_w W_\mu^3 + c_w B_\mu , \quad (1.18)$$

with c_w and s_w mixing angles, defined as:

$$\frac{g'}{\sqrt{g^2 + g'^2}} = \sin \theta_W = s_w , \quad (1.19)$$

$$\frac{g}{\sqrt{g^2 + g'^2}} = \cos \theta_W = c_w , \quad (1.20)$$

then, the mass terms are

$$M_W = \frac{1}{2}vg , \quad M_Z = \frac{gv}{2 \cos \theta_W} , \quad M_A = 0 . \quad (1.21)$$

In a similar manner, the scalar field Φ allows to introduce the fermion mass terms in the SM, through the Yukawa interactions of fermions and scalar, with coupling constants λ_f proportional to the fermion masses.

Finally, the Lagrangian responsible for the masses in the SM can be written as,

$$\mathcal{L} = \left[(D_\mu\Phi)^\dagger(D^\mu\Phi) - \mu^2\phi^\dagger\Phi - \lambda(\Phi^\dagger\Phi)^2 \right] \quad \leftarrow \text{Higgs sector} \quad (1.22)$$

$$+ \left[\lambda_2 \bar{L}\Phi e_R + i\lambda_u \bar{Q}\tau_2\Phi^* u_R + \lambda_d \bar{Q}\Phi d_R + \text{h.c.} \right] . \quad \leftarrow \text{Yukawa interactions}$$

1.2 Beyond the Standard Model: Effective Field Theory

Up to this point, the SM has been successful in predicting and explaining experimental data; for example, the discovery of the W/Z bosons (1983) [14] and the Higgs boson

(2012) [15, 16]. However, it suffers from fine tuning problems and it is unable to provide answers to several fundamental questions, which leads to consider scenarios Beyond the Standard Model (BSM).

In general, the SM can be thought of as a low energy approximation of a more fundamental theory. Then, to build a new appropriate quantum field theory, one could try to deform the SM and parameterize new physics in a model independent way using higher dimensional operators composed of the SM fields: an effective Lagrangian expansion [17].

To define a quantum field extension for the SM, as described in [18], it is essential to:

- **identify the relevant degrees of freedom**, or fields. The EFT will use the building blocks (described in table (1.2)) to compose new operators, which are related through unknown couplings, also known as *anomalous couplings*;
- **identify the symmetries and the interactions**. All the symmetries and interactions (as well as gauge and Lorentz invariance) from the SM are imposed;
- **find the expansion parameters**, or power counting. The EFT describes the new Lagrangian as an expansion in terms of an energy cut-off scale. To set the expansion parameters, it is important to count the mass dimension (described in the previous section).

The EFTs can be either a top-down description or a bottom-up one, as shown in the figure (1.3). For example, the Fermi theory for beta decay, described in the introduction of this work, is an important example of a bottom-up EFT.

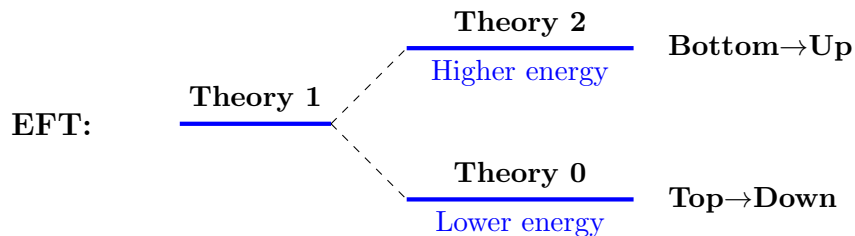


FIGURE 1.3: Effective Field Theory descriptions. The one used for this work is the bottom-up description (from SM to higher dimension operators for larger energies).

In general, this formalism is a good theoretical way to describe physics at some scale Λ , without knowing the detailed dynamics of the system. In this work, it is only of interest the bottom-up description, with Λ being the cut-off energy where new physics is expected to appear.

1.2.1 Building an SM bottom-up EFT

To rebuild the SM as an EFT, there are some necessary features that need to be considered when writing the effective Lagrangian:

- Starting with the 0th order element $\mathcal{L}^{(0)} = \mathcal{L}_{\text{SM}}$, the expansion of the SM as an effective Lagrangian can be constructed as,

$$\mathcal{L} = \mathcal{L}^{(0)} + \mathcal{L}^{(1)} + \mathcal{L}^{(2)} + \dots .$$

- One should write the most general set of interactions, preserving the symmetries $SU(3)_C \times SU(2)_L \times U(1)_Y$ and using the fields included in the SM⁴. For the purposes of this work, a linear realization is considered with the Higgs signature measured by the experiments.
- The SM includes all possible dim-4 operators. Assuming Lorentz and gauge invariance, new physics (NP) effects start to be described already by any operator \mathcal{O}_i with dimension 5 and larger. The Effective Lagrangian is the following:

$$\mathcal{L}_{\text{EFT}} = \mathcal{L}_{\text{SM}} + \underbrace{\sum_i c_i \mathcal{O}_i}_{\mathcal{L}_{\text{NP}}} \quad \text{with } [\mathcal{O}_i] = d > 4 .$$

- New particles are produced only at the cut-off energy scale ($m \approx \Lambda$) and not before, as they are not observed in the SM. The coefficient c_i is defined as

$$c_i = \frac{f_i}{\Lambda^{d-4}}$$

where f_i is the interaction coupling. These coefficients are unknown but can be constrained using experimental data, in a similar way to the β -decay example.

- When baryon and lepton numbers are conserved, only the operators with even dimension can be constructed (dim-6, dim-8, dim-10, ...). The restrictions on the coefficients and operators come from high precision measurements. For example, in the absence of any departure from the SM predictions for fermionic interactions, one might try to look for effects using bosonic fields operators. A more detailed explanation on the current experimental limits for the anomalous couplings can be found in [19].

⁴Note that the field content varies depending if a linear realization is considered or not. In a linear realization of the gauge symmetry $SU(2)_L \times U(1)_Y$, the Higgs doublet field Φ is included in the low-energy particle content (SM-Higgs doublet field). While in an $SU(2)_L \times U(1)_Y$ nonlinear realization (or non-decoupling) only the would-be Goldstone bosons which give masses to W^\pm and Z -bosons are included without the SM-Higgs boson.

- At low energies the effective Lagrangian should reduce to the SM, if no new lighter particles (below the cut-off energy) are discovered [20]. In addition, any extension of the SM should satisfy the S-matrix basic principles, e.g. unitarity, analyticity, etc.

1.2.2 Anomalous couplings in the electroweak sector

Precision tests are sensitive observables that allow verifying the effectiveness of the SM to describe the particle interactions up to very high energy scales, or to find direct evidence of new physics. For instance, now when the LHC is measuring again, a better understanding of the dynamics behind the Electroweak Symmetry Breaking (EWSB) is timely and topical; and, for instance, gauge boson self interactions are one of the more convenient places to search for BSM physics.

Therefore, this work will be focussed on new physics arising from VBS final states as deviations in the measurements of triple gauge couplings (TGCs) and quartic gauge couplings (QGCs), shown in figure (1.4).

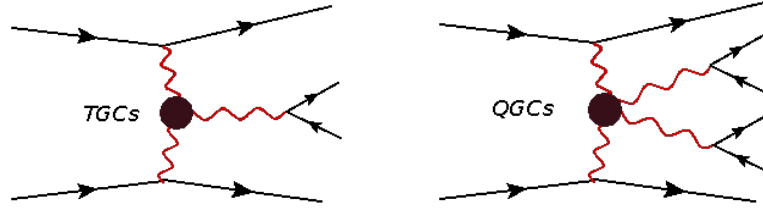


FIGURE 1.4: Collider gauge boson self interactions: triple gauge couplings and quartic gauge couplings with leptons plus 2 jets signature.

Acknowledging the bottom-up EFT prescription described previously and truncating the expansion to the lowest order possible, the bosonic interactions are affected by dimension 6 operators (\mathcal{O}_i) and dimension 8 operators (\mathcal{O}_{S_i} , \mathcal{O}_{T_i} and \mathcal{O}_{M_i} , whose indices will be explained in (1.3)). Then, the resulting effective Lagrangian is,

$$\mathcal{L}_{EFT} = \underbrace{\mathcal{L}_{SM}}_{dim-4} + \underbrace{\sum_i \frac{f_i}{\Lambda^2} \mathcal{O}_i}_{dim-6} + \underbrace{\sum_i \frac{f_{S_i}}{\Lambda^4} \mathcal{O}_{S_i} + \sum_i \frac{f_{T_i}}{\Lambda^4} \mathcal{O}_{T_i} + \sum_i \frac{f_{M_i}}{\Lambda^4} \mathcal{O}_{M_i}}_{dim-8}. \quad (1.23)$$

Using the VBFNLO definition for the field strength tensors⁵ [8] (without taking the $SU(3)$ part),

$$\hat{W}_{\mu\nu} = igT^i W_{\mu\nu}^i, \quad \hat{B}_{\mu\nu} = ig'Y B_{\mu\nu}, \quad (1.24)$$

⁵There is a difference between the anomalous couplings defined in VBFNLO and those defined in [21]. The conversion factors can be found in Appendix (B).

it is possible to define the bosonic operators.

Dimension 6 Operators: When baryon number conservation is imposed, there are in total 59 dim-6 operators [20], from which only 15 are bosonic operators. Dim-6 operators involve TGCs and QGCs, as it is shown in the table below,

| Operator | TGCs | QGCs |
|----------------------------------------------------------------------------------------|--------------------|------------------|
| $\mathcal{O}_{WWW} = \text{Tr}[\hat{W}_{\mu\nu}\hat{W}^{\nu\rho}\hat{W}_{\rho}^{\mu}]$ | ZWW, AWW | WWWW, ZZWW |
| $\mathcal{O}_W = (D_{\mu}\Phi)^{\dagger}\hat{W}^{\mu\nu}(D_{\nu}\Phi)$ | AWW, HWW, HZZ, HZA | ZZWW, ZAWW, AAWW |
| $\mathcal{O}_B = (D_{\mu}\Phi)^{\dagger}\hat{B}^{\mu\nu}(D_{\nu}\Phi)$ | AWW, HWW, HZA, HAA | |
| $\mathcal{O}_{\phi W} = (\Phi)^{\dagger}\hat{W}_{\mu\nu}\hat{W}^{\mu\nu}(\Phi)$ | HZA, HZA, HAA, HWW | |

In other words, due gauge invariance, deviations coming from dim-6 operators have effects on the QGCs and TGCs. As the TGCs are known to agree with the SM within a few percent [22–27], the QGCs will be more suitable for NP searches.

Effective operators with genuine QGCs but no TGCs are generated at tree level at dimension 8 [28].

Dim-8 Operators: They offer an independent parameterization of QGCs and also allow more searches to be done, as some new physics only appears for the first time in dim-8 operators (e.g. heavy resonances). A more detailed definition of the operators can be found in the section (1.3).

To simplify the notation, one can define the anomalous coupling as,

$$F_{S_i, T_i, M_i} = \frac{f_{S_i, T_i, M_i}}{\Lambda^4}. \quad (1.25)$$

1.3 Dim-8 operators for VBS

As stated before, the genuine bosonic quartic vertices including BSM effects are of dimension 8 or higher. The table (1.3) contains a summary from the dim-8 operators contributions to the different quartic vertices. The operators can be classified in three groups [8, 29]:

- **Operators using only $D_{\mu}\phi$ (\mathcal{O}_{S_i}):** They contain four covariant derivatives of the Higgs field and, therefore, mainly longitudinally polarized particles have dominant

effects in the observable calculations:

$$\mathcal{O}_{S0} = [(D_\mu \Phi)^\dagger D_\nu \Phi] \times [(D^\mu \Phi)^\dagger D^\nu \Phi] \quad (1.26)$$

$$\mathcal{O}_{S1} = [(D_\mu \Phi)^\dagger D^\mu \Phi] \times [(D_\nu \Phi)^\dagger D^\nu \Phi] \quad (1.27)$$

$$\mathcal{O}_{S2} = [(D_\mu \Phi)^\dagger D_\nu \Phi] \times [(D^\nu \Phi)^\dagger D^\mu \Phi] \quad (1.28)$$

- **Operators using only $\hat{W}_{\mu\nu}$ and $\hat{B}_{\mu\nu}$ (\mathcal{O}_{T_i}):** They contain four field strength tensors and mainly the transversely polarized particles have dominant effects in the observable calculation:

$$\mathcal{O}_{T0} = \text{Tr}[\hat{W}_{\mu\nu} \hat{W}^{\mu\nu}] \times \text{Tr}[\hat{W}_{\alpha\beta} \hat{W}^{\alpha\beta}] \quad (1.29)$$

$$\mathcal{O}_{T1} = \text{Tr}[\hat{W}_{\alpha\nu} \hat{W}^{\mu\beta}] \times \text{Tr}[\hat{W}_{\mu\beta} \hat{W}^{\alpha\nu}] \quad (1.30)$$

$$\mathcal{O}_{T2} = \text{Tr}[\hat{W}_{\alpha\mu} \hat{W}^{\mu\beta}] \times \text{Tr}[\hat{W}_{\beta\nu} \hat{W}^{\nu\alpha}] \quad (1.31)$$

$$\mathcal{O}_{T5} = \text{Tr}[\hat{W}_{\mu\nu} \hat{W}^{\mu\nu}] \times \hat{B}_{\alpha\beta} \hat{B}^{\alpha\beta} \quad (1.32)$$

$$\mathcal{O}_{T6} = \text{Tr}[\hat{W}_{\alpha\nu} \hat{W}^{\mu\beta}] \times \hat{B}_{\mu\beta} \hat{B}^{\alpha\nu} \quad (1.33)$$

$$\mathcal{O}_{T7} = \text{Tr}[\hat{W}_{\alpha\mu} \hat{W}^{\mu\beta}] \times \hat{B}_{\beta\nu} \hat{B}^{\nu\alpha} \quad (1.34)$$

$$\mathcal{O}_{T8} = \hat{B}_{\mu\nu} \hat{B}^{\mu\nu} \hat{B}_{\alpha\beta} \hat{B}^{\alpha\beta} \quad (1.35)$$

$$\mathcal{O}_{T9} = \hat{B}_{\alpha\mu} \hat{B}^{\mu\beta} \hat{B}_{\beta\nu} \hat{B}^{\nu\alpha} \quad (1.36)$$

The last two operators give rise to QGCs for neutral electroweak gauge bosons, which do not appear in the SM.

- **Operators using $D_\mu \phi$, $\hat{W}_{\mu\nu}$ and $\hat{B}_{\mu\nu}$ (\mathcal{O}_{M_i}):** They are a mixture of field strength tensors and two covariant derivatives. In this case, transverse and longitudinal polarizations have comparable contributions to the dominant effects,

$$\mathcal{O}_{M0} = \text{Tr}[\hat{W}_{\mu\nu} \hat{W}^{\mu\nu}] \times [(D_\beta \Phi)^\dagger D^\beta \Phi] \quad (1.37)$$

$$\mathcal{O}_{M1} = \text{Tr}[\hat{W}_{\mu\nu} \hat{W}^{\nu\beta}] \times [(D_\beta \Phi)^\dagger D^\mu \Phi] \quad (1.38)$$

$$\mathcal{O}_{M2} = [\hat{B}_{\mu\nu} \hat{B}^{\mu\nu}] \times [(D_\beta \Phi)^\dagger D^\beta \Phi] \quad (1.39)$$

$$\mathcal{O}_{M3} = [\hat{B}_{\mu\nu} \hat{B}^{\nu\beta}] \times [(D_\beta \Phi)^\dagger D^\mu \Phi] \quad (1.40)$$

$$\mathcal{O}_{M4} = [(D_\mu \Phi)^\dagger \hat{W}_{\beta\nu} D^\mu \Phi] \times \hat{B}^{\beta\nu} \quad (1.41)$$

$$\mathcal{O}_{M5} = [(D_\mu \Phi)^\dagger \hat{W}_{\beta\nu} D^\nu \Phi] \times \hat{B}^{\beta\mu} \quad (1.42)$$

$$\mathcal{O}_{M7} = [(D_\mu \Phi)^\dagger \hat{W}_{\beta\nu} \hat{W}^{\beta\mu} D^\nu \Phi] \quad (1.43)$$

| | WWWW | WWZZ | ZZZZ | WWAZ | WWAA | ZZZA | ZZAA | ZAAA | AAAA |
|----------------------------------------|------|------|------|------|------|------|------|------|------|
| $\mathcal{O}_{S_0}, \mathcal{O}_{S_1}$ | X | X | X | | | | | | |
| $\mathcal{O}_{M_0}, \mathcal{O}_{M_1}$ | X | X | X | X | X | X | X | | |
| \mathcal{O}_{M_7} | X | X | X | X | X | X | X | | |
| $\mathcal{O}_{M_2}, \mathcal{O}_{M_3}$ | | X | X | X | X | X | X | | |
| $\mathcal{O}_{M_4}, \mathcal{O}_{M_5}$ | | X | X | X | X | X | X | | |
| $\mathcal{O}_{T_0}, \mathcal{O}_{T_1}$ | X | X | X | X | X | X | X | X | X |
| \mathcal{O}_{T_2} | X | X | X | X | X | X | X | X | X |
| $\mathcal{O}_{T_5}, \mathcal{O}_{T_6}$ | | X | X | X | X | X | X | X | X |
| \mathcal{O}_{T_7} | | X | X | X | X | X | X | X | X |
| $\mathcal{O}_{T_8}, \mathcal{O}_{T_9}$ | | | X | | | X | X | X | X |

TABLE 1.3: Quartic vertices modified by dim-8 operators.

CHAPTER 2

Vector Boson Scattering

2.1 Particle scattering inside the colliders

The vast majority of the experiments in particle physics involve particle scattering, making necessary to understand the underlying physics inside the collider.

Consider a fixed target collision, where the particle beam has a rest mass m and total beam energy E_B , colliding with another particle with same mass but at rest. The energy available in the collision in the center-of-mass frame (CM-frame) of the two particles is [2]

$$s = E_{\text{CM}}^2 = 2m^2 + 2mE_B , \quad (2.1)$$

which means that at high energies ($E_B \gg m$), the energy available increases proportional to $\sqrt{E_B}$.

If instead two colliding beams are considered, with 4-momenta p_1 and p_2 , the energy available in the collision in the CM-frame is,

$$s = E_{\text{CM}}^2 = (p_1 + p_2)^2 . \quad (2.2)$$

Let $p_i = (E_i, \vec{p}_i)$, if $\vec{p}_1 = -\vec{p}_2$ in the collider, then

$$s = (E_1 + E_2)^2 .$$

For example, the LHC fires two proton beams, with $\sqrt{s} = 13$ TeV.

During a particle collision, the event rate of a specific process per second is given by,

$$\frac{dN}{dt} = L\sigma , \quad (2.3)$$

being L the luminosity controlled by the beam parameters of the collider, and σ an intrinsic quantity to the process, which allows to compare experiments with different beam intensities.

For example, for a $2 \rightarrow 2$ scattering the cross section σ could be calculated from the respective quantum field theory as a function of the scattering matrix element \mathcal{M} describing the interactions [30],

$$\frac{d\sigma}{d\Omega} = \frac{1}{2s} \frac{\beta}{32\pi^2} \sum |\mathcal{M}|^2 \quad (2.4)$$

with $\beta = |\vec{p}|/p^0$ the velocity of the produced particle and Ω a solid angle for the final state particles. The complete cross section for $2 \rightarrow n$ processes will be explained in more detailed in the section (2.2).

2.1.1 The S -matrix

It is clear now that the cross section is an important experimental quantity, which provides information about the underlying process. Therefore, it is necessary to understand how the system evolves from its initial state, $|i\rangle_{\text{in}}$, until the measurement of the cross section in a final state, $|f\rangle_{\text{out}}$.

The transition from ${}_{\text{out}}\langle f|i\rangle_{\text{in}}$ is given by a linear operator S , called the S -matrix (or scattering matrix) [31],

$${}_{\text{out}}\langle f|i\rangle_{\text{in}} = {}_{\text{in}}\langle f|S|i\rangle_{\text{in}} . \quad (2.5)$$

The S -matrix needs to be unitary to satisfy the fundamental principle of probability conservation,

$$SS^\dagger = S^\dagger S = \mathbb{1} . \quad (2.6)$$

Then, the S -matrix can be understood in the following way [32]: if the particles do not interact at all, S is just the identity operator, meanwhile the non-trivial interaction is defined by a matrix, T , such as:

$$S = \mathbb{1} + iT . \quad (2.7)$$

The T -matrix is related to the scattering amplitude \mathcal{M} (equation (2.4)) in the following way: given a scattering $a + b \rightarrow c + d + e + \dots$, with 4-momenta p_a, p_b, p_F respectively ($p_F = \sum_k (p_k)_{\text{out}}$), the T -matrix is,

$$\langle F|T|p_a, p_b\rangle = \langle F|T|i\rangle = (2\pi)^4 \delta^{(4)}(p_F - (p_a + p_b)) \mathcal{M}_{Fi} . \quad (2.8)$$

Thus, the T -matrix is an intrinsic quantity to the process, just like the cross section.

2.1.2 Detector jargon

In general, not only the integrated cross section is important, but also observables that could be related to the particle. It is therefore useful to define the differential cross section as a function of the observables of interest, in other words, $d\sigma/d(\text{observable})$.

At the LHC, the origin of the coordinate system in the detector is located in the nominal interaction point¹, as shown in figure (2.1) [33]: the beam direction defines the z -axis and the $x-y$ plane is transverse to the beam. The positive x -axis points from the interaction point to the center of the LHC ring, whereas the positive y -axis points upwards.

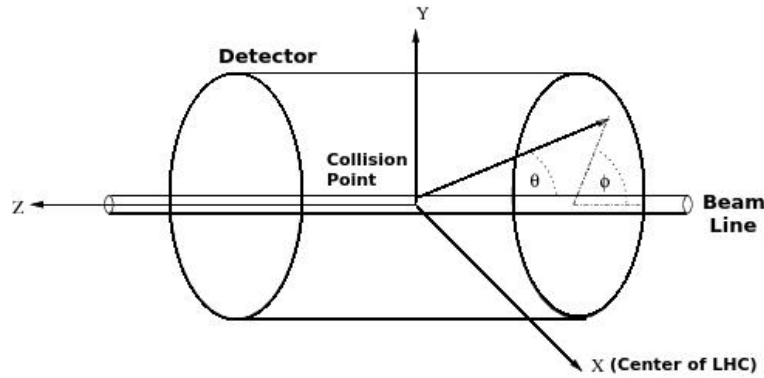


FIGURE 2.1: Coordinate system used by the ATLAS and CMS experiments at the LHC [33].

The azimuthal angle ϕ is measured around the beam axis, with $\phi = 0$ in the positive x -axis and increasing clocks-wise. The polar angle θ is the angle from the beam axis.

For a momentum $p = (E, p_x, p_y, p_z)$, the rapidity is defined as

$$y = \frac{1}{2} \log \frac{E + p_z}{E - p_z}, \quad (2.9)$$

which in the massless limit ($\beta \rightarrow 1$) gives the pseudo-rapidity,

$$\eta = \frac{1}{2} \log \left(\frac{1 + \cos \theta}{1 - \cos \theta} \right). \quad (2.10)$$

The transverse momentum p_T , the transverse energy E_T , the missing transverse energy \cancel{E}_T , and any other transverse variables, are defined in the x - y plane (transverse plane) unless stated otherwise.

The distance ΔR in the pseudorapidity-azimuthal angle space is defined as

$$\Delta R = \sqrt{\Delta\eta^2 + \Delta\phi^2}. \quad (2.11)$$

¹The nominal interaction point is the place designed for the collision to happen inside the detector.

The Mandelstam variables

The Mandelstam variables are independent of the frame of reference used. For a $2 \rightarrow 2$ scattering ($a + b \rightarrow c + d$), they are,

$$s = (p_a + p_b)^2 = (p_c + p_d)^2, \quad (2.12)$$

$$t = (p_a - p_c)^2 = (p_b - p_d)^2, \quad (2.13)$$

$$u = (p_a - p_d)^2 = (p_b - p_c)^2, \quad (2.14)$$

$$(2.15)$$

and for m_i the rest mass for any of the particles,

$$s + t + u = m_a^2 + m_b^2 + m_c^2 + m_d^2. \quad (2.16)$$

2.1.3 Vector Boson Scattering at the LHC

As it was stated in Chapter 1, the observation and deeper understanding of processes involving electroweak bosons have been one of the keys to reveal new physics. But the production of a pair of vector bosons cannot be directly measured in the detectors, as consequence of their lifetimes. Instead, it needs to be reconstructed from their decay products.

When a particle decays into several final states, the sum of the probability of all the possible decays must be equal to one. This introduces the concept of branching ratio BR [2],

$$\sum_i BR_i = 1.$$

If the vector boson decay channels are considered, they contain either leptons or hadrons in the final state. The decays are labeled as leptonic (zero hadrons), semileptonic (one vector boson decays to hadron) or hadronic (both vector bosons decays to hadrons) decays. Most of the vector bosons decay into hadronic channels (quark-antiquark pair), while the fully leptonic decay has a small branching ratio [30, 34]; e.g. the branching ratios for the W boson are (at tree level),

$$\begin{aligned} \text{BR}(W \rightarrow e\nu_e) = \text{BR}(W \rightarrow \mu\nu_\mu) = \text{BR}(W \rightarrow \tau\nu_\tau) &= \frac{1}{9}, \\ \text{BR}(W \rightarrow \text{hadrons}) &= \frac{2}{3}. \end{aligned}$$

Nevertheless, the focus of this thesis will be on the fully leptonic decay channels, as they have only a minor background from other processes, which implies that accurate

predictions for the signal and background processes are required. One could say then that the new physics findings are highly dependent on the ability to achieve this desired accuracy.

For this purpose, analytic phase-space integration becomes impractical, and instead numerical calculations using Monte Carlo programs are used.

2.2 VBFNLO

VBFNLO² [8] is a parton-level Monte Carlo program with a focus on hadron collider processes involving electroweak bosons, including diboson and triboson production as well as vector boson fusion and scattering, implemented to NLO QCD accuracy.

VBFNLO calculates cross sections and distributions of observables at the LHC for different processes, including gauge couplings from the EFT. The implemented signal and background processes are [8],

- Vector Boson Fusion (VBF) processes,
- Higgs production with two or three jets (1-loop electroweak corrections are also included for two jet final state),
- Higgs production in association with a photon + 2 jets,
- Vector Boson (VB) production + 2 jets,
- double VB production + 2 jets,
- double and triple VB production,
- double VB production in association with a hadronic jet,
- Higgs production via gluon fusion at LO.

This study of quartic gauge boson scattering requires diboson production plus two jets and fully leptonic decay of the vector bosons, as shown in figure (2.2).

2.2.1 Structure of VBFNLO

VBFNLO does the following [35]: it initializes the program, reads different input files (with the masses, couplings, desired process, etc.), calculates physical quantities (e.g.

²Vector **B**oson **F**usion processes at **NLO** QCD.

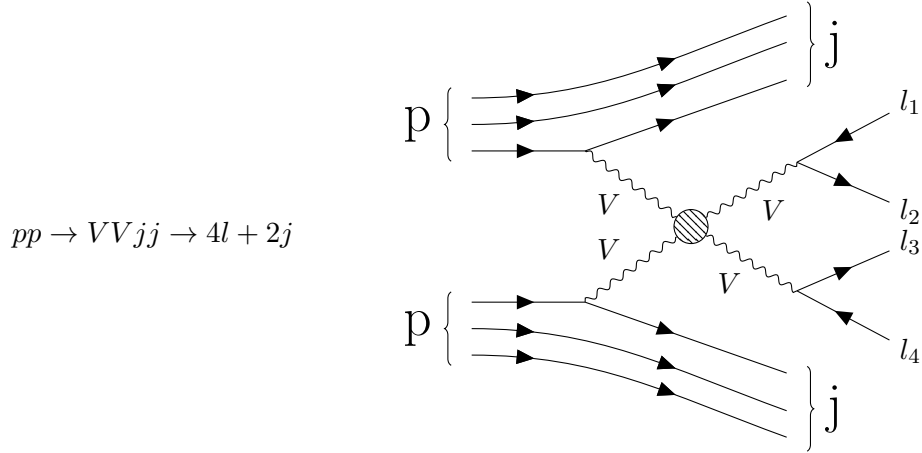


FIGURE 2.2: Quartic gauge boson scattering as implemented in VBFNLO.

branching ratios), does a phase space mapping and calculates the scattering amplitude for the given process, and finally calculates the cross section as a function of different observables that will be output as histograms, following the scheme shown in figure (2.3).

The main part of VBFNLO is the numerical integration at many phase space points of the cross section, as it integrates the phase space numerically using Monte Carlo integration to provide the differential distributions of arbitrary observables at the LHC [8].

For a process $pp \rightarrow X$ ($a_1 + a_2 \rightarrow \hat{x} \rightarrow b_1 b_2 \dots b_n$) the cross section is defined as [30],

$$\sigma = \int dx_1 dx_2 \sum f_{a_1/p}(x_1) f_{a_2/p}(x_2) \frac{1}{2s} \int d\phi_n(x_1 p + x_2 p; p_1 \dots p_n) \Theta(\text{cuts}) \quad (2.17)$$

$$\sum |\mathcal{M}|^2(a_1 a_2 \rightarrow b_1 b_2 \dots b_n)$$

with $f_{a_1/p}(x_1)$ the probability to find a parton a_1 inside one of the protons with momentum x_1 (a fraction of the proton momentum), and similarly $f_{a_2/p}(x_2)$. The summation is done for all the sub-processes; being $1/2s$ the flux factor³ and $d\phi_n$ the phase space integration⁴ defined as

$$d\phi_n(P; p_1 \dots p_n) = \prod_{i=1}^n \left(\frac{d^3 \mathbf{p}_i}{(2\pi)^3 2E_i} \right) (2\pi)^4 \delta^4 \left(P - \sum_i p_i \right), \quad (2.18)$$

and $\Theta(\text{cuts})$ the acceptance function [30].

³The “flux” factor includes the beam intensity and the target density. In other words, the flux factor corresponds to the amount of particles that pass each other per unit of area and per unit time.

⁴The Lorentz invariant “phase space” factor implies that experiments cannot observe individual states but integrate over a number of states.

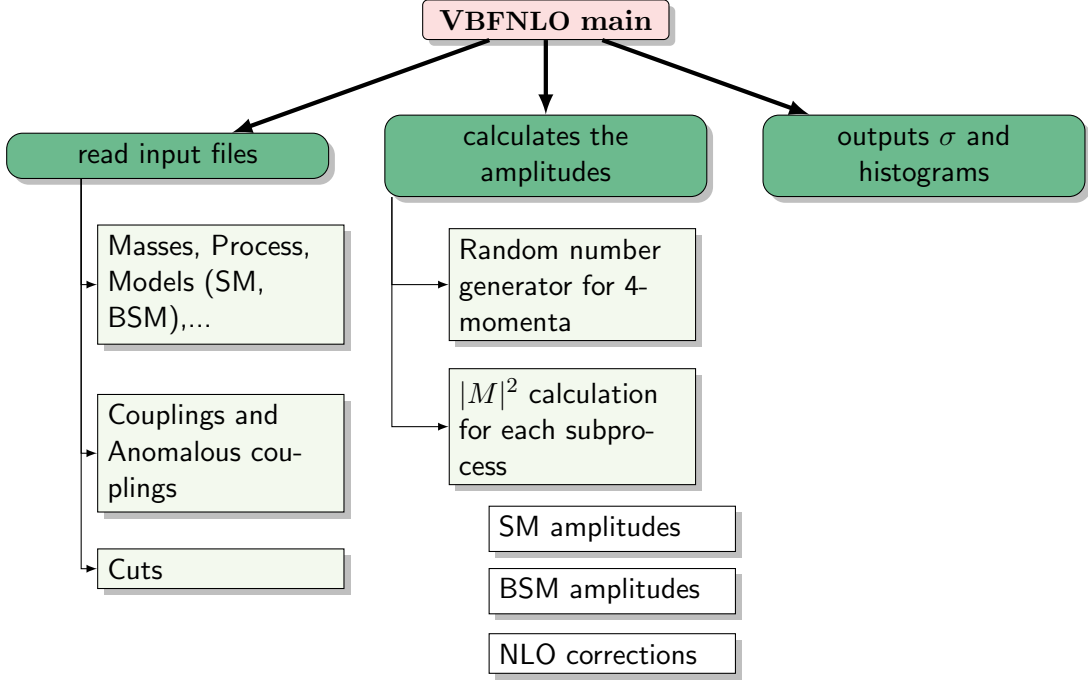


FIGURE 2.3: The structure in VBFNLO to calculate the cross sections and observables for different processes.

2.2.1.1 Calculation of the amplitudes

In VBFNLO, the calculation of any amplitude is split into the different contributing parts of the corresponding process, and later integrated to calculate the total cross section.

For example, for vector boson scattering, the amplitude is divided into the leptonic tensors and the quark currents, which could allow to calculate the anomalous coupling contributions to the leptonic tensor without any modification to the QCD calculations.

The amplitudes are calculated using HELAS [36] and MadGraph [37] subroutines. For instance, for vector boson anomalous couplings the scattering amplitude is the product of the quark decay currents $J_{p \rightarrow j V_i}$, and the anomalous amplitude \mathbf{M} for $V_1 V_2 \rightarrow 4f$,

$$\mathcal{M}_{pp \rightarrow 4fjj} = J_{p \rightarrow j V_1}^\mu J_{p \rightarrow j V_2}^\nu \mathbf{M}_{\mu\nu}^{\text{BSM}}(V_1 V_2 \rightarrow 4f) . \quad (2.19)$$

The amplitude subroutine distinguishes between SM calculations or BSM models, as well as LO or NLO calculations.

For the anomalous couplings calculations in Chapter 4, it is explained how the effective amplitudes are calculated using the Feynman diagrams and the HELAS subroutines.

PART II:

Unitarization in Monte Carlo Generators

CHAPTER 3

Restoring Unitarity for On-shell Scattering

3.1 The Unitarity Bounds

As mentioned in Chapter (2), the T matrix corresponds to the non-trivial scattering information defined in equation (2.7), which satisfies the unitarity condition established in equation (2.6). In other words,

$$-i(T - T^\dagger) = T^\dagger T . \quad (3.1)$$

Using equation (2.8) for a $2 \rightarrow 2$ scattering ($ab \rightarrow cd$), the unitarity condition (3.1) for the transition from an initial state $|i\rangle$ to a final state $|f\rangle$ is [31]

$$-i(\mathcal{M}_{fi} - \mathcal{M}_{if}^*) = \sum_n (2\pi)^4 \delta^4(P_n - P_i) \mathcal{M}_{nf}^* \mathcal{M}_{ni} , \quad (3.2)$$

where the sum runs over all the possible intermediate states $|n\rangle$ coupled to $|f\rangle$ and $|i\rangle$, and $P_i = p_a + p_b$.

The T -matrix has real and imaginary components, $T = \text{Re}(T) + i\text{Im}(T)$, where $\text{Re}(T)$ and $\text{Im}(T)$ are defined as Hermitian and anti-Hermitian matrices respectively. Therefore, one can write,

$$\text{Im}(T) = \frac{1}{2i} T - T^\dagger , \quad (3.3)$$

and

$$-i(\mathcal{M}_{fi} - \mathcal{M}_{if}^*) = 2(\text{Im}\mathcal{M})_{fi} = \sum_n (2\pi)^4 \delta^4(P_n - P_i) \mathcal{M}_{nf} \mathcal{M}_{ni} . \quad (3.4)$$

For $i = f$, expression (3.4) can be understood as the imaginary part of a forward scattering amplitude equivalent to the sum of all possible intermediate state particle contributions, as shown in figure (3.1).

$$2\text{Im} \left(\text{shaded circle with } p_a, p_a, p_b, p_b \right) = \sum_n \left(\text{shaded circle with } p_a, p_a, p_b, p_b \text{ and } n \text{ lines on the right} \right) \left(\text{shaded circle with } n \text{ lines on the left and } p_b, p_b, p_a, p_a \right)$$

FIGURE 3.1: The unitary relation for a forward $2 \rightarrow 2$ scattering amplitude.

Before trying to understand the consequences of the unitary relation in the calculation of σ , it is useful to introduce the Källén function $\lambda(x_1, x_2, x_3)$ [31],

$$\lambda(x_1, x_2, x_3) \equiv (x_1^2 + x_2^2 + x_3^2) - 2x_1x_2 - 2x_2x_3 - 2x_3x_1, \quad (3.5)$$

as a kinematical correction is needed for the phase space integration factor (2.18). Then, for a $2 \rightarrow 2$ scattering,

$$\begin{aligned} \sum_n (2\pi)^4 \delta^4(P_n - P_i) &= \sum_{c,d} \int \frac{d^3p_c d^3p_d}{(2\pi)^3(2E_c)(2\pi)^3(2E_d)} (2\pi)^4 \delta^4(p_c + p_d - P) \\ &= \sum_{c,d} \frac{\lambda^{\frac{1}{2}}(s, m_c^2, m_d^2)}{8s(2\pi)^2} \int d\Omega, \end{aligned} \quad (3.6)$$

where the sum runs over all pairs c, d into which $a + b$ can scatter.

The unitarity condition for $2 \rightarrow 2$ scattering, i.e. neglecting states $|n\rangle$ with 3 particles or more, then reads

$$2(\text{Im.}\mathcal{M})_{fi} = \sum_{c,d} \frac{\lambda^{\frac{1}{2}}(s, m_c^2, m_d^2)}{8s(4\pi^2)} \int \mathcal{M}_{nf}^* \mathcal{M}_{ni} d\Omega. \quad (3.7)$$

The total cross section for $ab \rightarrow cd$ ¹ can be expressed as

$$\sigma = \frac{1}{4[(p_a \cdot p_b)^2 - m_a^2 m_b^2]^{\frac{1}{2}}} \frac{\lambda^{\frac{1}{2}}(s, m_c^2, m_d^2)}{8s(2\pi)^2} \int |\mathcal{M}_{ni}|^2 d\Omega, \quad (3.8)$$

from which one derives the Optical Theorem for the total elastic cross section ($ab \rightarrow ab$), by setting $i = f$ in equation (3.7),

$$\sigma = \frac{1}{\lambda^{\frac{1}{2}}(s, m_a^2, m_b^2)} (\text{Im.}\mathcal{M})_{ii} \quad (3.9)$$

¹Case for non-identical particles.

3.1.1 The Partial Wave decomposition

Now let us use the helicity formalism from Jacob and Wick [38] for a $2 \rightarrow 2$ scattering, such as $(p_a, \lambda_a; p_b, \lambda_b) \rightarrow (p_c, \lambda_c; p_d, \lambda_d)$. The scattering amplitude \mathcal{M}_{fi} can be explicitly decomposed into partial wave amplitudes $A_{\lambda_a \lambda_b; \lambda_c \lambda_d}^j$,

$$\mathcal{M}_{fi}(s, \theta) = 16\pi \sum_j (2j+1) A_{\lambda_a \lambda_b; \lambda_c \lambda_d}^j(s) \mathcal{D}_{\lambda_a - \lambda_b; \lambda_c - \lambda_d}^{j*}(\theta), \quad (3.10)$$

with the Wigner \mathcal{D} functions as defined in the Appendix C.

Using the equations from section (3.1), it is possible to rewrite equation (3.2) as a matrix relation in helicity space and process space

$$A_{\lambda_a \lambda_b; \lambda_c \lambda_d}^j - A_{\lambda_c \lambda_d; \lambda_a \lambda_b}^{j*} = \sum_{c', d'} 2i \lambda^{\frac{1}{2}}(s, m_{c'}^2, m_{d'}^2) s^{-1} A_{\lambda_c \lambda_d; \lambda_a \lambda_b}^{j*} A_{\lambda_a \lambda_b; \lambda_c \lambda_d}^j. \quad (3.11)$$

Consider an elastic scattering with spinless particles. The partial wave decomposition is

$$M(s, \theta) = 16\pi \sum_{j=0}^{\infty} (2j+1) P^j(\cos \theta) a^j(s), \quad (3.12)$$

where $P^j(\cos \theta)$ are the Legendre polynomials².

The differential cross section (without the kinematical correction) is

$$\frac{d\sigma}{d\Omega} = \frac{1}{64\pi^2 s} |M|^2 \quad (3.13)$$

Now, substituting the equation (3.12) in (3.13) and using the orthogonality properties of the Legendre polynomials, the cross section can be rewritten as

$$\sigma = \frac{16\pi}{s} \sum_j (2j+1) |a^j(s)|^2. \quad (3.14)$$

Using the unitary relation (3.4) for the elastic scattering,

$$\sigma = \frac{\text{Im}M}{s} = \frac{16\pi}{s} \sum_j (2j+1) \text{Im}(a^j(s)) = \frac{16\pi}{s} \sum_j (2j+1) |a^j(s)|^2, \quad (3.15)$$

which is solved by

$$|a^j|^2 = \text{Im}(a^j),$$

²The Wigner \mathcal{D} functions reduce to the Legendre polynomials for spinless particles.

or

$$(\operatorname{Re}(a^j))^2 + \left(\operatorname{Im}(a^j) - \frac{1}{2}\right)^2 = \frac{1}{4}. \quad (3.16)$$

In general, for any scattering with spinless particles, the amplitude is bounded within a unitary circle (the Argand circle), as shown in figure (3.2),

$$|a^j|^2 \leq \operatorname{Im}(a^j), \quad |\operatorname{Re}(a^j)| \leq \frac{1}{2}. \quad (3.17)$$

These results are generalized for particles with spin and accordingly to the scattering amplitudes (and cross section). In other words, as the partial wave amplitudes are bounded, they are not allowed to grow proportional to the energy without becoming nonphysical.

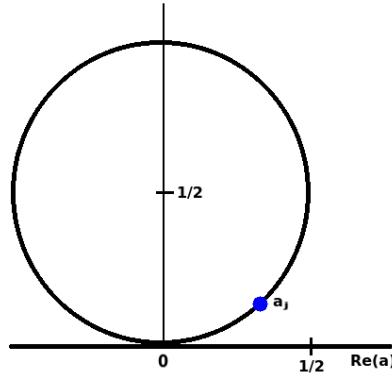


FIGURE 3.2: Unitary circle (Argand Circle) for the partial wave amplitudes: the amplitudes a^j (blue dot) must lay on the circle to satisfy the unitarity condition for elastic scattering.

3.2 AQCs Unitarity Violation

As shown in figure (3.3), the inclusion of higher dimension operators has as a consequence the growing of the cross section proportional to powers of s within energy regions reachable by the current experiments. That is, the amplitudes calculated using an effective Lagrangian could lead to non-physical cross sections if the EFT is used beyond its validity region, where the unitarity condition is not satisfied.

As nature will always guarantee unitarity conservation, it is necessary to remain within the limit set by the S -matrix on the squared amplitude $|M|^2$ to ensure a correct physical behavior. Moreover, unitarity considerations have proven to be powerful in pointing to the correct energy regions where new physics could arise.

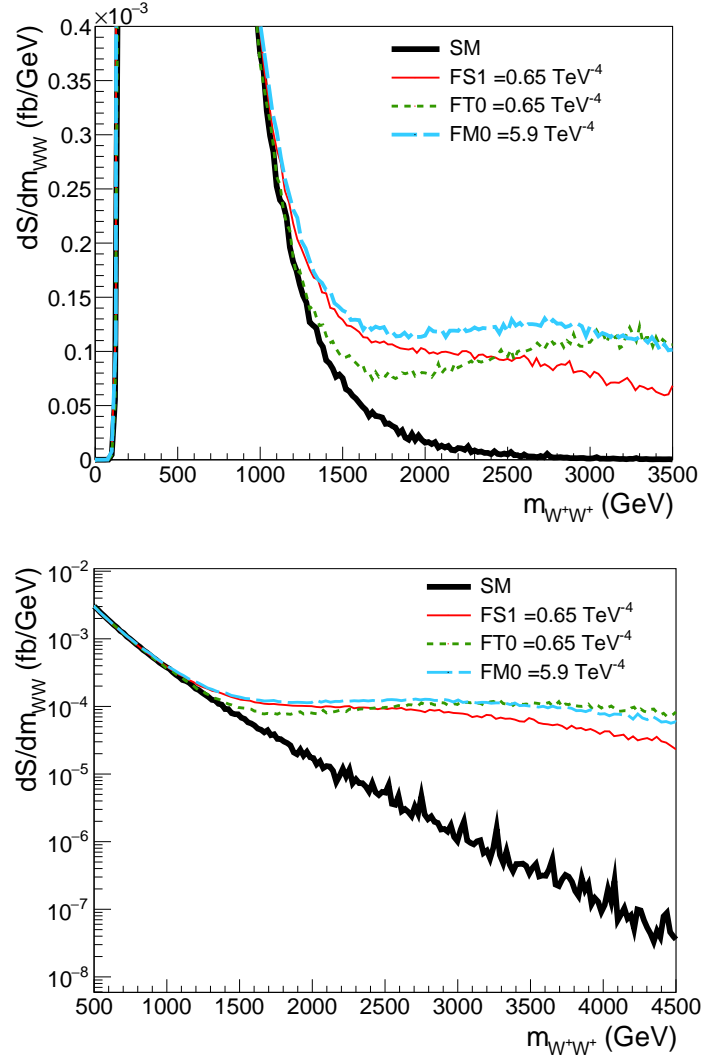
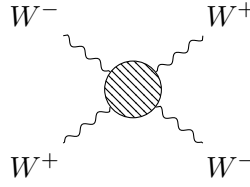


FIGURE 3.3: For $pp \rightarrow e^+ \nu_e \mu^+ \nu_\mu jj$ at 13 TeV, i.e. for off-shell $W^+W^+ \rightarrow W^+W^+$ scattering: invariant mass M_{WW} distribution. The plot shows the SM (leading order and with all possible contributions) in a black thick line and also some dim-8 operators (F_{S_1} , F_{T_0} , F_{M_0}) are included (red thinner line, green dotted line and light blue dashed line respectively). In general, depending on the coupling size, the cross section falls slower with respect to the SM, as the EFT is used beyond its validity region. The bottom plot shows the same results as the upper plot but in a semi-log scale to emphasize the EFT separation from the SM.

Example of unitarity restriction

Consider the scattering $W^+W^- \rightarrow W^+W^-$ within the SM, as shown in the following Feynman diagram,



Each of the diagrams in figure (3.4) has an individual contribution $a_i(s, \theta)$ to the scattering amplitude. Within the SM, the sum of all these contributions results in $a(s, \theta) = \sum_i a_i(s, \theta) \propto s/M_W^2$ [39].

As a consequence when $s \gg M_W$, the cross section σ grows proportional to s and the unitarity condition (3.17) is not satisfied. To restore unitarity, it is necessary to involve new physics that would modify the vertices for $W^+W^- \rightarrow W^+W^-$ scattering and cancel these contributions.

In this case, the inclusion of the Higgs contributions (shown in figure (3.5)) restores unitarity and satisfies the condition (3.17).

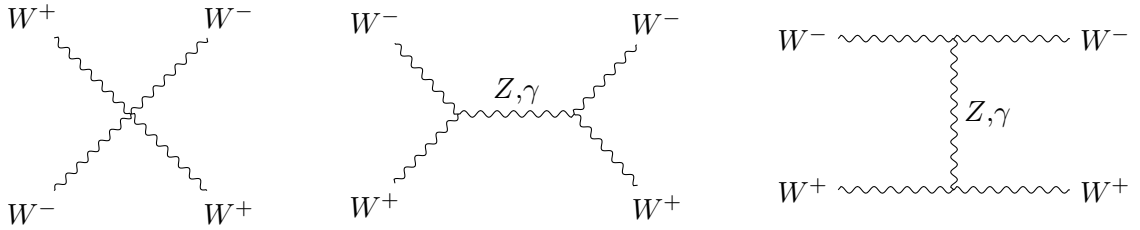


FIGURE 3.4: Contributions from the gauge couplings (TGC and QGC) for the scattering $W^+W^- \rightarrow W^+W^-$.

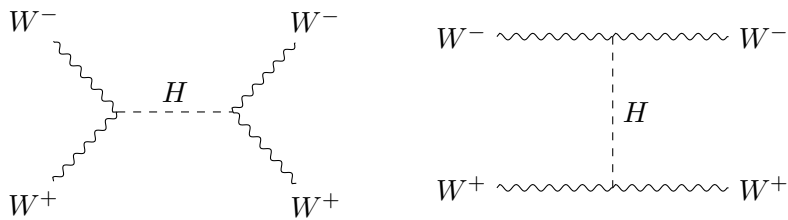


FIGURE 3.5: Contributions from the Higgs exchange for $W^+W^- \rightarrow W^+W^-$.

However, any extra perturbation in these couplings could eventually spoil the unitarity condition, making the bosonic couplings a sensitive observable to study in searches for new physics.

3.3 The K matrix and T-matrix

The T -matrix is one of the several matrices connected with the S -matrix, which can be used to characterize the collisions. For $S = 1 + iT$, it is possible to define

- the reactance matrix, X

$$X = i \frac{1 - S}{1 + S}, \quad (3.18)$$

- the reaction matrix, K

$$K = 2X = 2i \frac{1 - S}{1 + S}. \quad (3.19)$$

In other words, the K -matrix is the Cayley transform of the S -matrix.

Using the equations for the K -matrix (3.19) and for the T -matrix (2.7), it is possible to write the Heitler's equation, which will guarantee that the S -matrix is unitary,

$$T - \frac{1}{2}iKT = K. \quad (3.20)$$

These relations imply that any Hermitian K -matrix will produce a unitary S -matrix. A more detailed explanation of these matrices can be found in [40, 41].

3.4 Linear T-matrix on-shell unitarization

Using the Heitler's equation (3.20), it is possible to rewrite T as a function of the K -matrix [41],

$$T = K \left(\mathbf{1} - \frac{i}{2}K \right)^{-1}, \quad (3.21)$$

which satisfies the unitary condition (3.1) and keeps the S -matrix unitary. In other words, one can always write the matrix T in terms of a Hermitian matrix K .

For example, considering a $2 \rightarrow 2$ scattering with partial wave amplitudes a^j , i.e. the T -matrix is diagonal with elements a^j . Then, equation (3.21) can be understood as a projection onto a unitary circle, as shown in figure (3.6). Then, one could write equation (3.21) in terms of the eigen-amplitudes to determine the amplitude within the Argand circle,

$$a^j = \frac{k^j}{1 - \frac{i}{2}k^j}. \quad (3.22)$$

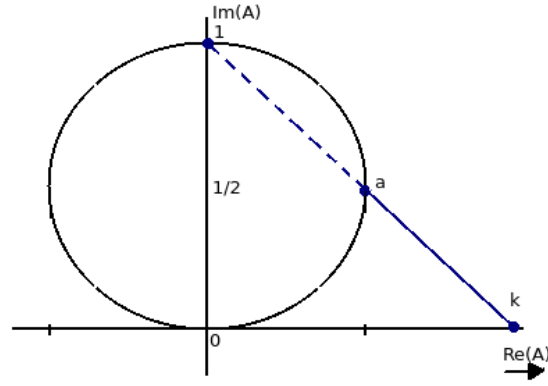


FIGURE 3.6: Stereographic projection onto the Argand Circle

One could use this expression (3.21) as an ansatz and expand it to arbitrary models of scattering matrix T_o , which main requirement is to be normal, $T_o^\dagger T_o = T_o T_o^\dagger$. Then,

$$T = \text{Re}(T_o) \left(\mathbf{1} - \frac{i}{2} T_o^\dagger \right)^{-1}. \quad (3.23)$$

This prescription is known as a T -matrix linear unitarization for normal matrices, defined for $2 \rightarrow 2$ scattering (a deeper study can be found in [42]).

Then, the T -matrix linear unitarization (3.23) is defined as

$$T = \text{Re}(T_o) \left(\mathbf{1} + \frac{i}{2} (T_o - T_o^\dagger) + \frac{1}{4} T_o^\dagger T_o \right)^{-1} \left(\mathbf{1} + \frac{i}{2} T_o \right). \quad (3.24)$$

CHAPTER 4

Restoring Unitarity for Off-shell processes

In Chapter 3, physical quantities for on-shell scattering and how to restore unitarity have been discussed. But within a collider VV processes are produced off-shell. Thus, a more general unitarization prescription is needed.

In this Chapter, some existing unitarization prescriptions are described in section (4.1). However, the aim of this work is to define a new unitarization (more) model independent for vector bosons produced at the LHC (or in general off-shell), without restrictions on the 4-momenta of the bosons.

On the following pages, a review of the ideas developed and implemented is made, explaining all the challenges necessary to overcome along the way, up to the final definition of the unitarization for off-shell VBS based on the on-shell T-matrix unitarization (in section (4.6)).

4.1 Previous Unitarization Efforts

As explained before, the inclusion of higher dimension operators leads to non-physical cross-section regions. Therefore, it is necessary to do a cut-off to truncate and discard any process out of the EFT validity region, or to modify the scattering amplitudes and enforce unitarity.

However, for dim-8 operators a cut-off does not seem to be optimal, as the unitarity bound for AQC is located within energy regions currently reachable by the LHC.

To modify the scattering amplitudes, the Form Factors and the K-matrix unitarization (both implemented in VBFNLO) could be used to push back the amplitudes to the region where $SS^\dagger = 1$ is satisfied, as shown in figure (4.1).

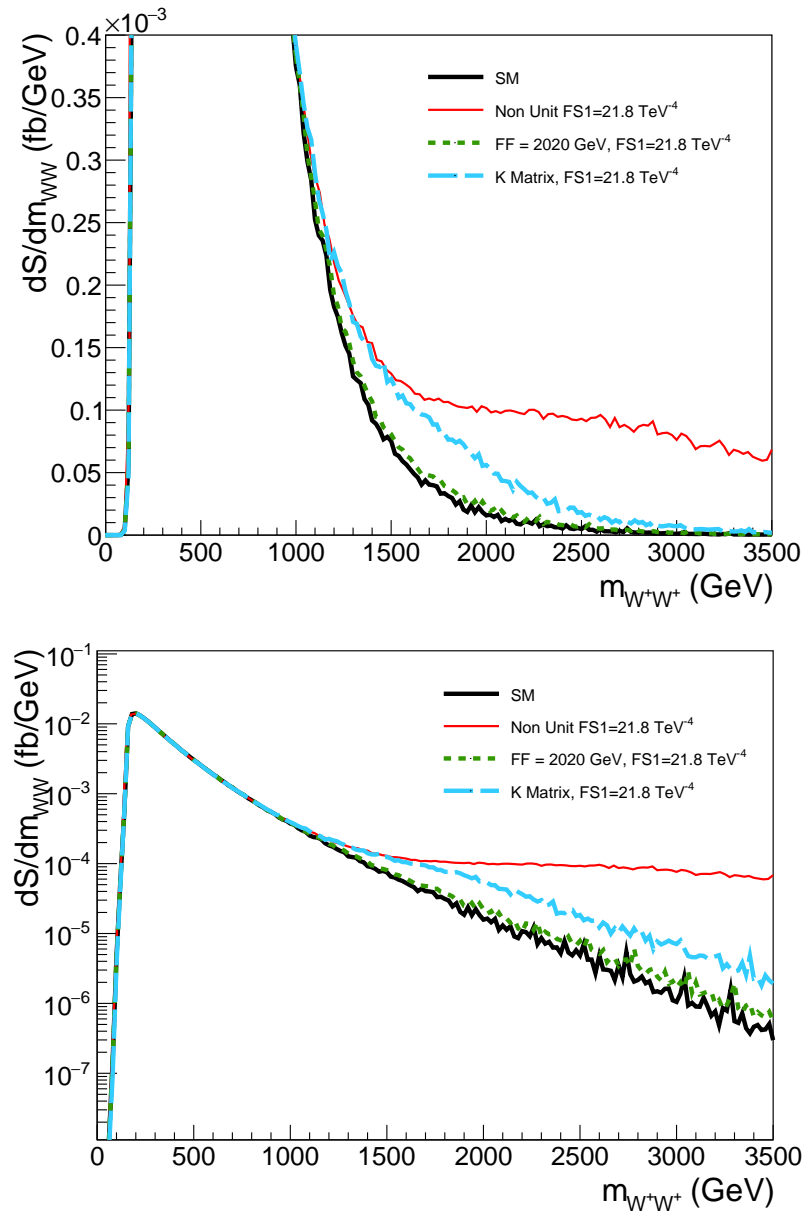


FIGURE 4.1: F_{S1} coupling for $pp \rightarrow W^+W^+jj$ scattering. The invariant mass distribution shows how the unitarization prescription pushes back the amplitudes outside the validity region of the EFT. The upper plot is non-log, while the bottom plot is a semi-log plot for the same results. Here, the SM distribution (black thicker line), the anomalous coupling without unitarization (red solid line), the form factor unitarization (calculated with the form factor tool) with $\Lambda = 2020$ GeV for $F_{S1} = 21.8$ TeV (green short dashed line) and the K-matrix unitarization (aquamarine long dashed line) are shown.

4.1.1 Form Factor unitarization

To suppress the raising behavior of the amplitudes and unitarity violation, one could use a form factor FF and multiply it to the couplings. In VBFNLO a dipole form factor is used,

$$FF = \frac{1}{\left(1 + \frac{s}{\Lambda_{FF}^2}\right)^p}, \quad (4.1)$$

where s is the squared invariant mass of the produced bosons, Λ_{FF} is the mass scale for new physics and p is the damping power (e.g. at least $p=2$ for dim-8) as explained in [8, 43].

To determine the form factor it is possible to use the calculation tool from VBFNLO (`calc_formfactor`), which computes the 0th partial wave of the amplitude for the on-shell VV scattering ($a^{j=0}$) and sets as unitarity criterion the real part of the partial wave to be less than $\frac{1}{2}$,

$$|\text{Re}(a^0)| \leq \frac{1}{2}. \quad (4.2)$$

The choice of Λ becomes a fine-tuning problem that will depend on the strength of the couplings.

4.1.2 K -matrix unitarization

Consider a diagonalizable K -matrix with eigenamplitude a_K . The corresponding unitarized eigenvalue a_u can be written using equation (3.21),

$$a_u = \frac{a_K}{1 - ia_K}, \quad (4.3)$$

which can be understood as the projection of the eigenvalue a_k onto the Argand Circle defined in Chapter 3, and which is calculated from the on-shell elastic VV scattering amplitude.

One could assume that, in a similar way to the SM, the longitudinally polarized vector boson contributions are dominant¹. Then, in the region where $p^0 \gg m_V$, the longitudinal polarization vector $\varepsilon_L^\mu(p)$ becomes parallel to the momentum p^μ ,

$$\varepsilon^\mu(p, \lambda) = \frac{p^\mu}{m_V} + \mathcal{O}\left(\frac{m}{p^0}\right). \quad (4.4)$$

¹The polarization vectors are defined in section (4.3).

Using the Mandelstam variables, one could rewrite

$$\varepsilon_1 \cdot \varepsilon_2 \varepsilon_3^* \cdot \varepsilon_4^* \simeq \frac{1}{\prod_i m_i} \frac{s^2}{4}, \quad (4.5)$$

$$\varepsilon_1 \cdot \varepsilon_3^* \varepsilon_2 \cdot \varepsilon_4^* \simeq \frac{1}{\prod_i m_i} \frac{t^2}{4}, \quad (4.6)$$

$$\varepsilon_1 \cdot \varepsilon_4^* \varepsilon_2 \cdot \varepsilon_3^* \simeq \frac{1}{\prod_i m_i} \frac{u^2}{4}. \quad (4.7)$$

and rewrite the amplitudes for the EFT using these definitions. For example, using the Feynman rules defined in Appendix A and the on-shell partial wave decomposition described in Chapter 3, it is possible to write a_k for the anomalous coupling F_{S_0} for the on-shell $W^+W^+ \rightarrow W^+W^+$ scattering,

$$a_k = F_{S_0} s^2. \quad (4.8)$$

Then, the unitarized amplitude can be written as (apart from constant factors),

$$a_u \propto \frac{F_{S_0} s^2}{1 - iF_{S_0} s^2}. \quad (4.9)$$

This assumption in the polarization vectors is useful to unitarize the amplitudes from F_{S_i} operators. However, as the F_{T_i} or F_{M_i} operators have more complicated structure, the unitarization cannot be achieved easily with this approach, as explained in [41, 44]. Thus, it is necessary to find a simpler unitarization prescription.

4.2 Off-shell Anomalous Quartic Couplings in VBFNLO

The off-shell VV scattering amplitude ($2 \rightarrow 6$, i.e. an 8 fermion amplitude) can be written as the result of the SM plus the anomalous part; namely,

$$\mathcal{M}_{8f} = \mathcal{M}_{8f}^{\text{SM}} + \underbrace{\left(J_{p \rightarrow jV}^\mu J_{p \rightarrow jV}^\nu \mathcal{M}_{\mu\nu}^{\text{AQC}}(VV \rightarrow 4f) \right)}_{\mathcal{M}_{8f}^{\text{AQC}}}, \quad (4.10)$$

where the SM part is unitary and includes all possible contributions (including the Higgs) without new physics; and $\mathcal{M}_{8f}^{\text{AQC}}$ has the contributions from the EFT higher dimension operators (as described in Chapter 1).

For example, consider the anomalous contribution for $pp \rightarrow VVjj \rightarrow 4l + 2j$, as shown in figure (2.2) in Chapter 2: for this quartic coupling the anomalous interaction can be

described as the product of *the quark currents*, **the VV scattering** ($VV \rightarrow VV$) and *the leptonic decay currents*, as shown in figure (4.2)². The amplitude is,

$$\mathcal{M}_{pp \rightarrow 4l+2j}^{\text{AQC}} = \underbrace{J_{p_1 \rightarrow jV_1}^{\mu_1} J_{p_2 \rightarrow jV_2}^{\mu_2}}_{\text{External quarks currents}} \underbrace{\mathbf{m}_{\mu_1\mu_2\mu_3\mu_4}}_{\text{VBS amplitude}} \underbrace{J_{V_3 \rightarrow \bar{l}\bar{l}}^{\mu_3} J_{V_4 \rightarrow \bar{l}\bar{l}}^{\mu_4}}_{\text{Leptons decay currents}}. \quad (4.11)$$

Because the currents J^μ are conserved, it satisfies

$$q_\mu \cdot J^\mu = 0, \quad (4.12)$$

so, one could include the following boson propagator in the VBS amplitude,

$$D_V^{\mu\nu}(q) = \frac{-i}{q^2 - m_V^2 + im_V\Gamma} \left(g^{\mu\nu} - \frac{q^\mu q^\nu}{q^2} \right), \quad (4.13)$$

as the $q^\mu q^\nu/q^2$ term disappears and could be replaced by $q^\mu q^\nu/m^2$.

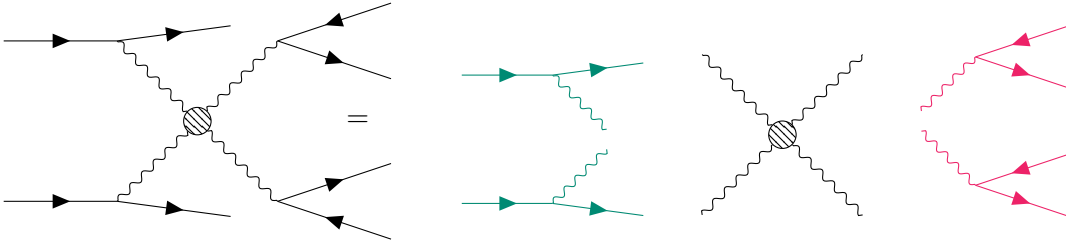


FIGURE 4.2: Feynman Diagram for off-shell VV scattering as implemented in VBFNLO for the anomalous quartic couplings.

In VBFNLO the scattering takes place in the Lab-Frame. As the interaction amplitude is Lorentz invariant for massless external particles, the results are independent of the frame. Thus, to ease the calculations and understanding of analytical expressions throughout this work, some of the quantities (e.g. the polarization vectors) are calculated in the CM-frame of the VV scattering.

4.3 On-Shell and Off-Shell polarization vectors

Before defining the polarization vectors, it is important to understand the notation used, as there is a distinction among the polarization vectors depending on whether the momenta were defined for an on-shell or off-shell process.

²This color scheme is used to distinguish between the different pieces of the amplitude as written in VBFNLO for AQC's.

For on-shell, the momenta notation is k^μ , which satisfies that $k^\mu k_\mu = k_0^2 - |\vec{k}|^2 = m_V^2$. For instance, the momenta for the vector bosons in the CM-frame and with the incoming bosons aligned with the z-axis are defined as,

- on-shell vector bosons: k_1, k_2, k_3, k_4 ,

$$\begin{array}{ll} \text{incoming bosons} & \text{outgoing bosons} \\ \bar{k}_1 = (0, 0, |k_1|) = k_1 \hat{e}_z & \bar{k}_3 = |k_3| (\sin \theta, 0, \cos \theta) \\ \bar{k}_2 = -\bar{k}_1 & \bar{k}_4 = -\bar{k}_3 \\ k_{\text{in}}^\mu = (E_{\text{in}}, \bar{k}_{\text{in}}) & k_{\text{out}}^\mu = (E_{\text{out}}, \bar{k}_{\text{out}}) \\ \text{where, } k^\mu k_\mu = m_V^2 & \text{(on-shell condition).} \end{array}$$

For off-shell, the notation is q^μ , which only satisfies that $q^\mu q_\mu = (q_0^2 - |\vec{q}|^2)$. It should be noted that for LHC processes the incoming bosons are space-like vectors with $q^\mu q_\mu < 0$, while the outgoing bosons are time-like with $q^\mu q_\mu > 0$. In a similar way the momenta for the vector bosons in the scattering are,

- off-shell vector bosons: q_1, q_2, q_3, q_4 ,

$$\begin{array}{ll} \text{incoming bosons} & \text{outgoing bosons} \\ \bar{q}_1 = (0, 0, |q_1|) = q_{\text{in}} \hat{e}_z & \bar{q}_3 = |\vec{q}_3| (\sin \theta, 0, \cos \theta) \\ \bar{q}_1 = -\bar{q}_2 & \bar{q}_3 = -\bar{q}_4 \\ q_{\text{in}}^\mu = (q_{\text{in}}^0, \bar{q}_{\text{in}}) & q_{\text{out}}^\mu = (q_{\text{out}}^0, \bar{q}_{\text{out}}) \end{array}$$

Finally, if no distinction is needed between on-shell/off-shell, the 4-momentum is simply called p^μ .

For each vector boson $V_{1\dots 4}$ a polarization vector is defined ($\varepsilon(q_{1\dots 4}, \lambda)$), which depends on the boson momentum. Broadly speaking, for $p^\mu = (p_0, p_x, p_y, p_z)$ the polarization vectors $\varepsilon(p, \lambda)$ are³

$$\varepsilon^\mu(p, 1) = \frac{1}{|\vec{p}|p_T} \begin{pmatrix} 0 \\ p_x p_z \\ p_y p_z \\ -p_T^2 \end{pmatrix}; \quad \varepsilon^\mu(p, 2) = \frac{1}{p_T} \begin{pmatrix} 0 \\ -p_y \\ p_x \\ 0 \end{pmatrix}; \quad (4.14)$$

$$\varepsilon^\mu(p, 3) = \frac{p_0}{\sqrt{|p_0^2 - |\vec{p}|^2} |\vec{p}|} \begin{pmatrix} \frac{|\vec{p}|^2}{p_0} \\ p_x \\ p_y \\ p_z \end{pmatrix}, \quad (4.15)$$

³For massive vector bosons.

with,

$$p_T = \sqrt{p_x^2 + p_y^2}, \quad \text{and } |\bar{p}| = \sqrt{p_x^2 + p_y^2 + p_z^2},$$

and λ the boson helicity. The longitudinal or transverse polarization vectors, with $\lambda = 0, \pm$, are defined as

$$\varepsilon^\mu(p, \pm) = \pm \frac{1}{\sqrt{2}} (-\varepsilon^\mu(p, 1) \mp i\varepsilon^\mu(p, 2)) \quad (4.16)$$

$$\varepsilon^\mu(p, 0) = \varepsilon^\mu(p, 3). \quad (4.17)$$

The polarization vectors also satisfy the following properties,

$$p^\mu \varepsilon_\mu(p, \lambda) = 0, \quad (4.18)$$

$$\varepsilon_\mu(p, \lambda) (\varepsilon^\mu(p, \lambda'))^* = -\mathcal{S}_\lambda(p^2) \delta_{\lambda\lambda'}, \quad (4.19)$$

here $\mathcal{S}_\lambda(p^2)$ gives a sign factor $+1$, except for longitudinal polarizations of space-like momenta, then $\mathcal{S}_0(p^2 < 0) = -1$.

Now, consider as an example the incoming bosons with a momentum p_i as described previously (p_i equal to q_1, q_2 or k_1, k_2). It is easy to show that the transverse polarization vectors do not depend explicitly on p_i^2 . Therefore, they are independent of the process being off-shell or on-shell.

The transverse polarization vectors ($\lambda = \pm$) are,

$$\varepsilon^\mu(p_i, \lambda = \pm) = \pm \frac{1}{\sqrt{2}} \begin{pmatrix} 0 \\ -1 \\ \mp i \operatorname{sign} \left[\frac{\bar{p}_i}{|\bar{p}_i|} \right] \\ 0 \end{pmatrix}. \quad (4.20)$$

The difference appears for the longitudinal polarization vector ($\varepsilon(q/k, 0)$), as a normalization factor (N_k for on-shell and N_q for off-shell) needs to be introduced,

$$\text{On-shell: } \varepsilon(k, 0) = \begin{pmatrix} \frac{|\bar{k}|}{m_V} \\ \frac{E}{m_V} \hat{k} \end{pmatrix} = N_k \begin{pmatrix} |\bar{k}| \\ E \hat{k} \end{pmatrix}, \quad (4.21)$$

$$\text{Off-shell: } \varepsilon(q, 0) = \begin{pmatrix} \frac{|\bar{q}|}{\sqrt{|q^2|}} \\ \frac{q^0}{\sqrt{|q^2|}} \hat{q} \end{pmatrix} = N_q \begin{pmatrix} |\bar{q}| \\ q^0 \hat{q} \end{pmatrix}. \quad (4.22)$$

The normalization factors are

$$N_k = \frac{1}{m_V} , \quad \text{for on-shell;} \quad (4.23)$$

$$N_q = \frac{1}{\sqrt{|q_{\text{in}}^2|}} , \quad \text{for off-shell.} \quad (4.24)$$

Generalizing these results for the outgoing vector bosons, too, it is possible to rewrite the polarization sums in terms of the normalization factors (with $n = 1, \dots, 4$),

$$\begin{aligned} \sum_{\lambda_n = \pm, 0} (\varepsilon^\mu(k_n, \lambda_n))^* \varepsilon^\nu(k_n, \lambda_n) &= -g^{\mu\nu} + \frac{k_n^\mu k_n^\nu}{m_n^2} \\ &= -g^{\mu\nu} + N_{k_n}^2 k_n^\mu k_n^\nu, \end{aligned} \quad (4.25)$$

for on-shell bosons. However, for off-shell bosons one need to redefine the polarization sum in the following way

$$\begin{aligned} \widetilde{\sum}_{\lambda_n = \pm, 0} (\varepsilon^\mu(q_n, \lambda_n))^* \varepsilon^\nu(q_n, \lambda_n) &\equiv \sum_{\lambda_n = \pm, 0} \mathcal{S}_{\lambda_n}(q_n^2) (\varepsilon^\mu(q_n, \lambda_n))^* \varepsilon^\nu(q_n, \lambda_n) \\ &= -g^{\mu\nu} + N_{q_n}^2 q_n^\mu q_n^\nu . \end{aligned} \quad (4.26)$$

In other words, for the incoming bosons ($i=1,2$), equation (4.26) can be rewritten as

$$\widetilde{\sum}_{\lambda_i = \pm, 0} (\varepsilon^\mu(q_i, \lambda_i))^* \varepsilon^\nu(q_i, \lambda_i) = \sum_{\lambda_i = \pm, 0} (\varepsilon^\mu(q_i, \lambda_i))^* \varepsilon^\nu(q_i, \lambda_i) - (\varepsilon^\mu(q_i, 0))^* \varepsilon^\nu(q_i, 0) \quad (4.27)$$

4.4 On-Shell/Off-Shell Matching

Using the polarization sum (4.26) for an off-shell process, the propagators (4.13) can be redefined as

$$D^{\mu\alpha}(q) = \underbrace{\frac{i}{q^2 - m_V^2 + im_V\Gamma}}_{c(q^2)} \widetilde{\sum}_{\lambda} \varepsilon^{*\mu}(q, \lambda) \varepsilon^\alpha(q, \lambda) = c(q^2) \widetilde{\sum}_{\lambda} \varepsilon^{*\mu}(q, \lambda) \varepsilon^\alpha(q, \lambda) . \quad (4.28)$$

Then, one could rewrite the anomalous amplitude $\mathcal{M}_{\mu\nu}^{\text{AQC}}$ from equation (4.10) as a function of the polarization vectors $\varepsilon(q_{1\dots 4}, \lambda_{1\dots 4})$,

$$\begin{aligned} \mathcal{M}_{\mu\nu}^{\text{AQC}}(VV \rightarrow 4f) &= \mathcal{F} \widetilde{\sum}_{\lambda_1 \lambda_2} \varepsilon_\mu^*(q_1, \lambda_1) \varepsilon_\nu^*(q_2, \lambda_2) \\ &\quad \times \widetilde{\sum}_{\lambda_3 \lambda_4} M(\varepsilon(q_1, \lambda_1) \varepsilon(q_2, \lambda_2); \varepsilon^*(q_3, \lambda_3) \varepsilon^*(q_4, \lambda_4)) Z_3(\lambda_3) Z_4(\lambda_4) , \end{aligned} \quad (4.29)$$

where $M(\varepsilon(q_{1\dots 4}, \lambda_{1\dots 4}))$ is the vector boson quartic vertex, which will be called (for readability purposes) $M_{\lambda_1\lambda_2\lambda_3\lambda_4}$,

$$M_{\lambda_1\lambda_2\lambda_3\lambda_4} = M(\varepsilon(q_1, \lambda_1)\varepsilon(q_2, \lambda_2); \varepsilon^*(q_3, \lambda_3)\varepsilon^*(q_4, \lambda_4)) , \quad (4.30)$$

and it is defined as

$$M_{\lambda_1\lambda_2\lambda_3\lambda_4} = \varepsilon^{\mu_1}(q_1, \lambda_1)\varepsilon^{\mu_2}(q_2, \lambda_2)\mathbf{m}_{\mu_1\mu_2\mu_3\mu_4}\varepsilon^{*\mu_3}(q_3, \lambda_3)\varepsilon^{*\mu_4}(q_4, \lambda_4) . \quad (4.31)$$

The other elements from equation (4.29) are

$$Z_3(\lambda_3) = \varepsilon_\rho(\lambda_3, q_3)J_{V_3 \rightarrow l\bar{l}}^\rho , \quad Z_4(\lambda_4) = \varepsilon_\gamma(\lambda_4, q_4)J_{V_4 \rightarrow l\bar{l}}^\gamma , \quad (4.32)$$

$$\mathcal{F} = \prod_{l=1}^4 c(q_l^2) . \quad (4.33)$$

Now, to recover the S-matrix unitarity property using an on-shell unitarization prescription (like the T-matrix described in Chapter 3), one could try to find an “on-shell/off-shell matching”, such that $M_{\lambda_1\lambda_2\lambda_3\lambda_4}$ can be replaced by the matrix element of the equivalent on-shell process. In other words,

$$M(\varepsilon(q_1, \lambda_1)\varepsilon(q_2, \lambda_2); \varepsilon^*(q_3, \lambda_3)\varepsilon^*(q_4, \lambda_4)) \Rightarrow M_{\text{on}}(\varepsilon(k_1, \lambda_1)\varepsilon(k_2, \lambda_2); \varepsilon^*(k_3, \lambda_3)\varepsilon^*(k_4, \lambda_4)) .$$

Once again, for readability purposes, the following notation will be used

$$(M_{\text{on}})_{\lambda_1\lambda_2\lambda_3\lambda_4} = M_{\text{on}}(\varepsilon(k_1, \lambda_1)\varepsilon(k_2, \lambda_2); \varepsilon^*(k_3, \lambda_3)\varepsilon^*(k_4, \lambda_4)) . \quad (4.34)$$

Note the following example: consider the on-shell scattering $W^+W^+ \rightarrow W^+W^+$. As explained in Appendix A, the matrix element for F_{S_0} is,

$$(M_{\text{on}})_{\lambda_1\lambda_2\lambda_3\lambda_4}(F_{S_0}) = 4F_{S_0}M_W^4 \varepsilon(k_1, \lambda_1) \cdot \varepsilon(k_2, \lambda_2) \varepsilon^*(k_3, \lambda_3) \cdot \varepsilon^*(k_4, \lambda_4) . \quad (4.35)$$

Then, one could replace (4.35) in (4.29),

$$\begin{aligned} \mathcal{M}_{\mu\nu}^{\text{AQC}}(VV \rightarrow 4f) &= \mathcal{F} \widetilde{\sum}_{\lambda_1\lambda_2} \varepsilon_\mu^*(q_1, \lambda_1)\varepsilon_\nu^*(q_2, \lambda_2) \\ &\times \widetilde{\sum}_{\lambda_3\lambda_4} (4F_{S_0}M_W^4 (\varepsilon(k_1, \lambda_1) \cdot \varepsilon(k_2, \lambda_2) \varepsilon^*(k_3, \lambda_3) \cdot \varepsilon^*(k_4, \lambda_4))) \\ &\times Z_3(\lambda_3)Z_4(\lambda_4) . \end{aligned} \quad (4.36)$$

As for on-shell processes $\mathcal{S}(k^2) = 1$, for the matching one consider $\widetilde{\sum} = \sum$. Then, the “On-shell/Off-shell” matching can be understood as the combination of on-shell and

off-shell polarization vectors, such as

$$\mathcal{M}_{\mu\nu} = \mathcal{F} \sum_{\lambda_1 \lambda_2} \overbrace{\varepsilon_\mu^*(q_1, \lambda_1) \varepsilon_\nu(q_2, \lambda_2)}^{\text{off-shell}} \sum_{\lambda_3 \lambda_4} \underbrace{\lambda_3 \lambda_4 (M_{\text{on}})_{\lambda_1 \lambda_2 \lambda_3 \lambda_4}}_{\text{on-shell}} \overbrace{Z_3(\lambda_3) Z_4(\lambda_4)}^{\text{off-shell}}, \quad (4.37)$$

where $(M_{\text{on}})_{\lambda_1 \lambda_2 \lambda_3 \lambda_4}$ could be unitarized using the on-shell prescriptions existing in the literature.

The following pages (until section (4.4)) are dedicated to describe the investigation done to find an accurate “on-shell/off-shell” matching without much success and the reasons (and challenges) behind these results, as a motivation for the subsequent unitarization prescription.

4.4.1 Polarization Vector Matching

The matching given in equation (4.37) requires a redefinition of the polarization sum, in order to obtain the correct propagators (as defined in equation (4.28)) using a combination of on-shell and off-shell polarization vectors,

$$\begin{aligned} \sum_{\lambda=\pm,0} (\varepsilon^\mu(q, \lambda))^* \varepsilon^\nu(k, \lambda) &= -g^{\mu\nu} + N_q^2 q^\mu k^\nu \\ &= -g^{\mu\nu} + \tilde{N} q^\mu N_k k^\nu, \end{aligned} \quad (4.38)$$

where \tilde{N} is the normalization factor for the off-shell polarization vectors in the on-/off-shell matching, such that it guarantees

$$\tilde{N} N_k = N_q^2. \quad (4.39)$$

Therefore,

$$\tilde{N} = \frac{m}{q^2}. \quad (4.40)$$

Then, the longitudinal polarization vectors for the matching need to be defined as,

$$\begin{aligned} \varepsilon^\mu(q, \lambda = 0) &= \tilde{N} (|\vec{q}|, q_0 \hat{q}) \\ &= \frac{m}{q^2} (|\vec{q}|, q_0 \hat{q}), \quad \text{for off-shell,} \end{aligned} \quad (4.41)$$

and

$$\begin{aligned} \varepsilon^\mu(k, \lambda = 0) &= N_k (|\vec{k}|, k_0 \hat{k}) \\ &= \frac{1}{m} (|\vec{k}|, k_0 \hat{k}), \quad \text{for on-shell.} \end{aligned} \quad (4.42)$$

4.4.2 Calculating the New Amplitude

To calculate the new amplitude using equation (4.37), with the vector boson propagator as defined in equation (4.38), one needs to find the momenta k_i for the on-shell scattering amplitude.

In the on-shell scattering CM-Frame, the following expressions are true:

$$E_1 = \frac{s + m_{V_1}^2 - m_{V_2}^2}{2\sqrt{s}}, \quad (4.43)$$

$$E_2 = \frac{s + m_{V_2}^2 - m_{V_1}^2}{2\sqrt{s}}, \quad (4.44)$$

$$E_3 = \frac{s + m_{V_3}^2 - m_{V_4}^2}{2\sqrt{s}}, \quad (4.45)$$

$$E_4 = \frac{s + m_{V_4}^2 - m_{V_3}^2}{2\sqrt{s}}. \quad (4.46)$$

Then, for example, for $W^+W^+ \rightarrow W^+W^+$ on-shell scattering,

$$E_1 = E_2 = E_3 = E_4 = \frac{\sqrt{s}}{2}. \quad (4.47)$$

To satisfy the on-shell condition given in section (4.3), the space component should satisfy

$$\bar{k}_i^2 = E_i^2 - m_{V_i}^2. \quad (4.48)$$

The momentum k_i^μ is obtained from the off-shell momentum q_i^μ calculated with VBFNLO, as it will be explained below in section (4.4.2.1).

To correctly define the on-shell space component, it is essential to conserve the same vector direction from the off-shell bosons. Therefore, one can define the scattering angle (θ) for the outgoing on-shell bosons in the following way,

$$\cos \theta = \frac{q_{3z}}{|\bar{q}_3|}. \quad (4.49)$$

Then, using

$$\beta = \sqrt{1 - \frac{4m_W^2}{s}}, \quad (4.50)$$

one finds that, for the on-shell $W^+W^+ \rightarrow W^+W^+$ example, the momenta is:

- for the incoming bosons $\bar{k}_1 = -\bar{k}_2$, and

$$k_1^\mu = \frac{\sqrt{s}}{2} (1, 0, 0, \beta); \quad (4.51)$$

- for the outgoing bosons $\bar{k}_3 = -\bar{k}_4$, and

$$k_3^\mu = \frac{\sqrt{s}}{2} (1, \beta \sin \theta, 0, \beta \cos \theta) . \quad (4.52)$$

4.4.2.1 From q_i^μ to k_i^μ

Throughout this work, different relationships between q_i^μ and k_i^μ were studied for the “on-shell/off-shell” matching equation (4.37). The resulting observable distributions were compared with the pure off-shell results (usual VBFNLO results for $pp \rightarrow VVjj$ scattering) for different anomalous couplings, as explained below. To avoid the SM dominant contributions to the distributions, and to compare purely the results from anomalous couplings, large couplings were taken (between 100 TeV^{-4} and 1000 TeV^{-4}).

The results here shown are for $W^+W^+ \rightarrow W^+W^+$ scattering.

1. Same center of mass energy:

One could set the on-shell and off-shell scattering to have the same center of mass energy. In other words, they should satisfy

$$s = (q_1 + q_2)^2 = (k_1 + k_2)^2 . \quad (4.53)$$

Using equations (4.51) and (4.52), the momenta and polarization vectors were calculated for the matching.

- **Matching for F_{S_i} couplings:**

Near the energy threshold $\sqrt{s} = \Lambda_u$ where F_{S_i} breaks unitarity ($\Lambda_u < 1 \text{ TeV}$), the “on-shell/off-shell” matching agrees within 20% difference with the pure off-shell results, as shown in Figure (4.3). Above this region, it agrees within 10% or better.

Whereas the contribution is mainly coming from the longitudinal polarization, one might accept this result as a first confirmation of the matching working in a reasonable way. Nevertheless, before using any unitarization scheme, it is important to confirm a proper behavior for the rest of the AQC's.

- **Matching for F_{T_i} and F_{M_i} couplings:**

For F_{T_i} and F_{M_i} , the disagreement between the observable distributions from off-shell results and the matching can be observed up to very large energies ($E_{\text{CM}} \geq 3 \text{ TeV}$), as it is shown in figure (4.4) for F_{T_0} . A thorough understanding of these unforeseen results is necessary.

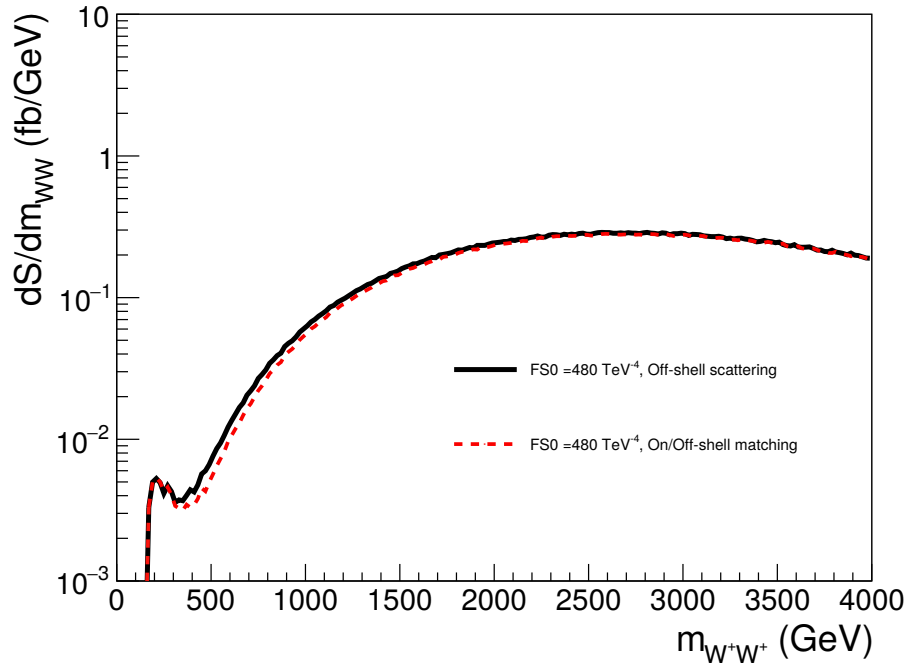


FIGURE 4.3: Semi-log invariant mass distribution for $F_{S_0} = 480 \text{ TeV}^{-4}$. Comparison between the off-shell scattering (pure off-shell polarization vectors and momenta, black thick line) and the “on-shell/off-shell” matching (red dashed line) that satisfies equation (4.53).

In this example, the matrix element is calculated using the Feynman rules from Appendix A. Then, $(M_{\text{on}})_{\lambda_1 \lambda_2 \lambda_3 \lambda_4}$ is

$$\begin{aligned}
 M(F_{T_0}) \propto & [(p_3 \cdot \varepsilon_2)(p_2 \cdot \varepsilon_3^*) - (\varepsilon_3^* \cdot \varepsilon_2)(p_3 \cdot p_2)] \\
 & \times [(p_4 \cdot \varepsilon_1)(p_1 \cdot \varepsilon_4^*) - (\varepsilon_4^* \cdot \varepsilon_1)(p_4 \cdot p_1)] \\
 & + [(p_3 \cdot \varepsilon_1)(p_1 \cdot \varepsilon_3^*) - (\varepsilon_3^* \cdot \varepsilon_1)(p_3 \cdot p_1)] \\
 & \times [(p_4 \cdot \varepsilon_2)(p_2 \cdot \varepsilon_4^*) - (\varepsilon_4^* \cdot \varepsilon_2)(p_4 \cdot p_2)]. \quad (4.54)
 \end{aligned}$$

In the F_{T_0} invariant mass distribution shown in figure (4.4), it is possible to observe that far from the energy threshold where unitarity is broken $k_i \approx q_i$. And therefore, $\varepsilon_{1,2}(k, \pm) = \varepsilon_{1,2}(q, \pm)$ and $\varepsilon_{3,4}(k, \pm) = \varepsilon_{3,4}(q, \pm)$. Then, the dominant contributions for $(M_{\text{on}})_{\lambda_1 \lambda_2 \lambda_3 \lambda_4}$ come from transverse polarization vectors,

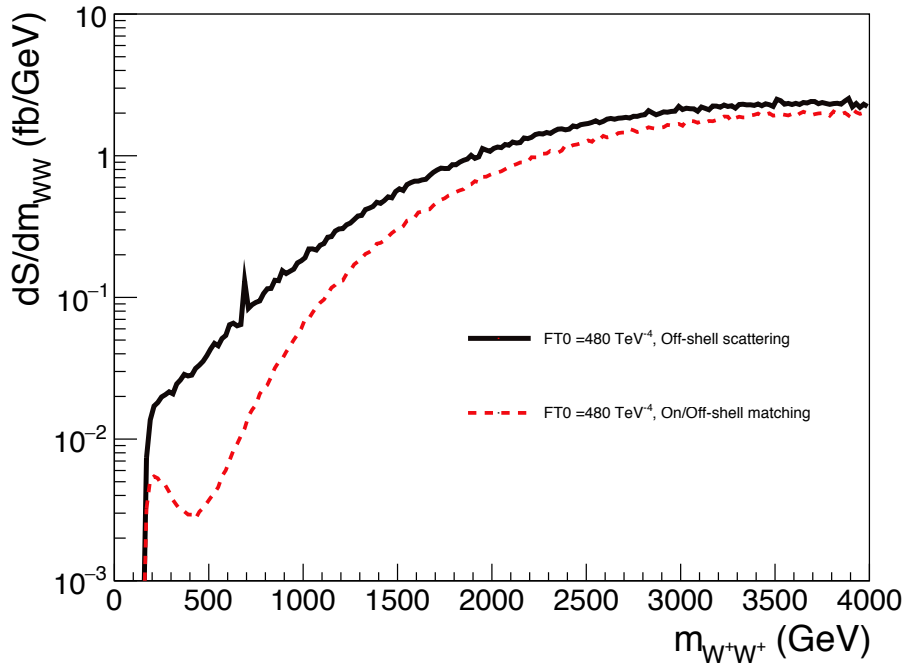


FIGURE 4.4: Semi-log invariant mass distribution for $F_{T_0} = 480 \text{ TeV}^{-4}$. Comparison between the off-shell scattering (pure off-shell polarization vectors and momenta, black thick line) and the “on-shell/off-shell” matching (red dashed line) that satisfies equation (4.53).

$$\begin{array}{ll}
 --++ & - (1 + \cos \theta^2) F_{T_0} s^2 \\
 -+-+ & - \frac{1}{2} (1 + \cos \theta)^2 F_{T_0} s^2 \\
 -++- & - \frac{1}{2} (-1 + \cos \theta)^2 F_{T_0} s^2 \\
 +- -+ & - \frac{1}{2} (-1 + \cos \theta)^2 F_{T_0} s^2 \\
 +-+- & - \frac{1}{2} (1 + \cos \theta)^2 F_{T_0} s^2 \\
 ++-- & - (1 + \cos \theta^2) F_{T_0} s^2
 \end{array}$$

while the rest of the helicities combination contributions is negligible. This complies with the agreement between the pure off-shell results and the on-shell/off-shell matching for very large energies.

Near the threshold, however, all the helicity combinations have non-trivial contributions to the matrix element. Thus, contributions from $\varepsilon(\lambda = 0)$ are also expected. In other words, the first suspicion for the observed behavior comes from the non-leading terms.

To test this idea and understand better the contributions from different helicities combinations to the amplitude, $(M_{\text{on}})_{\lambda_1 \lambda_2 \lambda_3 \lambda_4}$ was calculated considering different contributions for the matching.

Figure (4.5) exhibits that for the invariant mass distribution the contributions from non-leading terms are negligible with respect to the leading ones. Even more, it shows that the total cross section is primarily the result from the leading contributions, also in the region where non-leading contributions are expected. These results lead to consider a similar decomposition for the pure off-shell amplitude calculation as a comparison.

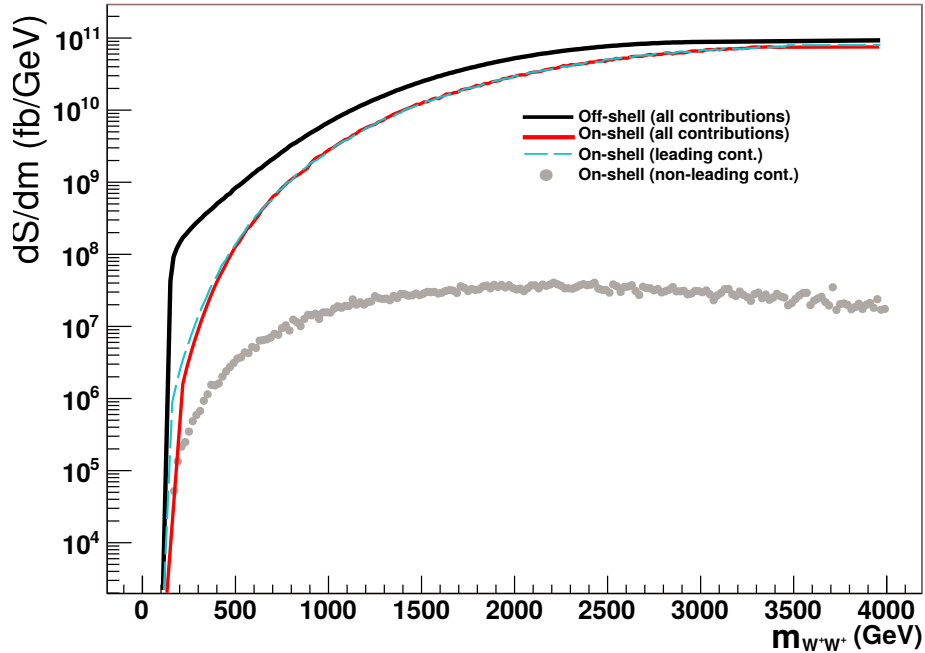


FIGURE 4.5: Semi-log invariant mass distribution for $F_{T_0} = 1000 \text{ TeV}^{-4}$, with a cut for the SM contributions ($E_{cm} > 100 \text{ GeV}$). The black thick line shows the off-shell distribution, while the red thinner line the matching distribution. The dashed aquamarine line (on top of the red one) shows the leading terms distribution. The gray dots distribution shows all the non-leading terms contributions.

Figure (4.6) shows the off-shell results for all the helicities contributions and only the leading terms, and the equivalent matching results. Here it is clear that the on-shell/off-shell matching does not reproduce correctly the contribution from the non-leading terms in the region where they are expected. Thus, one might wonder the origin of these difference between the non-leading contributions for the off-shell and the matching results.

A deeper numerical analysis of these results indicated that near the threshold there are large virtualities contributing to small E_{CM} . In the pure off-shell matrix elements, these cancellations are counterbalanced by the off-shell momenta components. However, for the “on-shell/off-shell” matching, these large virtualities introduce large cancellations in the non-leading terms contributing to the amplitude. Therefore, it would be useful to construct the

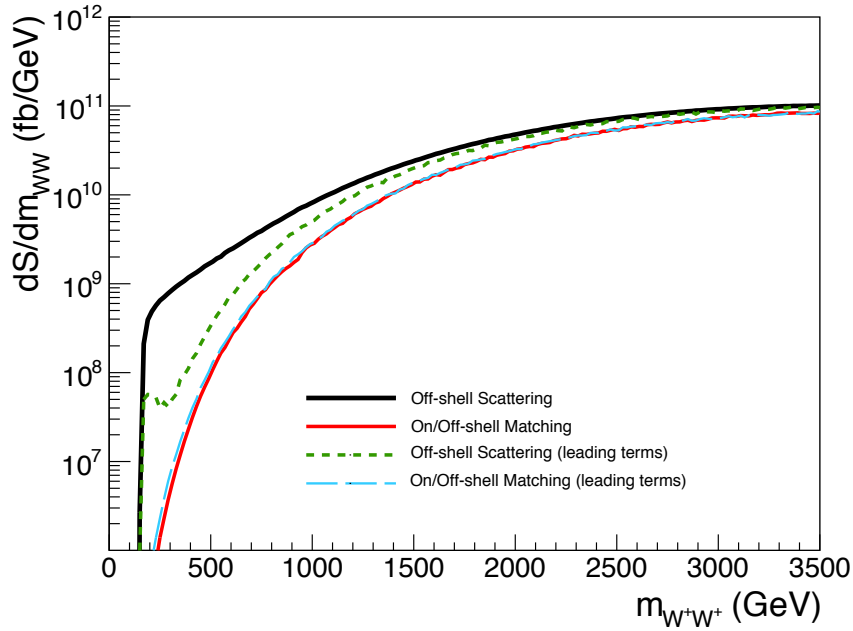


FIGURE 4.6: Semi-log invariant mass distribution for $F_{T_0} = 1000 \text{ TeV}^{-4}$, with a cut for the SM contributions ($E_{cm} > 100 \text{ GeV}$). The black thick line shows the off-shell distribution, while the red thinner line the matching distribution. The dashed aquamarine line (on top of the red one) shows the leading terms distribution and the green short dashed line shows the leading terms contributions for off-shell.

on-shell momenta in such a way, that the cancellations can be rectified near the threshold.

2. On-shell momenta $\bar{k}_1 \equiv \bar{q}_1$:

One could construct the on-shell momenta from $\bar{k}_1 = \bar{q}_1$. Then, using the on-shell condition,

$$\Rightarrow E_1 = \sqrt{m_V^2 + \bar{q}_1^2}.$$

From equations (4.51) and (4.52),

$$s = 4 (m_V^2 + \bar{q}_1^2),$$

it is easy to obtain the momenta for all the bosons in the on-shell scattering.

The differential cross section distribution as a function of the invariant mass is shown in figure (4.7) for F_{T_0} . The result is compared to the previous on-shell momenta computation ($s = E_{CM}^2$) and to the off-shell distribution. It can be observed that there are large cancellations, even for the leading terms, which discards this on-shell momenta construction.

A similar construction with $\bar{k}_1 = \bar{q}_3$ was done. Nevertheless, the observable distributions have similar results as $\bar{k}_1 = \bar{q}_1$.

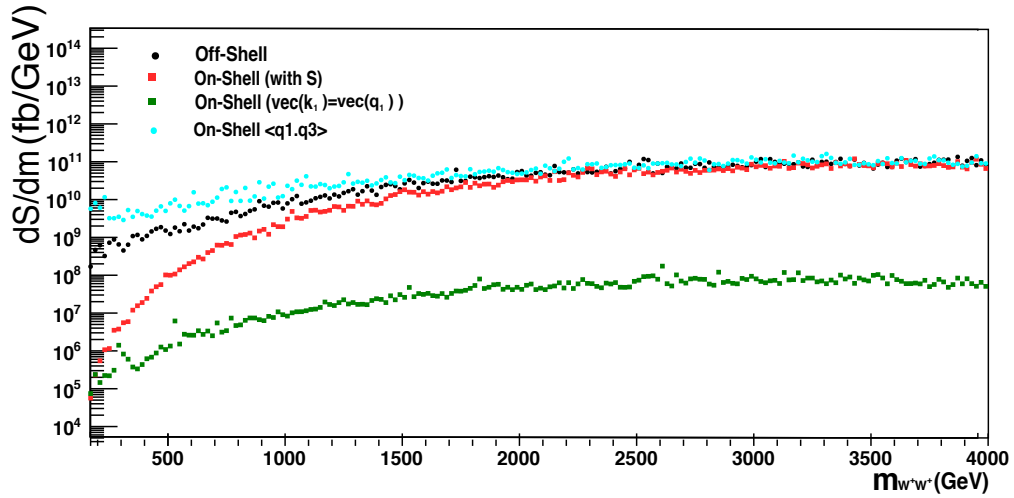


FIGURE 4.7: Semi-log invariant mass distribution for $F_{T_0} = 1000 \text{ TeV}^{-4}$, with a cut for the SM contributions ($E_{\text{CM}} > 100 \text{ GeV}$). The black dotted distribution shows the off-shell results, the red distribution the on-shell momenta construction with $s = (q_1^2 + q_2^2)$, the green distribution shows the on-shell momenta built from $\vec{k}_1 = \vec{q}_1$, and the aquamarine distribution the average construction for testing the origin of the cancellations.

3. On-shell momenta from an average $\langle \vec{q}_1, \vec{q}_3 \rangle$:

The main purpose for this on-shell momenta construction is a deeper understanding of the cancellations that appear in the on-shell/off-shell matching. Therefore, it is important to keep in mind that this on-shell construction is not theoretically motivated, but rather an artificial tool.

So far, the main problem seemed to be the large virtualities of the bosons, which are not cancelled as required around the threshold in the “on-shell/off-shell” matching. Then, one could include explicitly the missing cancellations, by defining an average between \vec{q}_1 , \vec{q}_3 in the following way: consider $\vec{q}_1 = (0, 0, z_1)$ and $\vec{q}_3 = (x_3, 0, z_3)$. The on-shell momenta can be defined as $\vec{k}_1 = |\vec{q}| \hat{q}_1$, with

$$|\vec{q}| \equiv \sqrt{|\vec{q}_1| |\vec{q}_3|} = \sqrt{|z_1| |\sqrt{x_3^2 + z_3^2}|}. \quad (4.55)$$

Then, the Lorentz invariant s for the scattering is defined as

$$s = 4 \left(m_V^2 + |z_1| |\sqrt{x_3^2 + z_3^2}| \right). \quad (4.56)$$

Using equations (4.51) and (4.52), all the on-shell momenta can be computed. The resulting invariant mass distribution is also shown in figure (4.7). For this case, the difference with the off-shell distribution is smaller than it has been with the

previous on-shell momenta construction. This result confirms the inability to cancel the large virtualities for small E_{CM} without introducing some arbitrary model to define the on-shell momenta. And, although it reproduces a closer behavior to the off-shell, there is no specific reason why one should define the on-shell vectors using this particular construction.

In summary, the “on-shell/off-shell” matching is not an appropriate approach to find an analytical way to unitarize the amplitudes with a pure on-shell unitarization scheme. Instead, a numerical unitarization is required.

4.5 Numerical T-matrix unitarization for off-shell processes

Instead of the “on-shell/off-shell” matching, the matrix element $\mathcal{M}_{\mu\nu}$

$$\mathcal{M}_{\mu\nu} = \mathcal{F} \sum_{\lambda_1 \lambda_2} \widetilde{\varepsilon}_\mu^*(q_1, \lambda_1) \varepsilon_\nu(q_2, \lambda_2) \sum_{\lambda_3 \lambda_4} \underbrace{M_{\lambda_1 \lambda_2 \lambda_3 \lambda_4}}_{\text{to unitarize}} Z_3(\lambda_3) Z_4(\lambda_4), \quad (4.57)$$

will be written with all the polarization vectors defined off-shell. Then, a numerical implementation of the T-matrix unitarization described in Chapter 3 is used to unitarize $M_{\lambda_1 \lambda_2 \lambda_3 \lambda_4}$.

However, as the T-matrix unitarization still requires an on-shell like behavior, the longitudinal polarization vectors are redefined as,

$$\varepsilon^\mu(q, \lambda = 0) = \tilde{N}(|\vec{q}|, q_0 \hat{q}), \quad (4.58)$$

$$\varepsilon'^\mu(q, \lambda = 0) = N_k(|\vec{q}|, q_0 \hat{q}) \quad (4.59)$$

and $M_{\lambda_1 \lambda_2 \lambda_3 \lambda_4}$ is now redefined as a function of $\varepsilon'(q, \lambda)$ (the transverse polarization vectors are the same, $\varepsilon'(q, \pm) = \varepsilon(q, \pm)$),

$$\begin{aligned} M_{\lambda_1 \lambda_2 \lambda_3 \lambda_4} &= M(\varepsilon'(q_1, \lambda_1), \varepsilon'(q_2, \lambda_2); \varepsilon'^*(q_3, \lambda_3), \varepsilon'^*(q_4, \lambda_4)) \\ &= \varepsilon'^{\mu_1}(q_1, \lambda_1) \varepsilon'^{\mu_2}(q_2, \lambda_2) \mathbf{m}_{\mu_1 \mu_2 \mu_3 \mu_4} \varepsilon'^{* \mu_3}(q_3, \lambda_3) \varepsilon'^{* \mu_4}(q_4, \lambda_4) \end{aligned} \quad (4.60)$$

For example, the amplitude for the F_{S_0} coupling for $W^+ W^+ \rightarrow W^+ W^+$ scattering is,

$$M_{\lambda_1 \lambda_2 \lambda_3 \lambda_4} \propto F_{S_0} (\varepsilon'(q_1, \lambda_1) \cdot \varepsilon'(q_2, \lambda_2) \varepsilon'^*(q_3, \lambda_3) \cdot \varepsilon'^*(q_4, \lambda_4)) . \quad (4.61)$$

4.5.1 Partial Wave Decomposition for off-shell processes

The partial wave decomposition explained in Chapter 3 also needs to be extended for the VV off-shell production. Considering the four λ_i helicities (12 \rightarrow 34) and using the Wigner-Eckart theorem [31], the partial wave decomposition as defined in equation (3.10) is

$$M_{\lambda_1\lambda_2\lambda_3\lambda_4}(\theta, q^2) = 16\pi \sum_{j=0}^2 (2j+1) a_{\lambda_1\lambda_2\lambda_3\lambda_4}^j(q^2) d_{\alpha\beta}^j(\theta) \quad (4.62)$$

where $\alpha = \lambda_1 - \lambda_2$ and $\beta = \lambda_3 - \lambda_4$. The partial wave amplitudes $a_{\lambda_1\lambda_2\lambda_3\lambda_4}^j(q^2)$ ⁴ will be projected onto the Argand circle (as described in Chapter 3) and unitarized.

In order to find the $a_{\lambda_1\lambda_2\lambda_3\lambda_4}^j$ corresponding to the amplitude $M_{\lambda_1\lambda_2\lambda_3\lambda_4}$, the previous equation can be rewritten as a product of vectors, such as

$$M_{\lambda_1\lambda_2\lambda_3\lambda_4}(\theta_i, q^2) = 16\pi \begin{pmatrix} d_{\alpha\beta}^0 & 3d_{\alpha\beta}^1 & 5d_{\alpha\beta}^2 \end{pmatrix}(\theta_i) \cdot \begin{pmatrix} a_{\lambda_1\lambda_2\lambda_3\lambda_4}^0 \\ a_{\lambda_1\lambda_2\lambda_3\lambda_4}^1 \\ a_{\lambda_1\lambda_2\lambda_3\lambda_4}^2 \end{pmatrix}(q^2). \quad (4.63)$$

Therefore, using three arbitrary angles, e.g. $\theta_i = \pi/3, \pi/2, 2\pi/3$ ($i=1,2,3$), the Wigner amplitudes $a_{\lambda_1\lambda_2\lambda_3\lambda_4}^j$ are obtained from the inversion of the full matrix. In other words,

$$\begin{pmatrix} a_{\lambda_1\lambda_2\lambda_3\lambda_4}^0 \\ a_{\lambda_1\lambda_2\lambda_3\lambda_4}^1 \\ a_{\lambda_1\lambda_2\lambda_3\lambda_4}^2 \end{pmatrix}(q^2) = \frac{1}{16\pi} \begin{pmatrix} d_{\alpha\beta}^0(\theta_1) & 3d_{\alpha\beta}^1(\theta_1) & 5d_{\alpha\beta}^2(\theta_1) \\ d_{\alpha\beta}^0(\theta_2) & 3d_{\alpha\beta}^1(\theta_2) & 5d_{\alpha\beta}^2(\theta_2) \\ d_{\alpha\beta}^0(\theta_3) & 3d_{\alpha\beta}^1(\theta_3) & 5d_{\alpha\beta}^2(\theta_3) \end{pmatrix}^{-1} \begin{pmatrix} M_{\lambda_1\dots}(\theta_1, q^2) \\ M_{\lambda_1\dots}(\theta_2, q^2) \\ M_{\lambda_1\dots}(\theta_3, q^2) \end{pmatrix}. \quad (4.64)$$

For example, consider the $W^+W^+ \rightarrow W^+W^+$ scattering. The figures (4.8) and (4.9) show the contributions from the partial wave amplitudes to the total scattering amplitudes for F_{S_1} and F_{M_0} , respectively.

It is easy to observe that for F_{S_1} , the partial wave $j = 0$ gives the largest contribution to the amplitude (one can show that for F_{T_0} this statement is also true). However, for F_{M_0} , $j = 1$ gives the largest contribution to the amplitude.

4.5.2 From On-shell to Off-shell T-matrix

It is possible to write the partial wave amplitude $a_{\lambda_1\lambda_2\lambda_3\lambda_4}^j$ as a matrix a^j , with $m \times n$ components (a_{mn}^j). Here $m = (\lambda_1, \lambda_2)$ and $n = (\lambda_3, \lambda_4)$ gives all the possible helicities

⁴The on-shell partial wave amplitude $a_{\lambda_1\lambda_2\lambda_3\lambda_4}^j$ is a function of s . However, for off-shell processes, it is a function of s and all vector boson virtualities, q_i^2 , with $i = 1, \dots, 4$. These 5 invariants are collectively denoted by q^2 .

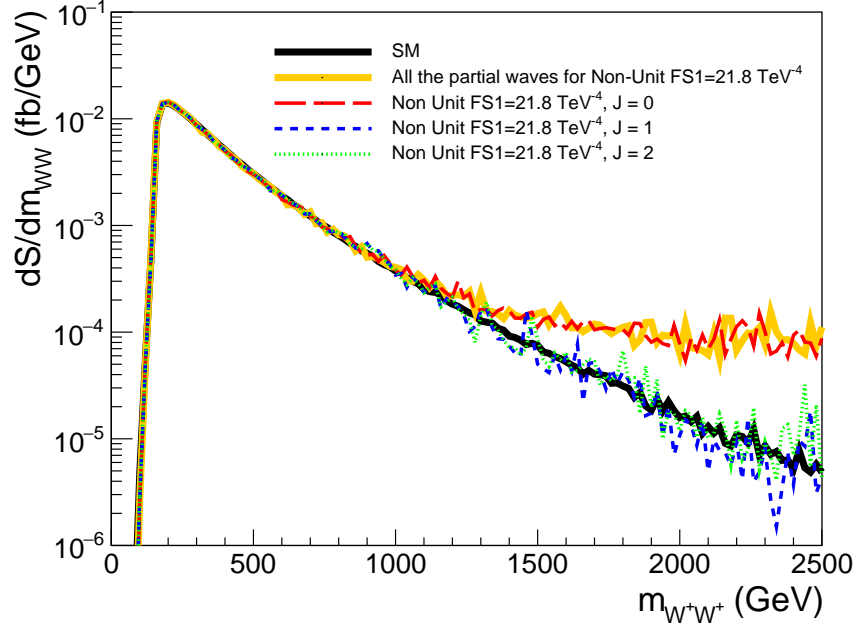


FIGURE 4.8: Partial wave amplitude ($j=0,1,2$) contribution to the total amplitude in the invariant mass distribution for F_{S_1} coupling (semi-log plot). The yellow thick line shows the total amplitude (as shown in equation (4.62)), the red dashed line is the contribution from $j = 0$, the blue thick dash line is $j = 1$ and the dot-dashed green line $j = 2$.

combinations for the incoming and outgoing bosons, respectively. For instance, for $W^+W^+ \rightarrow W^+W^+$ scattering, there are 9 possible helicity combinations as shown in table (4.1); then, $a_{m \times n}^j = a_{9 \times 9}^j$ matrix.

| | 1 | 2 | 3 | 4 | 5 | 6 | 7 | 8 | 9 |
|--------------------------|-----|-----|-----|-----|-----|-----|-----|-----|-----|
| (λ_i, λ_j) | - - | - 0 | - + | 0 - | 0 0 | 0 + | + - | + 0 | + + |

TABLE 4.1: Helicities combination for $W^+W^+ \rightarrow W^+W^+$: $(\lambda_1, \lambda_2) \rightarrow m$ and $(\lambda_3, \lambda_4) \rightarrow n$ mapping.

Using the T -matrix unitarization equation (3.23), one could define the matrix u^j , with $m \times n$ components (u_{mn}^j), as the partial wave amplitude which will restore the S -matrix unitarity,

$$u^j = \text{Re}(a^j) \left(\mathbb{1} + \frac{1}{4} (a^j)^\dagger a^j \right)^{-1} \left(\mathbb{1} + \frac{i}{2} a^j \right). \quad (4.65)$$

Then, the matrix element $M_{\lambda_1 \lambda_2 \lambda_3 \lambda_4}$ from equation (4.62) can be redefined as $M u_{\lambda_1 \lambda_2 \lambda_3 \lambda_4}$,

$$M u_{\lambda_1 \lambda_2 \lambda_3 \lambda_4}(\theta, q^2) = 16\pi \sum_{j=0}^2 (2j+1) d_{\alpha\beta}^j(\theta) u_{(\lambda_1, \lambda_2), (\lambda_3, \lambda_4)}^j(q^2). \quad (4.66)$$

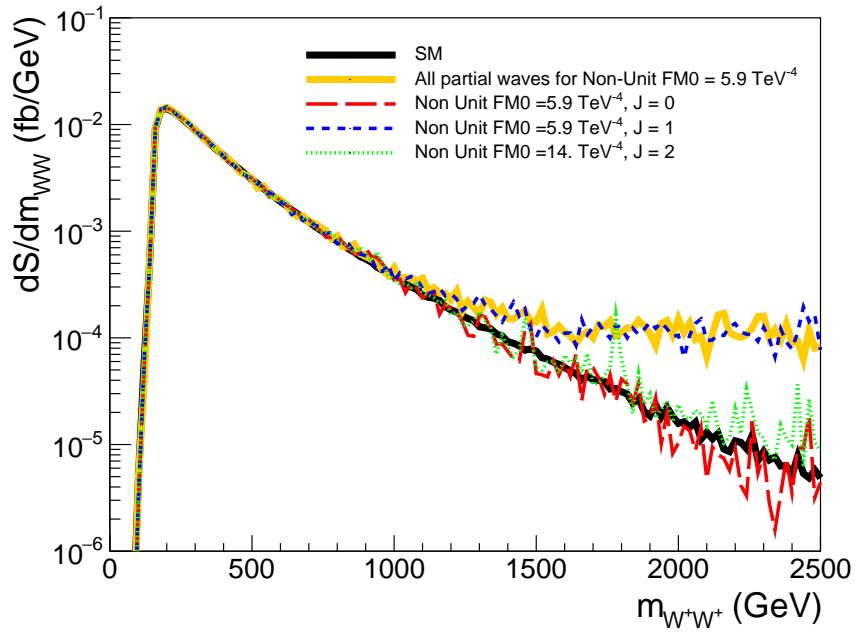


FIGURE 4.9: Partial wave amplitude ($j=0,1,2$) contribution to the total amplitude in the invariant mass distribution for F_{M_0} coupling. The yellow thick line shows the total amplitude (as shown in equation (4.62)), the red dashed line is the contribution from $j = 0$, the blue thick dash line is $j = 1$ and the dot-dashed green line $j = 2$.

Now, to solve the equation (4.65), it is necessary to find $(\mathbb{1} + \frac{1}{4}(a^j)^\dagger a^j)^{-1}$. One could consider the following,

$$u^j = \underbrace{\text{Re}(a^j)}_B \left(\underbrace{\mathbb{1} - \frac{i}{2}(a^j)^\dagger}_{A^{-1}} \right)^{-1}.$$

For example, for $W^+W^+ \rightarrow W^+W^+$ scattering, this can be rewritten as a 9×9 matrix product,

$$T_{u \ 9 \times 9}^j = B_{9 \times 9}^j \left(A_{9 \times 9}^j \right)^{-1}, \quad (4.67)$$

which means that it is necessary to calculate a 9×9 matrix inversion. Yet inverting a matrix is neither numerically stable nor desirable (due to calculation time), in particular for other processes where the matrices are larger than 9×9 .

Instead, it is better to solve the system of equations to find the matrix u^j ⁵. Some of the factorization methods implemented in VBFNLO to solve equation (4.67) are described in Appendix D.

To verify that the T -matrix unitarization is working, it is fundamental to test that the S -matrix is indeed unitary, using equation (3.1) described in Chapter 3. One finds

⁵A deeper explanation on how to solve the system of equations is discussed in Appendix D.

numerical invalidity of the unitary relation, which implies some failure in the implementation of the unitarization model for off-shell scattering.

4.5.3 Testing the unitary condition: a non-symmetric amplitude

After different numerical tests were done with VBFNLO, it was found that the unitary relation is not satisfied. The partial wave amplitude $a_{\lambda_1\lambda_2\lambda_3\lambda_4}^j$ does not form a normal matrix for the off-shell processes considered. Thus, T-matrix unitarization cannot be used, unless a new matrix satisfying the following equation (4.68) is defined,

$$[T_o, T_o^\dagger] = 0 . \quad (4.68)$$

Therefore, it is vital to find a normal matrix related to $M_{\lambda_1\lambda_2\lambda_3\lambda_4}$.

In general, any matrix A could be decomposed as a symmetric matrix plus an asymmetric one, such as

$$A = A_{\text{sym}} + A_{\text{asym}} , \quad (4.69)$$

with

$$A_{\text{sym}} = \frac{1}{2} (A + A^\dagger) , \quad (4.70)$$

$$A_{\text{asym}} = \frac{1}{2} (A - A^\dagger) . \quad (4.71)$$

For VV on-shell production, one could think to rewrite the partial wave amplitude using the equations (4.69), (4.70) and (4.71), as all the symmetric matrices are normal and the asymmetric contributions are expected to be negligible in the phenomenologically important region of small boson virtualities.

Then, the symmetric matrix will be unitarized. One might be tempted to write the following,

$$(a_{m,n}^j)_{\text{sym}} = \frac{1}{2} (a_{m,n}^j + a_{n,m}^{*j}) , \quad (4.72)$$

with $m = (\lambda_1, \lambda_2)$ and $n = (\lambda_3, \lambda_4)$.

Figure (4.10) shows the invariant mass distribution for F_{S_0} coupling, where the symmetric and asymmetric results behave as expected. But, once the coupling structure includes not only the polarization vectors but the 4-momenta q_i contributions, e.g. F_{T_0} , it is not possible to rewrite the partial wave amplitude using equations (4.69) and (4.70), as shown in figure (4.11). This behavior is a clear consequence of the vector boson large virtualities, which were not considered in this approach, and which establishes a clear distinction between the incoming and outgoing particles.

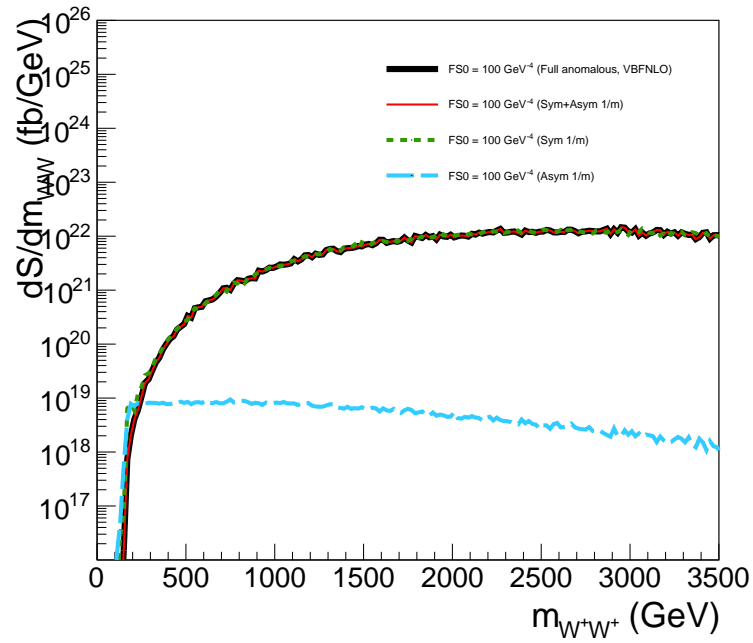


FIGURE 4.10: Semi-log invariant mass distribution for $W^+W^+ \rightarrow W^+W^+$ F_{S_0} coupling. The total amplitude is compared with the symmetric and asymmetric components: the black thick line is the non-unitarized amplitude, the red thinner line is the sum of the sym+asym, the green small dashed line on top of the other two is the symmetric component and the aquamarine large dashed line is the asymmetric part.

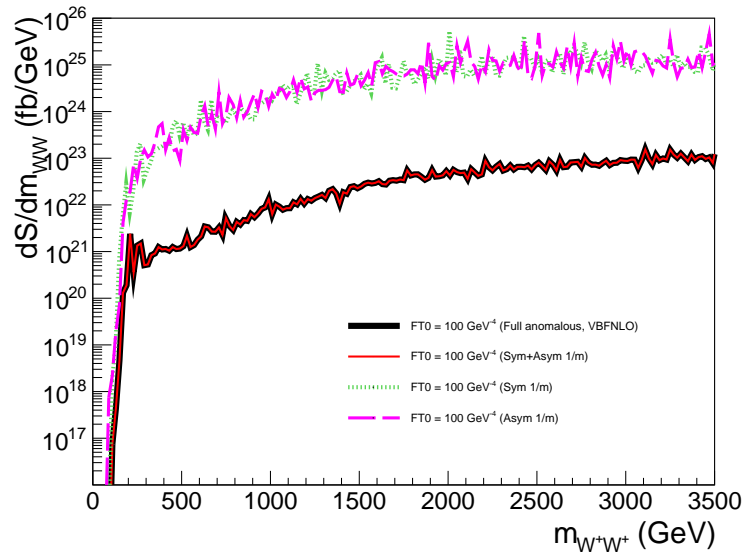


FIGURE 4.11: Semi-log invariant mass distribution for $W^+W^+ \rightarrow W^+W^+$ F_{T_0} coupling. The total amplitude is compared with the symmetric and asymmetric components: the black thick line is the non-unitarized amplitude, the red thinner line is the sum of the sym+asym. Here the green small dashed line is the symmetric component and the pink large dashed line is the asymmetric part, both above the non-unitarized distribution.

In summary, a new normal matrix is needed to define the unitarization prescription for $2 \rightarrow 6$ vector boson off-shell scattering.

4.6 Off-shell T-matrix for VBS

So far, the issues in the unitarization are a result of considering $V_1 V_2 \rightarrow V_3 V_4$ as an on-shell scattering, and trying to solve everything without taking the different virtualities q_i^2 of the 4 bosons V_i into account. Note that even for $W^+ W^+ \rightarrow W^+ W^+$ the virtualities render the V_i distinguishable.

In this section, one should consider the matrix element as a combination of all the possible scatterings for the 4 bosons involved, for any $2 \rightarrow 6$ process. Then, the most general matrix one could write for the scattering is:

$$\begin{pmatrix} V_1 V_2 \rightarrow V_1 V_2 & V_3 V_4 \rightarrow V_1 V_2 \\ V_1 V_2 \rightarrow V_3 V_4 & V_3 V_4 \rightarrow V_3 V_4 \end{pmatrix}. \quad (4.73)$$

As the incoming bosons are space like (s), while the outgoing bosons are time like (t), this can be understood as

$$\begin{pmatrix} s \rightarrow s & t \rightarrow s \\ s \rightarrow t & t \rightarrow t \end{pmatrix},$$

where $s \rightarrow t$ is the partial wave amplitude from $M(\varepsilon(q_1, \lambda_1)\varepsilon(q_2, \lambda_2); \varepsilon^*(q_3, \lambda_3)\varepsilon^*(q_4, \lambda_4))$ used previously. Then,

$$a_{s \rightarrow t}^j = a_{\lambda_1 \lambda_2 \lambda_3 \lambda_4}^j(q^2),$$

and $t \rightarrow s = (s \rightarrow t)^\dagger$.

Here, $s \rightarrow s$ is the partial wave amplitude from $M(\varepsilon(q_{1s}, \lambda_1)\varepsilon(q_{2s}, \lambda_2); \varepsilon^*(q_{3s}, \lambda_3)\varepsilon^*(q_{4s}, \lambda_4))$, with 3-momentum directions given by the corresponding q_i , but

$$q_{1s}^2 = q_{3s}^2 = q_1^2, \quad (4.74)$$

$$q_{2s}^2 = q_{4s}^2 = q_2^2, \quad (4.75)$$

then,

$$a_{s \rightarrow s}^j = a_{\lambda_1 \lambda_2 \lambda_3 \lambda_4}^j(q_s^2). \quad (4.76)$$

And, $t \rightarrow t$ is the partial wave amplitude from $M(\varepsilon(q_{1t}, \lambda_1)\varepsilon(q_{2t}, \lambda_2); \varepsilon^*(q_{3t}, \lambda_3)\varepsilon^*(q_{4t}, \lambda_4))$, with the momenta similarly defined with

$$q_{1t}^2 = q_{3t}^2 = q_3^2 \quad (4.77)$$

$$q_{2t}^2 = q_{4t}^2 = q_4^2 \quad (4.78)$$

then,

$$a_{t \rightarrow t}^j = a_{\lambda_1 \lambda_2 \lambda_3 \lambda_4}^j(q_t^2). \quad (4.79)$$

To simplify the calculations, and as it is only of interest to find a normal matrix related to $V_1 V_2 \rightarrow V_3 V_4$, a new interaction matrix to be unitarized could be defined as

$$T = \begin{pmatrix} 0 & A^\dagger \\ A & 0 \end{pmatrix} = T^\dagger, \quad (4.80)$$

with

$$A = a_{s \rightarrow t} = (a_{t \rightarrow s})^\dagger, \quad (4.81)$$

$$A^\dagger = a_{t \rightarrow s}, \quad (4.82)$$

and therefore, $[T, T^\dagger] = 0$.

Replacing equation (4.80) in the equation (3.23) to find the unitarized amplitude,

$$T_u = T \left(\mathbb{1} - \frac{i}{2} T^\dagger \right)^{-1} = \begin{pmatrix} U_1(s \rightarrow s) & U_2(t \rightarrow s) \\ \mathbf{U}_3(s \rightarrow t) & U_4(t \rightarrow t) \end{pmatrix}.$$

The encircled quantity U_3 is the unitary amplitude to be replaced in the equation (4.66).

Using block matrix algebra,

- $\mathbb{1} + \frac{i}{2} T^\dagger = \begin{pmatrix} \mathbb{1} & \frac{i}{2} A(t \rightarrow s) \\ \frac{i}{2} A^\dagger(s \rightarrow t) & \mathbb{1} \end{pmatrix},$
- $(T^\dagger)^2 = \begin{pmatrix} A(t \rightarrow s) A^\dagger(s \rightarrow t) & 0 \\ 0 & A^\dagger(t \rightarrow s) A(s \rightarrow t) \end{pmatrix},$
- $\left(\mathbb{1} + \frac{1}{4} (T^\dagger)^2 \right)^{-1} = \begin{pmatrix} (\mathbb{1} + \frac{1}{4} A(t \rightarrow s) A^\dagger(s \rightarrow t))^{-1} & 0 \\ 0 & (\mathbb{1} + \frac{1}{4} A^\dagger(s \rightarrow t) A(t \rightarrow s))^{-1} \end{pmatrix}.$

Then,

$$T_u = \begin{pmatrix} A \left(\mathbb{1} + \frac{1}{4} A^\dagger A \right)^{-1} \frac{i}{2} A^\dagger & A \left(\mathbb{1} + \frac{1}{4} A^\dagger A \right)^{-1} \\ \mathbf{A}^\dagger \left(\mathbb{1} + \frac{1}{4} \mathbf{A} \mathbf{A}^\dagger \right)^{-1} & A^\dagger \left(\mathbb{1} + \frac{1}{4} A A^\dagger \right)^{-1} \frac{i}{2} A \end{pmatrix}. \quad (4.83)$$

If the linear T-matrix unitarization scheme is considered, U_3 (inside the blue circle area) gives only the real part of the unitarization. Therefore, a complex part needs to be added to satisfy the T-matrix definition, similar to the equations (3.23) and (4.65). It is important to consider the type of vectors that would form the imaginary component of $U_3(s \rightarrow t)$, as it is a $s \rightarrow t$ process. In the limit where $q_i^2 \sim m_V^2$, $A_{s \rightarrow t} \rightarrow A_{t \rightarrow t}$, which makes $A(t \rightarrow t)$ the most reasonable choice for the imaginary part.

Therefore, the new off-shell unitarization scheme for $2 \rightarrow 6$ VBS is defined as,

$$T_u(s \rightarrow t) = A_{s \rightarrow t} \left(\mathbb{1} + \frac{1}{4} A_{t \rightarrow s} A_{s \rightarrow t} \right)^{-1} + \frac{i}{2} A_{s \rightarrow t} A_{t \rightarrow t} \left(\mathbb{1} + \frac{1}{4} A_{t \rightarrow s} A_{s \rightarrow t} \right)^{-1},$$

or simplified,

$$T_u(s \rightarrow t) = A_{s \rightarrow t} \left(\mathbb{1} + \frac{i}{2} A_{t \rightarrow t} \right) \left(\mathbb{1} + \frac{1}{4} A_{t \rightarrow s} A_{s \rightarrow t} \right)^{-1}. \quad (4.84)$$

To corroborate the results from this new unitarization scheme, a good idea is to compare the observable distributions using the K-matrix unitarization and the new T-matrix unitarization for F_{S_1} and $F_{S_0} = F_{S_2}$; for example, the invariant mass plot shown in figure (4.12).

This plot (4.12) shows that between 0 and 700 GeV the new T-matrix unitarization, the K-matrix unitarization and the non-unitarized distributions are in agreement. After 700 GeV (for $F_{S_1} = 400 \text{ TeV}^{-4}$), the T-matrix unitarization distribution lies below the K-matrix within less than 20% difference.

But, it is once again necessary to test the unitarization for another couplings and to examine whether or not this unitarization prescription is valid.

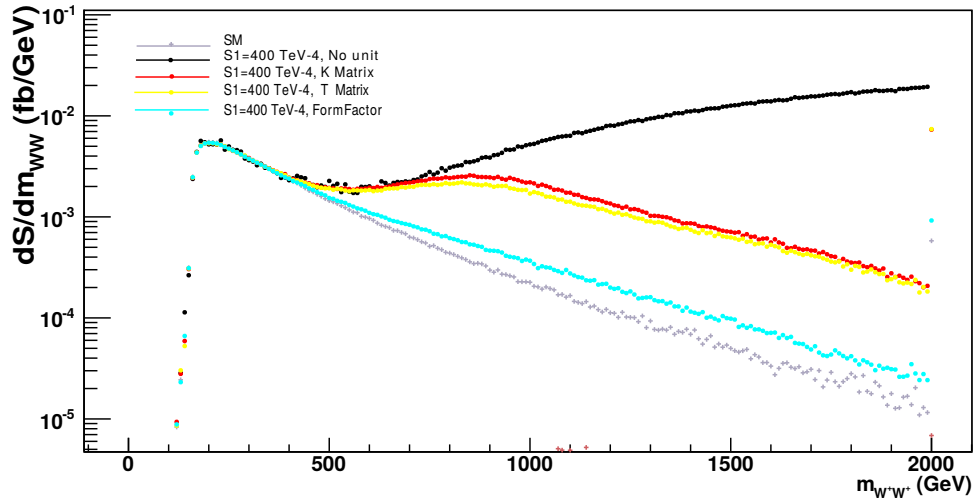


FIGURE 4.12: Off-shell T-matrix unitarization for $F_{S_1}=400 \text{ TeV}^{-4}$ for $W^+W^+ \rightarrow W^+W^+$ scattering. The invariant mass distribution shows: gray dots the SM, aquamarine dots the form factor unitarization, the yellow line the new off-shell T-matrix unitarization, the red line the K-matrix unitarization and the black line the non-unitarized distribution.

The results for F_{T_0} (without any extra cut) are shown in figure (4.13), whose unexpected behavior (observed in purple triangular markers) implies a deficiency in the unitarization approach used. For a better understanding, and based on previous experiences from the virtualities' influence on the transverse and mixed couplings, cuts on the invariant mass and the virtuality values of the incoming bosons were implemented, to suppress the large contributions.

A first suspicion lies on the alignment of the $A_{t \rightarrow t}$ and $A_{t \rightarrow s} A_{s \rightarrow t}^\dagger$ eigenvectors, which might not necessarily be orthogonal and, therefore, the denominator does not achieve the necessary suppression on the growth of the amplitudes. Nevertheless, a deeper investigation and proper understanding on this effect needs to be done and it was not the topic of this work.

Instead, to guarantee proper cancellations and implement a unitarization scheme which will restore unitarity, one can modify the equation (4.84) using instead the maximum eigenvalue⁶ of the matrix $(A_{t \rightarrow s} A_{s \rightarrow t}^\dagger)$.

The final T-matrix unitarization model for off-shell VBS ($2 \rightarrow 6$) is,

$$T_u(s \rightarrow t) = A_{s \rightarrow t} \left(\mathbf{1} + \frac{i}{2} A_{t \rightarrow t} \right) \left(\mathbf{1} + \frac{1}{4} E_{\max} \right)^{-1}, \quad (4.85)$$

⁶To calculate the maximum eigenvalue, different algorithms were implemented in VBFNLO. They are explained in the Appendix E.

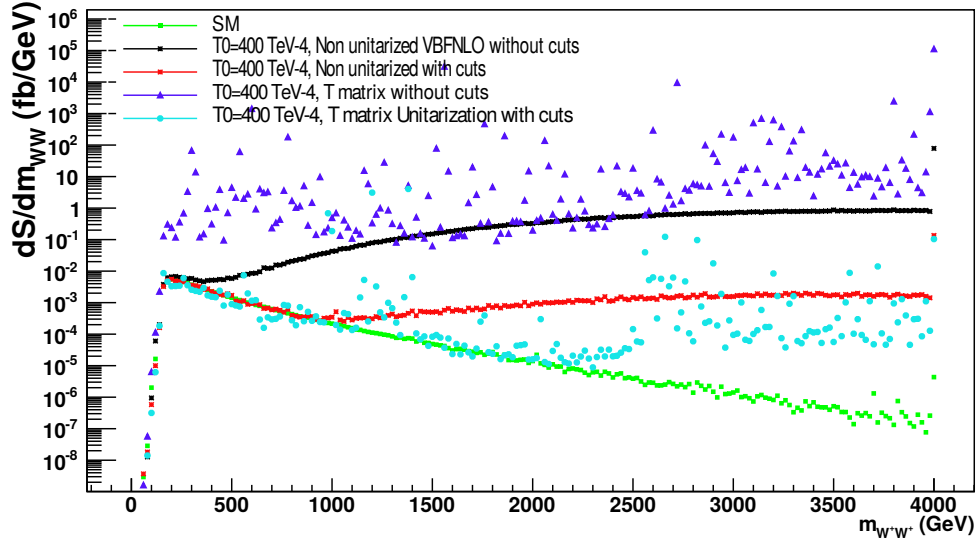


FIGURE 4.13: Off-shell T -matrix unitarization for $F_{T_0}=400 \text{ TeV}^{-4} W^+W^+ \rightarrow W^+W^+$ scattering. The invariant mass distribution shows: green line the SM, black line the non-unitarized anomalous coupling distribution, the red line same distribution with cuts on the incoming virtualities; the blue triangular dots are the off-shell linear T -matrix unitarization and the aquamarine dots are same distribution with cuts on the incoming virtualities.

where the maximum eigenvalue is $E_{\max} = \max(\lambda(A_{t \rightarrow s} A_{s \rightarrow t}^\dagger))$. The distribution obtained using this expression can be observed in figure (4.14) for F_{S_1} coupling and figure (4.15) for F_{T_0} .

The off-shell linear T -matrix unitarization for $2 \rightarrow 6$ processes is fully implemented in VBFNLO for $W^+W^+ \rightarrow W^+W^+$ and it includes NLO QCD corrections for all the couplings. For example, figure (4.16) shows these results for F_{S_1} .

The implementation of this approach in VBFNLO is described in Appendix F.

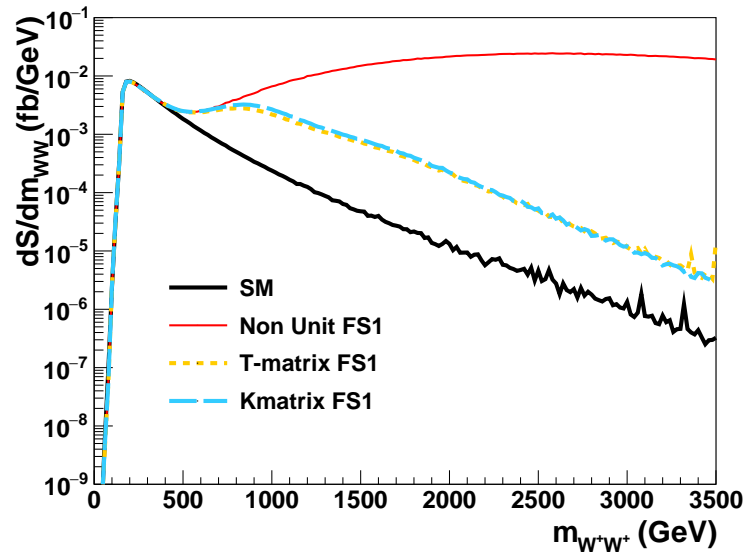


FIGURE 4.14: Semi-log invariant mass distribution for $F_{S_1} = 400 \text{ TeV}^{-4}$, $W^+W^+ \rightarrow W^+W^+$ scattering at 13 TeV. The black solid line is the SM distribution, the red thinner solid line the anomalous coupling without unitarization, the dashed aquamarine line the K -matrix unitarization distribution and the dotted yellow line the new off-shell linear T -matrix unitarization, as defined in equation (4.85).

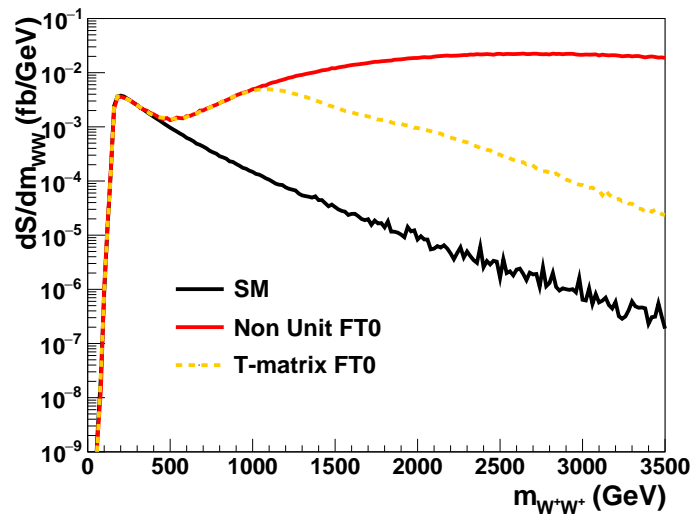


FIGURE 4.15: Semi-log invariant mass distribution for $F_{T_0} = 400 \text{ TeV}^{-4}$, $W^+W^+ \rightarrow W^+W^+$ scattering. The black solid line is the SM distribution, the red thinner solid line the anomalous coupling without unitarization and the dotted yellow line the new off-shell linear T -matrix unitarization, as defined in equation (4.85).

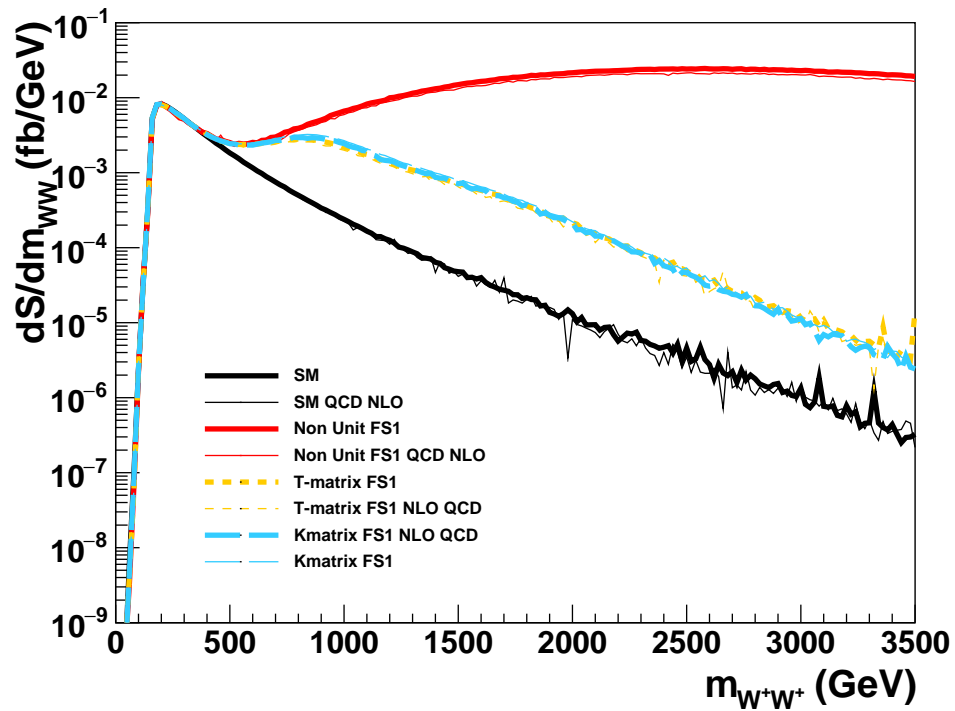


FIGURE 4.16: Semi-log invariant mass distribution for $F_{S_1} = 400 \text{ TeV}^{-4}$, $W^+W^+ \rightarrow W^+W^+$ scattering at 13 TeV including NLO QCD corrections (thinner lines). The black solid line is the SM distribution, the red solid line the anomalous coupling without unitarization, the dashed aquamarine line the K -matrix unitarization distribution and the dotted yellow line the new off-shell linear T -matrix unitarization, as defined in equation (4.85).

CHAPTER 5

Limits for Anomalous Couplings at 13 TeV collisions

In this chapter, to illustrate the importance of the unitarization for off-shell processes at the LHC, an analysis on the current limits for $W^+W^+ \rightarrow W^+W^+$ for the CMS results¹ [45] at $\sqrt{s} = 13$ TeV and integrated luminosity of $35.9 \pm 0.9\text{fb}^{-1}$ is done.

If the unitarity is not restored for the anomalous couplings, two possible scenarios might happen: either the new physics limits are beyond the EFT validity, or the new limits could rule out regions where new physics might appear.

5.1 Electroweak production of same-sign W boson pairs

The final states considered for this process are $2j + 4l$: $\mu^+\mu^+\nu_\mu\nu_\mu jj$, $e^+e^+\nu_e\nu_e jj$, $e^+\mu^+\nu_e\nu_\mu jj$ and their charge conjugates. The following cuts were implemented:

- $m_{ll} > 20$ GeV,
- $p_T^{\text{miss}} > 40$ GeV,
- $p_T^l > 20$ GeV,
- $\eta_l < 2.5$,
- $R_{jj} = 0.4$,
- $p_T^j > 30$ GeV,
- $|\eta_j| < 5$,
- $m_{jj} > 500$ GeV,
- $\Delta\eta_{jj} > 2.5$.

The observed limits on the AQC from the CMS experiment at 13 TeV for the dim-8 operators are shown in the table 5.1. These limits are calculated without considering

¹At the moment this work was written, the ATLAS experiment have not released new results at 13 TeV on their limits for anomalous couplings.

any unitarization formalism. The table has the values in the Éboli convention (used in [45]) and VBFNLO convention.

| Coefficient | CMS¹(13 TeV) | CMS²(13 TeV) |
|--------------------|--------------------------------|--------------------------------|
| F_{S_0} | [-7.7,7.7] | [-7.7,7.7] |
| F_{S_1} | [-21.6,21.8] | [-21.6,21.8] |
| F_{M_0} | [-6.0,5.9] | [-14.3398,14.5829] |
| F_{M_1} | [-8.7,9.1] | [-22.1174,21.1452] |
| F_{M_6} | [-11.9,11.8] | [-28.6797,28.9227] |
| F_{M_7} | [-13.3,12.9] | [-31.3532,32.3254] |
| F_{T_0} | [-0.62,0.65] | [-3.6625,3.8397] |
| F_{T_1} | [-0.28,0.31] | [-1.6540,1.8312] |
| F_{T_2} | [-0.89,1.02] | [-5.2574,6.0254] |

¹ Éboli convention (used in [45]).

² VBFNLO notation.

TABLE 5.1: Observed limits on the dim-8 anomalous couplings: the first and second columns are the limits obtained by the CMS experiment at 13 TeV [45].

This chapter will be focused mainly on the couplings F_{S_1} , F_{M_0} and F_{T_0} .

5.1.1 QGCs Unitary Bound

First, the SM cross section obtained by the CMS experiment [45] and the one calculated by VBFNLO are compared for $W^+W^+ \rightarrow W^+W^+$ scattering, to ensure that the cuts are the same and the results are in agreement within a few percent difference. The CMS fiducial cross section is $\sigma_{SM} = 3.83 \pm 0.66$ (stat) ± 0.35 (syst) fb; while the result for the same process calculated by VBFNLO is $\sigma_{SM} = 3.5690 \pm 0.0015 \pm 0.0426$.

Using the Form Factor tool from VBFNLO described in Chapter 4 [43], the energy threshold Λ_{unit} where the unitarity condition is broken for the $2 \rightarrow 2$ scattering is calculated, using the partial wave amplitude $j = 0$ as unitarity criterion. In other words,

$$|\text{Re}(a^{j=0})| \leq \frac{1}{2}.$$

In other words, for energies $\sqrt{s} \geq \Lambda_{\text{unit}}$, the amplitudes saturate the unitarity bound.

The table (5.2) shows the unitarity bounds for some couplings within the limits given in table (5.1). This unitarity bound will be useful to compare the saturation observed in the invariant mass distributions for the VV scattering.

It is important to note * in table (5.2), as for F_{M_i} couplings the dominant partial wave amplitude contribution is $j = 1$ (recalling Chapter 4). Thus, the bounds are obtained using crossing symmetry².

| Coupling (TeV^{-4}) | Λ_{unit} |
|--------------------------------|-------------------------|
| $F_{S_0} =$ | 7.7 1989.0 GeV |
| $F_{S_1} =$ | 21.8 2020.0 GeV |
| $F_{M_0}^* =$ | 5.9 2028.0 GeV |
| $F_{M_1}^* =$ | 9.1 2638.0 GeV |
| $F_{M_6}^* =$ | 11.8 2033.0 GeV |
| $F_{M_7}^* =$ | 12.9 2829.0 GeV |
| $F_{T_0} =$ | 0.65 3326.0 GeV |
| $F_{T_1} =$ | 0.31 3385.0 GeV |
| $F_{T_2} =$ | 1.02 3388.0 GeV |

TABLE 5.2: Unitary bound for different QGCs using the limits from table (5.1) and calculated using the partial wave 0 for the $2 \rightarrow 2$ process (Form factor tool in VBFNLO).

5.1.2 EFT with unitarization: coupling limits

To find the new limits, the following procedure is followed,

1. The cross section σ_{AQC} is calculated using the limits for the couplings F_{S_1} , F_{M_0} and F_{T_0} from table (5.1) without any unitarization.
2. The cross section $\sigma_{\text{AQC} - T\text{-matrix}}$ is computed with F_{S_1} , F_{M_0} and F_{T_0} , using the T -matrix unitarization.
3. The coupling's value is slowly raised until $\sigma_{\text{AQC} - T\text{-matrix}} \equiv \sigma_{\text{AQC}}$ is achieved. Therefore, the new limit will be lying in the unitarity saturation bound for that cross section.

The table 5.3 shows the new limits for F_{S_1} , F_{M_0} and F_{T_0} .

The figures (5.1) and (5.2) show the differential cross section distributions as a function of m_{WW} and m_{ll} for F_{S_1} and F_{T_0} (respectively).

The importance of the unitarization can be observed in these plots, as one can distinguish the red area between the non-unitarized distribution and the unitarized one, which

²For a $2 \rightarrow 2$ scattering, the crossing symmetry relates amplitudes by transforming ingoing particles into outgoing antiparticles.

| Coupling (TeV^{-4}) | CMS (13 TeV) | New limits |
|--------------------------------|--------------|--------------|
| F_{S_1} | [-21.6,21.8] | [-50.0,60.3] |
| F_{M_0} | [-8.7,9.1] | [-20.0,14.5] |
| F_{T_0} | [-0.62,0.65] | [-1.35,1.60] |

TABLE 5.3: New limits on the dim-8 anomalous couplings (using Éboli convention); the first column shows the observed results by the CMS experiment (5.1) and the second column the new limits for all the number of events expected according to [45].

saturates the unitarity bound previously calculated. Any measurement done in this red area is within a parameter region that breaks unitarity.

The plots also show that there is a suppression for the non-unitarized distribution below the interception between the unitarized and non-unitarized distributions (shown as a blue area). This could increase the probability of measuring any deviation from the SM for the coupling in that region.

As the new limits reach the unitarity saturation bound for the respective process, the intersection of the m_{VV} distributions (T -matrix and non-unitarized, with blue and red lines respectively) shows the energy threshold Λ_{unit} , which should agree with the results from table (5.2).

For example, for F_{S_1} the m_{VV} distribution shows Λ_{unit} around 2 TeV, in agreement with the results in table (5.2); while figure (5.2) shows Λ_{unit} around 2.9 TeV, being a clue that a more precise calculation of the limit needs to be investigated.

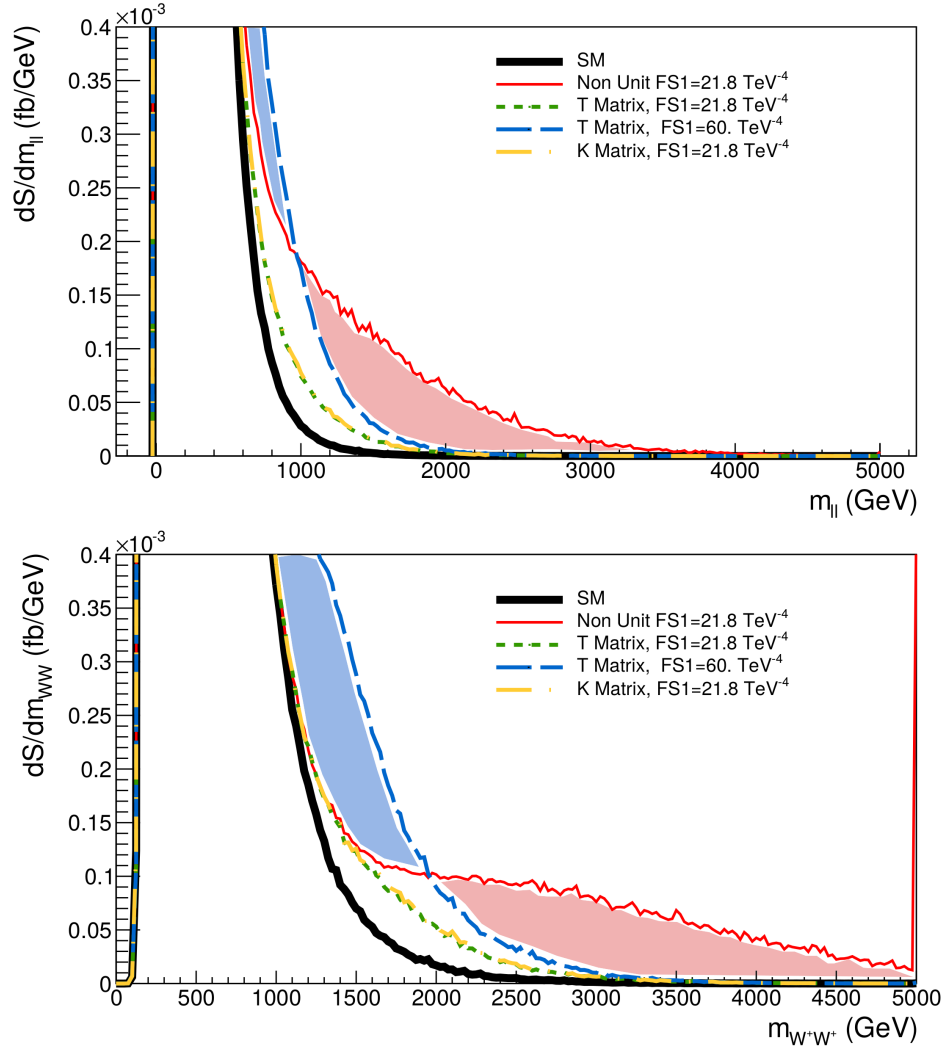


FIGURE 5.1: The upper plot shows the differential cross section as a function of the charged leptons invariant mass, m_{ll} , while the bottom plot shows a similar distribution but as a function of the invariant mass m_{WW} for F_{S_1} coupling. The black thick line is the SM distribution, the red thinner line is F_{S_1} distribution without unitarization, the green short dashed line is the T -matrix unitarization with the CMS F_{S_1} value, while the blue large dashed line is the T -matrix unitarization with the new limit. The yellow dashed-dotted line is the K -matrix for the CMS value. The red area shows the region where the parameter region is not valid, while the blue area shows the region where the non-unitarity distribution underestimates allowed deviations from the SM distributions.

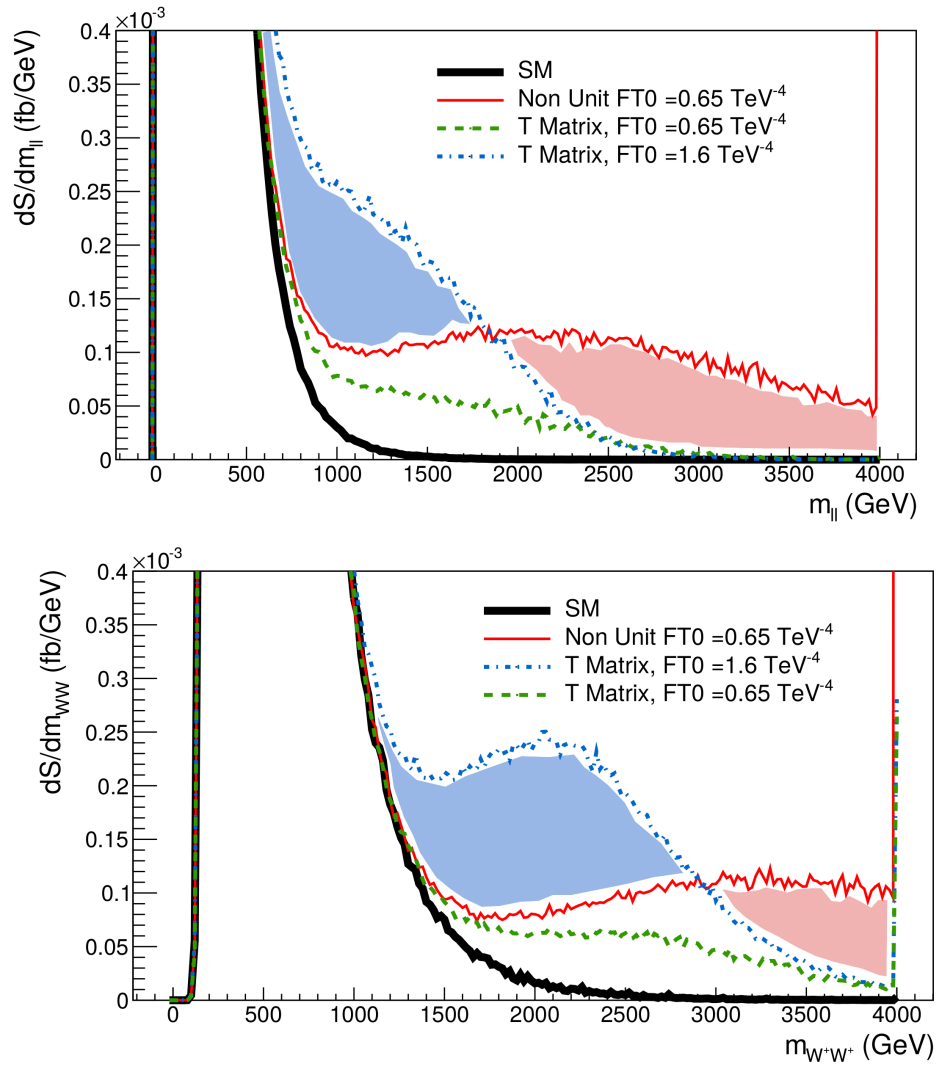


FIGURE 5.2: The upper plot shows the differential cross section as a function of the charged leptons invariant mass, m_{ll} , while the bottom shows a similar distribution but as a function of the invariant mass m_{WW} for F_{T_0} coupling. The black thick line is the SM distribution, the red thinner line is F_{T_0} distribution without unitarization, the green large dashed line is the T -matrix unitarization with the CMS F_{T_0} value, while the blue dotted line is the T -matrix unitarization with the new limit. The red area shows the region where the parameter region is not valid, while the blue area shows the region where the non-unitarity distribution underestimates allowed deviations from the SM distributions.

5.1.3 More Observables

To appreciate the importance of the unitarization for the anomalous couplings, one could study some measurable observables and the effects in their distributions if a unitarization scheme is used.

An extra cut in the invariant mass of the charge leptons, $m_{ll} \leq 500\text{GeV}$, which will guarantee that the SM effects are negligible.

- **DY(11-12)**

ΔY_{l1-l2} is defined as,

$$\Delta Y_{l1-l2} = |Y_{l1} - Y_{l2}|. \quad (5.1)$$

Figure (5.3) shows the differential cross section as a function of $|\Delta Y_{l1-l2}|$ for F_{T_0} . The solid thicker black line shows the SM, the thinner solid red line shows the cross sections for the F_{T_0} coupling using the current CMS limit at 13 TeV. The green dashed line shows the cross sections using the T -matrix unitarization using the CMS limit. The blue dotted-dashed line shows a new limit for F_{T_0} , if the T -matrix unitarization is used.

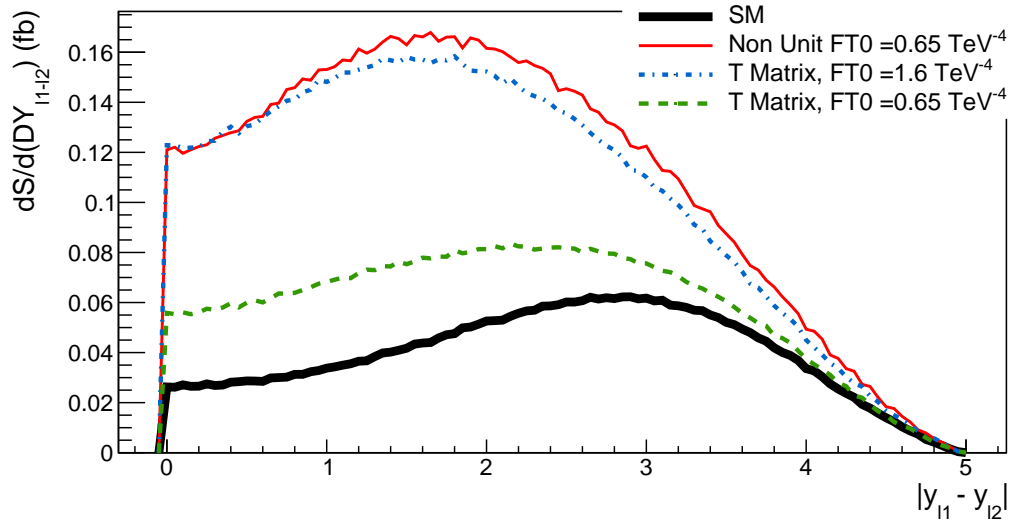


FIGURE 5.3: Differential cross sections for the process $pp \rightarrow W^+W^+jj$ as function of ΔY_{l1-l2} for F_{T_0} .

Figure (5.3) shows the distribution for F_{S_1} . The solid thicker black line shows the SM, the thinner solid red line shows the cross sections for the coupling using the current CMS limit at 13 TeV. The green dashed line shows the cross sections using the T -matrix unitarization using the CMS limit. The blue long dashed line shows a new limit for F_{S_1} , if the T -matrix unitarization is used. The other value for F_{S_1}

using the T-matrix shows how the saturation of the unitarity bound is achieved (aquamarine dotted-dashed line). The K -matrix unitarization is also shown with the long dashed-dotted yellow line using the CMS limit.

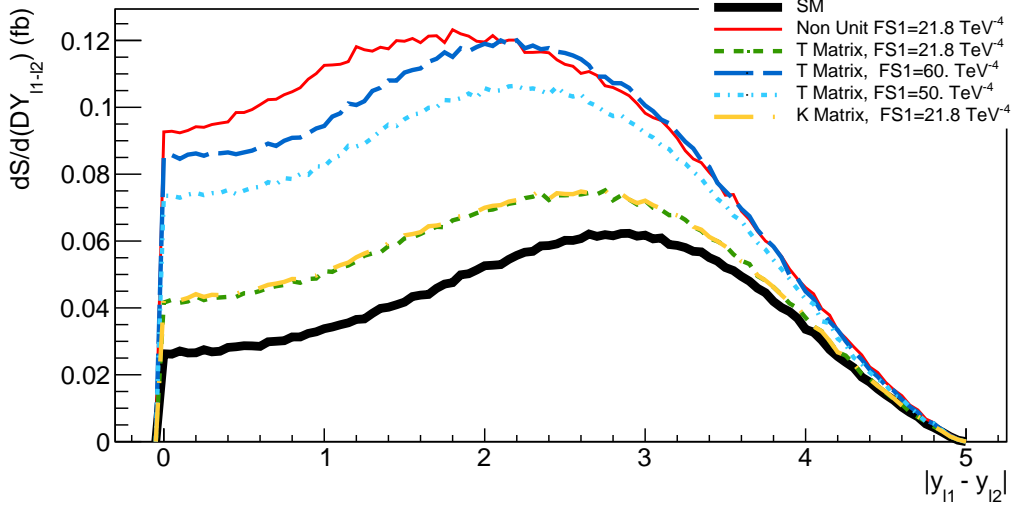


FIGURE 5.4: Differential cross sections for the process $pp \rightarrow W^+W^+jj$ as function of ΔY_{l1-l2} for F_{S_1} .

- **phi_jj**

The differential cross section as a function of the ϕ_{jj} is shown in figure (5.5). The solid thicker black line shows the Standard Model, the thinner solid red line shows the cross sections for the F_{T_0} coupling using the CMS limits at 13 TeV. The green dashed line shows the distribution using the T -matrix unitarization with the CMS limit. The blue dashed-dotted line shows a possible new limit for F_{T_0} , if the T -matrix unitarization is used.

- Y_l^*

Figure (5.6) describes how central the leptons are for F_{S_1} coupling. Y_l^* is defined as,

$$Y_l^* = Y_l - \left(\frac{Y_{j1} + Y_{j2}}{2} \right). \quad (5.2)$$

The solid thicker black line shows the SM, the thinner solid red line shows the cross sections for the F_{S_1} coupling using the CMS limits at 13 TeV. The green dashed line shows the distribution using the T -matrix unitarization with the CMS limit. The blue dashed-dotted line shows a possible new limit for F_{T_0} , if the T -matrix unitarization is used. The yellow dotted-long dashed line shows the CMS limit using the K -matrix unitarization.

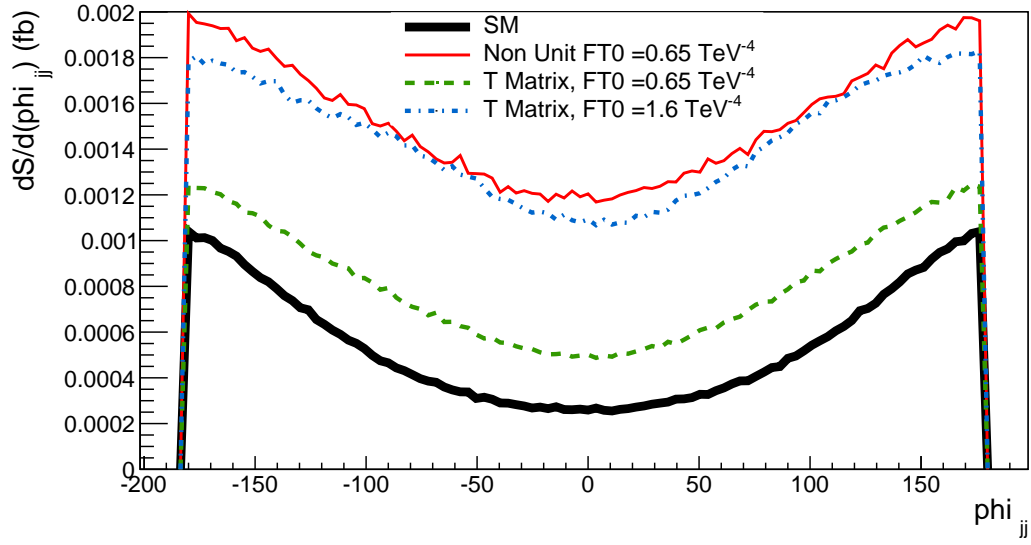


FIGURE 5.5: Differential cross sections for the process $pp \rightarrow W^+W^+jj$ as function of ϕ_{jj} for F_{T_0} .

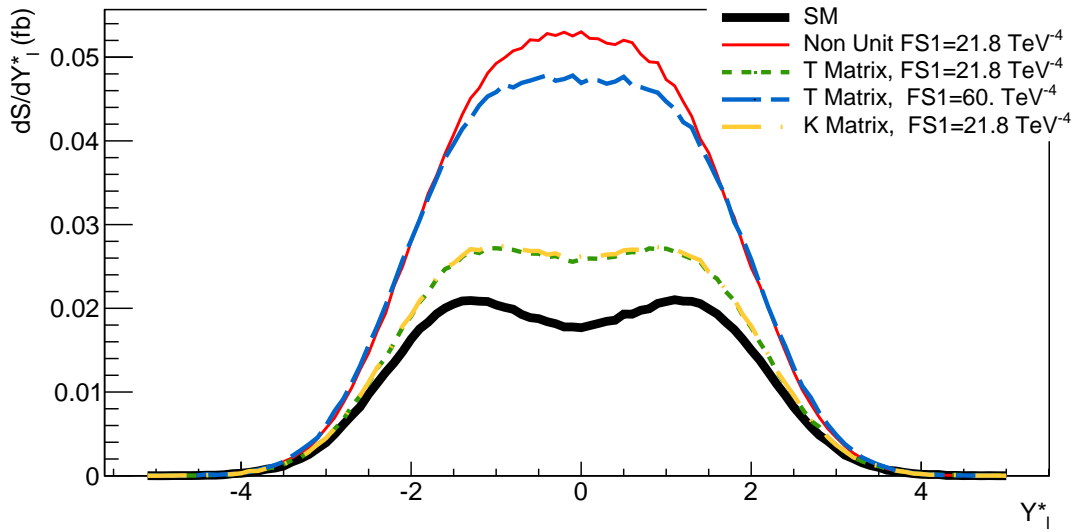


FIGURE 5.6: Differential cross sections for the process $pp \rightarrow W^+W^+jj$ as function of Y_l^* for F_{S_1} .

Summary

The effective Lagrangian formalism is a good theoretical way to describe BSM scenarios, as deviations from the SM can be parameterized in a convenient way using the SM fields. In general, the anomalous couplings associated with the vector boson scattering provide a very sensitive probe for new physics.

Despite this, using the EFT beyond its validity region leads to non-physical cross sections, which violate the unitarity condition from the S-matrix. Therefore, through this work a better understanding of the unitarity prescriptions for $2 \rightarrow 6$ processes at the LHC and the challenges involved was attempted.

For on-shell VV production, the K -matrix and T -matrix schemes have been previously studied [41], and they were used as a reference in this thesis to define a new prescription. However, the underlying phenomena for the off-shell VV production requires a thorough analysis to find a suitable unitarization scheme, such that the non-unitarized amplitude will be projected onto the Argand circle.

From Chapter 4, it is clear that for off-shell VV production, large virtualities of the vector bosons have important contributions, in particular at small s . For example, the $VV \rightarrow VV$ scattering amplitudes form non-diagonalizable matrices, and it is not possible to rewrite them in terms of the symmetric/asymmetric components. This characteristic off-shellness of the bosons was an important challenge in each of the attempts to find a unitarized scattering amplitude.

Although there have been studies before on the validity of the K -matrix and T -matrix extension for on-shell/off-shell processes [46, 47], this work has been mainly dedicated to the validity of these approaches for vector boson scattering at the LHC. In summary, the most important message from this thesis is the relation for the unitarization described in Chapter 4,

$$T_u(s \rightarrow t) = A_{s \rightarrow t} \left(\mathbf{1} + \frac{i}{2} A_{t \rightarrow t} \right) \left(\mathbf{1} + \frac{1}{4} \mathbf{E}_{\max} \right)^{-1}.$$

Using this scattering matrix, which is compatible with unitarity, does result in less constrained limits on new physics, as shown in Chapter 5.

To develop the unitarization model here defined, the off-shell $W^+W^+ \rightarrow W^+W^+$ scattering has been used and fully implemented for AQC's in VBFNLO. Now, with a working framework and theory, it might be simpler to implement in the future more vector boson processes and do more analyses on EFT for the electroweak sector. Processes including the Z/γ bosons might also bring new challenges, as it has not been trivial to find a unitarization prescription for space-like bosons going to time-like bosons.

APPENDIX A

Feynman Rules

As mentioned in Chapter 2, VBFNLO [8] uses the HELAS [36] subroutines to compute the amplitudes. However, for the anomalous couplings the amplitudes are calculated using FeynRules [48]. The results of these calculations are compared with previous works on anomalous couplings (e.g. [43, 44]) and implemented in **anomal4ON.F**.

At the moment of this work, only $W^+W^+ \rightarrow W^+W^+$ was fully implemented and functional, while $W^+W^- \rightarrow W^+W^-$ and $WZ \rightarrow WZ$ are work in progress.

Below the amplitudes $M_{\lambda_1\lambda_2\lambda_3\lambda_4}$ of equation 4.30 are given for the various dimension 8 operators¹, using the following notation

$$\begin{aligned}\varepsilon(p_1, \lambda_1) &= \varepsilon_1, & \varepsilon(p_2, \lambda_2) &= \varepsilon_2, \\ \varepsilon(p_3, \lambda_3) &= \varepsilon_3, & \varepsilon(p_4, \lambda_4) &= \varepsilon_4.\end{aligned}$$

Anomalous Couplings for $W^+W^+ \rightarrow W^+W^+$

F_{S_0} :

$$4F_{S_0} m_W^4 \varepsilon_1 \cdot \varepsilon_2 \varepsilon_3^* \cdot \varepsilon_4^* \tag{A.1}$$

F_{S_1} :

$$2F_{S_1} m_W^4 (\varepsilon_1 \cdot \varepsilon_3^* \varepsilon_2 \cdot \varepsilon_4^* + \varepsilon_1 \cdot \varepsilon_4^* \varepsilon_2 \cdot \varepsilon_3^*) \tag{A.2}$$

F_{S_2} :

$$2F_{S_2} m_W^4 (\varepsilon_1 \cdot \varepsilon_4^* \varepsilon_2 \cdot \varepsilon_3^* + \varepsilon_1 \cdot \varepsilon_3^* \varepsilon_2 \cdot \varepsilon_4^*) \tag{A.3}$$

F_{T_0} :

$$\begin{aligned}8F_{T_0} (gw^4) &((q_3 \cdot \varepsilon_2 q_2 \cdot \varepsilon_3^* - \varepsilon_3^* \cdot \varepsilon_2 q_3 \cdot q_2)(q_4 \cdot \varepsilon_1 q_1 \cdot \varepsilon_4^* - \varepsilon_4^* \cdot \varepsilon_1 q_4 \cdot q_1) \\ &+ (q_3 \cdot \varepsilon_1 q_1 \cdot \varepsilon_3^* - \varepsilon_3^* \cdot \varepsilon_1 q_3 \cdot q_1)(q_4 \cdot \varepsilon_2 q_2 \cdot \varepsilon_4^* - \varepsilon_4^* \cdot \varepsilon_2 q_4 \cdot q_2))\end{aligned} \tag{A.4}$$

¹Couplings involving another processes are explained in [43] (in German).

F_{T_1} :

$$\begin{aligned}
F_{T_1}(gw^4) & ((q_3 \cdot \varepsilon_2 q_2 \cdot \varepsilon_3^* - \varepsilon_3^* \cdot \varepsilon_2 q_3 \cdot q_2)(q_4 \cdot \varepsilon_1 q_1 \cdot \varepsilon_4^* - \varepsilon_4^* \cdot \varepsilon_1 q_4 \cdot q_1) \quad (\text{A.5}) \\
& + (q_3 \cdot \varepsilon_1 q_1 \cdot \varepsilon_3^* - \varepsilon_3^* \cdot \varepsilon_1 q_3 \cdot q_1)(q_4 \cdot \varepsilon_2 q_2 \cdot \varepsilon_4^* - \varepsilon_4^* \cdot \varepsilon_2 q_4 \cdot q_2) \\
& + 2(q_3 \cdot \varepsilon_4^* q_4 \cdot \varepsilon_3^* - \varepsilon_3^* \cdot \varepsilon_4^* q_3 \cdot q_4)(q_1 \cdot \varepsilon_2 q_2 \cdot \varepsilon_1 - \varepsilon_1 \cdot \varepsilon_2 q_1 \cdot q_2))
\end{aligned}$$

 F_{T_2} :

$$\begin{aligned}
F_{T_2}(gw^4) & (2q_1 \cdot \varepsilon_3^* q_2 \cdot \varepsilon_4^* q_4 \cdot \varepsilon_1 q_3 \cdot \varepsilon_2 + q_4 \cdot \varepsilon_3^* q_1 \cdot \varepsilon_4^* q_2 \cdot \varepsilon_1 q_3 \cdot \varepsilon_2 \quad (\text{A.6}) \\
& + 2q_2 \cdot \varepsilon_3^* q_1 \cdot \varepsilon_4^* q_3 \cdot \varepsilon_1 q_4 \cdot \varepsilon_2 + q_1 \cdot \varepsilon_3^* q_3 \cdot \varepsilon_4^* q_2 \cdot \varepsilon_1 q_4 \cdot \varepsilon_2 \\
& + q_4 \cdot \varepsilon_3^* q_2 \cdot \varepsilon_4^* q_3 \cdot \varepsilon_1 q_1 \cdot \varepsilon_2 + q_2 \cdot \varepsilon_3^* q_3 \cdot \varepsilon_4^* q_4 \cdot \varepsilon_1 q_1 \cdot \varepsilon_2 \\
& + \varepsilon_3^* \cdot \varepsilon_4^* \varepsilon_1 \cdot \varepsilon_2 (q_3 \cdot q_2 q_4 \cdot q_1 + q_3 \cdot q_1 q_4 \cdot q_2) \\
& + \varepsilon_1 \cdot \varepsilon_2 (-q_4 \cdot \varepsilon_3^* (q_2 \cdot \varepsilon_4^* q_3 \cdot q_1 + q_1 \cdot \varepsilon_4^* q_3 \cdot q_2) \\
& + q_2 \cdot \varepsilon_3^* (q_1 \cdot \varepsilon_4^* q_3 \cdot q_4 - q_3 \cdot \varepsilon_4^* q_4 \cdot q_1) \\
& + q_1 \cdot \varepsilon_3^* (q_2 \cdot \varepsilon_4^* q_3 \cdot q_4 - q_3 \cdot \varepsilon_4^* q_4 \cdot q_2)) \\
& - \varepsilon_3^* \cdot \varepsilon_4^* (+q_2 \cdot \varepsilon_1 (q_4 \cdot \varepsilon_2 q_3 \cdot q_1 + q_3 \cdot \varepsilon_2 q_4 \cdot q_1) \\
& + q_1 \cdot \varepsilon_2 (q_4 \cdot \varepsilon_1 q_3 \cdot q_2 + q_3 \cdot \varepsilon_1 q_4 \cdot q_2) \\
& - q_1 \cdot q_2 (q_4 \cdot \varepsilon_1 q_3 \cdot \varepsilon_2 + q_3 \cdot \varepsilon_1 q_4 \cdot \varepsilon_2)) \\
& + \varepsilon_3^* \cdot \varepsilon_1 \varepsilon_4^* \cdot \varepsilon_2 (2 \cdot q_3 \cdot q_2 q_4 \cdot q_1 + q_3 \cdot q_4 q_1 \cdot q_2) \\
& + \varepsilon_3^* \cdot \varepsilon_2 \varepsilon_4^* \cdot \varepsilon_1 (2 \cdot q_3 \cdot q_1 q_4 \cdot q_2 + q_3 \cdot q_4 q_1 \cdot q_2) \\
& - \varepsilon_4^* \cdot \varepsilon_2 (+q_1 \cdot \varepsilon_3^* (q_2 \cdot \varepsilon_1 q_3 \cdot q_4 + 2 \cdot q_4 \cdot \varepsilon_1 q_3 \cdot q_2) \\
& + q_2 \cdot \varepsilon_3^* (2 \cdot q_3 \cdot \varepsilon_1 q_4 \cdot q_1 - 2 \cdot q_4 \cdot \varepsilon_1 q_3 \cdot q_1) \\
& + q_4 \cdot \varepsilon_3^* (q_3 \cdot \varepsilon_1 q_1 \cdot q_2 - q_2 \cdot \varepsilon_1 q_3 \cdot q_1)) \\
& - \varepsilon_3^* \cdot \varepsilon_2 (+2q_2 \cdot \varepsilon_4^* (q_4 \cdot \varepsilon_1 q_3 \cdot q_1 - q_3 \cdot \varepsilon_1 q_4 \cdot q_1) \\
& + q_1 \cdot \varepsilon_4^* (q_2 \cdot \varepsilon_1 q_3 \cdot q_4 + 2q_3 \cdot \varepsilon_1 q_4 \cdot q_2) \\
& + q_3 \cdot \varepsilon_4^* (q_4 \cdot \varepsilon_1 q_1 \cdot q_2 - q_2 \cdot \varepsilon_1 q_4 \cdot q_1)) \\
& - \varepsilon_4^* \cdot \varepsilon_1 (+q_2 \cdot \varepsilon_3^* (q_1 \cdot \varepsilon_2 q_3 \cdot q_4 + 2 \cdot q_4 \cdot \varepsilon_2 q_3 \cdot q_1) \\
& + q_1 \cdot \varepsilon_3^* (2 \cdot q_3 \cdot \varepsilon_2 q_4 \cdot q_2 - 2 \cdot q_4 \cdot \varepsilon_2 q_3 \cdot q_2) \\
& + q_4 \cdot \varepsilon_3^* (q_3 \cdot \varepsilon_2 q_1 \cdot q_2 - q_1 \cdot \varepsilon_2 q_3 \cdot q_2)) \\
& - \varepsilon_3^* \cdot \varepsilon_1 (+q_2 \cdot \varepsilon_4^* (q_1 \cdot \varepsilon_2 q_3 \cdot q_4 + 2 \cdot q_3 \cdot \varepsilon_2 q_4 \cdot q_1) \\
& + q_1 \cdot \varepsilon_4^* (2 \cdot q_4 \cdot \varepsilon_2 q_3 \cdot q_2 - 2 \cdot q_3 \cdot \varepsilon_2 q_4 \cdot q_2) \\
& + q_3 \cdot \varepsilon_4^* (q_4 \cdot \varepsilon_2 q_1 \cdot q_2 - q_1 \cdot \varepsilon_2 q_4 \cdot q_2)))
\end{aligned}$$

F_{M_0} :

$$\begin{aligned}
2F_{M_0}(gw^2)(m_W^2)(\varepsilon_3^* \cdot \varepsilon_2(q_4 \cdot \varepsilon_1 q_1 \cdot \varepsilon_4^* - \varepsilon_4^* \cdot \varepsilon_1(q_3 \cdot q_2 + q_4 \cdot q_1)) & \quad (\text{A.7}) \\
+ \varepsilon_3^* \cdot \varepsilon_1(q_4 \cdot \varepsilon_2 q_2 \cdot \varepsilon_4^* - \varepsilon_4^* \cdot \varepsilon_2(q_3 \cdot q_1 + q_4 \cdot q_2)) & \\
+ q_3 \cdot \varepsilon_1 q_1 \cdot \varepsilon_3^* \varepsilon_4^* \cdot \varepsilon_2 + q_3 \cdot \varepsilon_2 q_2 \cdot \varepsilon_3^* \varepsilon_4^* \cdot \varepsilon_1) &
\end{aligned}$$

 F_{M_1} :

$$\begin{aligned}
(F_{M_1}/2)(gw^2)(m_W^2)(\varepsilon_1 \cdot \varepsilon_2(q_3 \cdot \varepsilon_4^*(q_1 \cdot \varepsilon_3^* + q_2 \cdot \varepsilon_3^*) & \quad (\text{A.8}) \\
+ q_4 \cdot \varepsilon_3^*(q_1 \cdot \varepsilon_4^* + q_2 \cdot \varepsilon_4^*)) & \\
+ \varepsilon_4^* \cdot \varepsilon_2(q_2 \cdot \varepsilon_3^*(q_3 \cdot \varepsilon_1 - q_4 \cdot \varepsilon_1) & \\
+ q_4 \cdot \varepsilon_1 q_1 \cdot \varepsilon_3^* - q_4 \cdot \varepsilon_3^* q_2 \cdot \varepsilon_1) & \\
+ \varepsilon_3^* \cdot \varepsilon_2(q_2 \cdot \varepsilon_4^*(q_4 \cdot \varepsilon_1 - q_3 \cdot \varepsilon_1) & \\
+ q_3 \cdot \varepsilon_1 q_1 \cdot \varepsilon_4^* - q_3 \cdot \varepsilon_4^* q_2 \cdot \varepsilon_1) & \\
+ \varepsilon_4^* \cdot \varepsilon_1(q_1 \cdot \varepsilon_3^*(q_3 \cdot \varepsilon_2 - q_4 \cdot \varepsilon_2) & \\
- q_4 \cdot \varepsilon_3^* q_1 \cdot \varepsilon_2 + q_4 \cdot \varepsilon_2 q_2 \cdot \varepsilon_3^*) & \\
- \varepsilon_3^* \cdot \varepsilon_1(q_1 \cdot \varepsilon_4^*(q_3 \cdot \varepsilon_2 - q_4 \cdot \varepsilon_2) & \\
+ q_3 \cdot \varepsilon_4^* q_1 \cdot \varepsilon_2 - q_3 \cdot \varepsilon_2 q_2 \cdot \varepsilon_4^*) & \\
+ \varepsilon_3^* \cdot \varepsilon_4^*(q_1 \cdot \varepsilon_2(q_3 \cdot \varepsilon_1 + q_4 \cdot \varepsilon_1) & \\
+ q_2 \cdot \varepsilon_1(q_3 \cdot \varepsilon_2 + q_4 \cdot \varepsilon_2)) & \\
- \varepsilon_3^* \cdot \varepsilon_4^* \varepsilon_1 \cdot \varepsilon_2(q_3 \cdot q_1 + q_3 \cdot q_2 + q_4 \cdot q_1 + q_4 \cdot q_2) & \\
- \varepsilon_3^* \cdot \varepsilon_1 \varepsilon_4^* \cdot \varepsilon_2(q_3 \cdot q_2 + q_4 \cdot q_1) & \\
- \varepsilon_3^* \cdot \varepsilon_2 \varepsilon_4^* \cdot \varepsilon_1(q_3 \cdot q_1 + q_4 \cdot q_2)) &
\end{aligned}$$

 F_{M_7} :

$$\begin{aligned}
-(F_{M_7}/2)(gw^2)(m_W^2)(\varepsilon_1 \cdot \varepsilon_2(q_3 \cdot \varepsilon_4^*(q_1 \cdot \varepsilon_3^* + q_2 \cdot \varepsilon_3^*) & \quad (\text{A.9}) \\
+ q_4 \cdot \varepsilon_3^*(q_1 \cdot \varepsilon_4^* + q_2 \cdot \varepsilon_4^*)) & \\
+ \varepsilon_3^* \cdot \varepsilon_4^*(q_1 \cdot \varepsilon_2(q_3 \cdot \varepsilon_1 + q_4 \cdot \varepsilon_1) & \\
+ q_2 \cdot \varepsilon_1(q_3 \cdot \varepsilon_2 + q_4 \cdot \varepsilon_2)) & \\
- \varepsilon_3^* \cdot \varepsilon_4^* \varepsilon_1 \cdot \varepsilon_2(q_3 \cdot q_1 + q_3 \cdot q_2 + q_4 \cdot q_1 + q_4 \cdot q_2) & \\
- q_3 \cdot \varepsilon_4^* q_1 \cdot \varepsilon_2 \varepsilon_3^* \cdot \varepsilon_1 - q_3 \cdot \varepsilon_4^* q_2 \cdot \varepsilon_1 \varepsilon_3^* \cdot \varepsilon_2 & \\
- q_4 \cdot \varepsilon_3^* q_1 \cdot \varepsilon_2 \varepsilon_4^* \cdot \varepsilon_1 - q_4 \cdot \varepsilon_3^* q_2 \cdot \varepsilon_1 \varepsilon_4^* \cdot \varepsilon_2) &
\end{aligned}$$

APPENDIX B

VBFNLO and Éboli convention

VBFNLO defines the field strenghts as

$$\begin{aligned}\hat{W}_{\mu\nu} &= igT^A W_{\mu\nu}^A, \\ \hat{B}_{\mu\nu} &= ig'Y B_{\mu\nu}, \\ D_\mu &= \partial_\mu + igT^A W_\mu^A + ig'Y B_\mu,\end{aligned}$$

which gives compatible normalizations for operators with field strengths and covariant derivatives due to the identity

$$[D_\mu, D_\nu] = \hat{W}_{\mu\nu} + \hat{B}_{\mu\nu}. \quad (\text{B.1})$$

In contrast, in [21] a different strenght field definition is used:

$$\begin{aligned}\hat{W}_{\mu\nu} &= T^A W_{\mu\nu}^A \\ \hat{B}_{\mu\nu} &= B_{\mu\nu}.\end{aligned}$$

This means that the coupling must be rescaled between VBFNLO and the Éboli convention [49],

| VBFNLO | Éboli |
|--------------|------------------------------------------------|
| $f_{S0,1}$ | $f_{S0,1}^{\text{Éboli}}$ |
| $f_{M0,1}$ | $-\frac{1}{g^2} f_{M0,1}^{\text{Éboli}}$ |
| $f_{M2,3}$ | $-\frac{4}{g'^2} f_{M2,3}^{\text{Éboli}}$ |
| $f_{M4,5}$ | $-\frac{2}{gg'} f_{M4,5}^{\text{Éboli}}$ |
| $f_{M6,7}$ | $-\frac{1}{g^2} f_{M6,7}^{\text{Éboli}}$ |
| $f_{T0,1,2}$ | $\frac{1}{g^4} f_{T0,1,2}^{\text{Éboli}}$ |
| $f_{T5,6,7}$ | $\frac{4}{g^2 g'^2} f_{T5,6,7}^{\text{Éboli}}$ |
| $f_{T8,9}$ | $\frac{16}{g'^4} f_{T8,9}^{\text{Éboli}}$ |

APPENDIX C

Wigner \mathcal{D} -function

The Wigner \mathcal{D} -functions are obtained from the $SU(2)$ representations of angular momentum J . If one would consider a rotation R_θ , with θ the angle around the y-axis¹, the \mathcal{D} functions are defined as [31] ,

$$\mathcal{D}_{\alpha,\beta}^J (R_\theta^{-1}) = \mathcal{D}_{\beta,\alpha}^{J*}(\theta) = d_{\beta,\alpha}^J(\theta) , \quad (\text{C.1})$$

where $d_{\beta,\alpha}^J(\theta)$ are the elements of Wigner's (small) d-matrix.

Now, for the Wigner-Eckart theorem used previously in Chapter 4, it was calculated $\mathcal{D}_{\alpha,\beta}^{J*}(\theta)$ matrix, with $\alpha = \lambda_1 - \lambda_2$ and $\alpha = \lambda_3 - \lambda_4$ (for $12 \rightarrow 34$ processes), and $J=0,1,2$ (for vector boson $j=1$). Some useful properties from the d-functions are,

- $d_{\alpha,\beta}^J(\theta) = (-1)^{\alpha-\beta} d_{-\alpha,-\beta}^J(\theta) = (-1)^{\alpha-\beta} d_{\beta,\alpha}^J(\theta)$
- $d_{\alpha,\beta}^j(\theta) = (-1)^{j+\alpha} d_{\alpha,-\beta}^j(\pi - \theta)$

The Wigner d-functions implemented for the unitarization are described in the Particle Data booklet [34].

| | $j = 0$ | $j = 1$ | $j = 2$ |
|-----------|---------|---------------------------------|-----------------------------------------------|
| d_{00} | 1 | $\cos \theta$ | $\frac{1}{3}(3 \cos^2 \theta - 1)$ |
| d_{10} | - | $-\frac{\sin \theta}{\sqrt{2}}$ | $-\sqrt{\frac{3}{2}} \sin \theta \cos \theta$ |
| d_{11} | - | $\frac{1+\cos \theta}{2}$ | $\frac{1+\cos \theta}{2}(2 \cos \theta - 1)$ |
| d_{1-1} | - | $\frac{1-\cos \theta}{2}$ | $\frac{1-\cos \theta}{2}(2 \cos \theta + 1)$ |
| d_{20} | - | - | $\frac{\sqrt{6}}{4} \sin^2 \theta$ |
| d_{2-1} | - | - | $-\frac{1-\cos \theta}{2} \sin \theta$ |
| d_{2-2} | - | - | $\left(\frac{1-\cos \theta}{2}\right)^2$ |
| d_{21} | - | - | $-\frac{1+\cos \theta}{2} \sin \theta$ |
| d_{22} | - | - | $\left(\frac{1+\cos \theta}{2}\right)^2$ |

¹In this work only one rotation angle is considered.

APPENDIX D

Factorization methods

It was explained before that a matrix inversion was necessary to unitarize the scattering amplitude.

$$T_u^j = \underbrace{\text{Re}(T_o^j)}_B \underbrace{\left(\mathbb{1} + \frac{1}{4} T_o^j T_o^{j\dagger} \right)^{-1}}_{C^{-1} = C_{\text{inv}}} \underbrace{\left(\mathbb{1} + \frac{i}{2} T_o^{j\dagger} \right)}_A ,$$

$$\therefore T_{u \ 9 \times 9}^j = B_{9 \times 9}^j C_{\text{inv} \ 9 \times 9}^j A_{9 \times 9}^j . \quad (\text{D.1})$$

However, this calculation is numerically non-stable and, in general, *there is hardly ever a good reason to invert a matrix* [50].

Instead, from the computational point of view, it is better to implement an algorithm where a system of equations is solved. The following are some of the factorization methods used during this work.

LU decomposition and factorization

Consider a non-singular square matrix A . Then, it is possible to decompose A into a lower and an upper triangular square matrix (L and U , respectively)

$$A = LU . \quad (\text{D.2})$$

For example,

$$\begin{bmatrix} a_{11} & a_{12} & a_{13} \\ a_{21} & a_{22} & a_{23} \\ a_{31} & a_{32} & a_{33} \end{bmatrix} = \begin{bmatrix} L_{11} & 0 & 0 \\ L_{21} & L_{22} & 0 \\ L_{31} & L_{32} & L_{33} \end{bmatrix} \begin{bmatrix} U_{11} & U_{12} & U_{13} \\ 0 & U_{22} & U_{23} \\ 0 & 0 & U_{33} \end{bmatrix} .$$

Using this, one could solve a system of equations with an LU -factorization, where the solution for $Ax = B$ is obtained by:

$$Ax = B \Rightarrow L(Ux) = B , \quad (\text{D.3})$$

which will simplify solving the system of equations.

QR Factorization

For any matrix A , one could decompose it as the product of a square orthogonal matrix ($Q^\top = Q^{-1}$) times an upper triangular matrix,

$$A_{mn} = Q_{mm} \cdot R_{mn} . \quad (\text{D.4})$$

For example,

$$\begin{bmatrix} a_{11} & a_{12} & a_{13} & a_{14} \\ a_{21} & a_{22} & a_{23} & a_{24} \\ a_{31} & a_{32} & a_{33} & a_{34} \end{bmatrix} = \begin{bmatrix} Q_{11} & Q_{12} & Q_{13} \\ Q_{21} & Q_{22} & Q_{23} \\ Q_{31} & Q_{32} & Q_{33} \end{bmatrix} \begin{bmatrix} R_{11} & R_{12} & R_{13} & R_{14} \\ 0 & 0 & R_{23} & R_{24} \\ 0 & 0 & 0 & R_{34} \end{bmatrix} .$$

Then, to solve a system of equations $A x = B$,

$$\begin{aligned} A x &= B \\ Q \cdot R x &= B \\ \Rightarrow R x &= Q^\top B \end{aligned} \quad (\text{D.5})$$

In general, to implement a QR factorization, an algorithm is needed to obtain Q and R [51]. For instance, the Householder algorithm is implemented in VBFNLO for this purpose, as it is the most widely used (in matlab, c++, etc.).

Summary Computational factorization

The table (D.1) [52] gives a summary on different algorithms available¹ numerically equivalent, but with different running times.

The factorization methods are implemented in the subroutine **SOE_Decompositions.F** in VBFNLO.

¹However, only Partial Pivote LU, Householder QR and Column Pivote Householder QR were used for this project

| Decomposition | Requirements of the matrix | Computational Speed | Algorithm reliability and accuracy |
|--------------------------------|-----------------------------------|---------------------|------------------------------------|
| Partial Pivote LU | Invertible | Fast | Depends on compiler |
| Full Pivote LU | N/A | Slow | Reliable |
| Householder QR | N/A | Fast | Depends on compiler |
| Column Pivote Householder QR | N/A | Fast | Good |
| Full Pivote Householder QR | N/A | Slow | Reliable |
| LLT | Positive definite | Very Fast | Depends on compiler |
| $LDLT$ | Positive or negative semidefinite | Very fast | good |

TABLE D.1: Comparison between different factorization methods available. A symmetric matrix A is positive definite if $v^*Av > 0, \forall v \neq 0$. On the other hand, a symmetric matrix A is positive semidefinite if $v^*Av \geq 0, \forall v \neq 0$, while is negative semidefinite if $v^*Av \leq 0, \forall v \neq 0$

APPENDIX E

Eigenvalues calculation in VBFNLO

In Chapter 4, the maximum eigenvalue of the matrix $(A_{t \rightarrow s} A_{s \rightarrow t})$ was introduced for the T-matrix off-shell unitarization. In general, the eigenvalues of a matrix B can be calculated using the *characteristic equation* from the matrix,

$$\det(B - \lambda \mathbf{1}) = 0 ; \quad (\text{E.1})$$

but an efficient and fast algorithm that would calculate the eigenvalues for large matrices is necessary for VBFNLO.

For the following approaches, consider B as a $n \times n$ matrix with n eigenvalues; then, the sum of all the eigenvalues is equal to the trace of B , while the product of the n eigenvalues is the same as the determinant of B .

Approximate calculation

Eigenvalues using the trace of a matrix

A simplified calculation of the eigenvalues can be obtained using the trace of a matrix. As defined before,

$$\text{tr}(B) = \sum_i^{i=n} \lambda_i . \quad (\text{E.2})$$

As the unitarization requires only the maximum eigenvalue, one could in principle consider that one of the λ is much larger than the others; therefore,

$$\sum_i \lambda_i = \lambda_{\max} + \sum_{k \neq \max}^{k=n-1} \frac{\lambda_k}{\lambda_{\max}} .$$

In general,

$$\text{tr}(B^k) = \sum_i \lambda_i^k .$$

And then, an approximate value of the maximum eigenvalue can be obtained from the following relation,

$$\lambda_{\max} \sim \frac{\text{tr}(B^2)}{\text{tr}(B)}. \quad (\text{E.3})$$

As there is no guarantee that the maximum eigenvalue in the matrix will be much larger than the others, nor that it does not repeat itself, a constant factor is needed for the implementation in VBFNLO (e.g $x = 1/3$). In other words,

$$\lambda_{\max} = x \frac{\text{tr}(B^2)}{\text{tr}(B)}. \quad (\text{E.4})$$

Tarazaga eigenvalue calculation

If the matrix B is also symmetric, the Tarazaga method [53] can be used instead for the approximate calculation of the eigenvalues. Tarazaga proves that, for each λ_i with $i = 1, \dots, n$

$$\left\| \lambda_{\max} - \frac{\text{tr}(B)}{n} \right\| \leq \sqrt{\frac{n-1}{n} \left(\|B\|_F - \frac{\text{tr}(B)^2}{n} \right)},$$

where $\|B\|_F$ is the Frobenius norm, defined as

$$\|B\|_F \equiv \sqrt{\text{Tr}(BB^\dagger)}.$$

Therefore, the maximum eigenvalue could be determined from

$$\lambda_{\max} = \frac{\text{tr}(B)}{n} + \sqrt{\frac{n-1}{n} \left(\|B\|_F - \frac{\text{tr}(B)^2}{n} \right)} \quad (\text{E.5})$$

Full eigenvalue calculation

QR factorization

One option to calculate the exact eigenvalues is using the QR factorization described in the appendix (D). The matrix B is redefined as $B = QR$, using the algorithms described before, Q and R are calculated, with R a $n \times n$ upper triangular matrix and Q an orthogonal matrix. Then,

- let $B_0 = Q_0 R_0$, the initial B matrix,
- while B_i is not a diagonal matrix,

$$Q_i R_i = B_{i-1}, \quad (\text{E.6})$$

- let $B_i = R_i Q_i$.

If the algorithm converges, the resulting diagonal matrix B_i will contain the eigenvalues on the main diagonal [54].

Figure (E.1) shows the difference in the distribution using the calculation methods here explained, for a coupling mixture ($F_{S_1} + F_{T_2} + F_{M_0}$). It is easy to observe that the eigenvalues obtained from the trace method give a good approximation near the threshold Λ_{unit} , yet the eigenvalues for larger m_{VV} are underestimated with respect to the exact eigenvalues distribution. All the other algorithms have distributions with less than 10% difference.

For this work the QR factorization was used to calculate the distributions in Chapter 5. However, all the algorithms are available in VBFNLO.

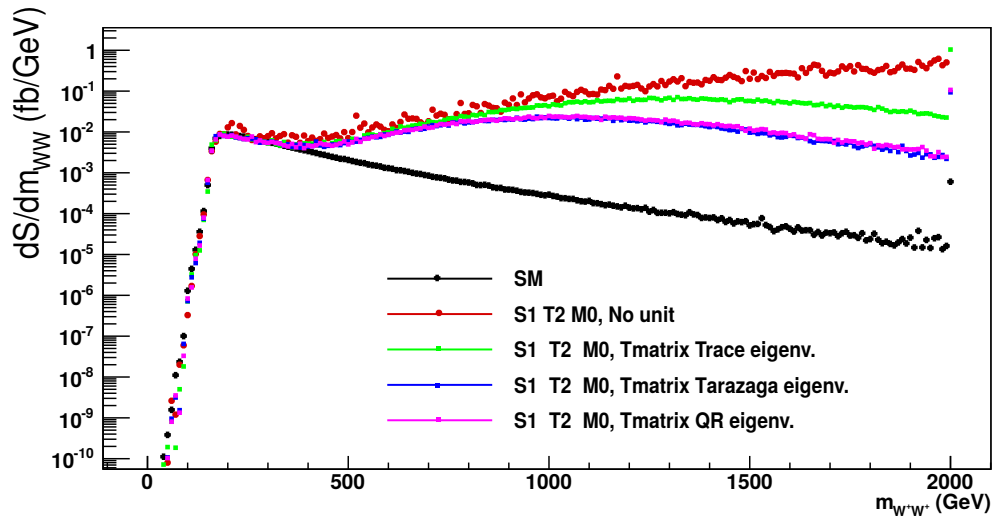


FIGURE E.1: Comparison between the different eigenvalue calculation methods using a combination anomalous couplings ($F_{S_1} + F_{T_2} + F_{M_0}$) for $W^+W^+ \rightarrow W^+W^+$ (semi-log plot). The plot shows the SM (black), the non-unitarized distribution (red), the T -matrix unitarization using the trace method (green), the T -matrix unitarization using the Tarazaga method (blue) and the exact eigenvalue calculation using the QR method (pink).

APPENDIX F

VBFNLO implementation

Implementation in VBFNLO

The T-matrix unitarization is implemented in VBFNLO, described previously in the Chapter 2. The new subroutines will follow the flow diagram in figure (F.1) to calculate the unitarized amplitudes.

The following subroutines were implemented:

1. The VBFNLO subroutine **amplitudes** calls the respective subroutine to calculate the squared matrix amplitude for the desired process. E.g., **m2s_qqwppqq.F** for $W^+W^+ \rightarrow W^+W^+$ (or its NLO version). This subroutine would decide if the SM is calculated or a BSM model. If EFT are calculated, it can decide between no-unitarization, form factor, K-matrix (for F_{S_i}) or the T-matrix here described.
2. For the T-matrix unitarization, **m2s_qqwppqq.F** calls: Helas subroutines for the currents, the boosting and rotating transformations (**rotCM.F**) and wpptowpp-Wigner (**towpm_on.F**).
3. Within **towpm_on.F**, one can find **wpptowpp_wigner**, which uses explicitly the polarization vectors instead of the propagators. It calls to **voffxx** (off-shell polarization vectors, using the normalization factor previously defined) and **www_onamon4** (**anomal4ON.F**). It also does the partial wave decomposition using the **wigner_d**, **www-wigner** and **tmatrix** subroutines.
4. **anomal4ON.F**: uses the Feynman rules calculated with FeynRules to calculate the $VV \rightarrow VV$ amplitudes using the polarization vectors.
5. Inside **wigner.F** one could find: **www-wigner**, which calculates the numerical partial wave decomposition for the **www** vertex, it calls the anomalous coupling and the inverse of the wigner D-matrix; **wigner-d** calculates the Wigner d-function; while **inv_wigner** calculates the inverse of the Wigner D-matrix.

6. **Tmatrix.F**: **tmatrix** subroutine rewrites the amplitude as a matrix 9×9 (for $W^+W^+ \rightarrow W^+W^+$) and calculates the T-matrix unitarization for the amplitudes. There is no need to invert the matrix anymore, but to calculate the eigenvalues. Then, **SOE_decomposition.F** or **eigenvalues.F** are called.
7. **SOE_decomposition.F**: contains different algorithms for the eigenvalue calculations, as well as different factorization systems to solve any system of equations. The subroutine **eigenvalues.F** was used previously for the FormFac tool.

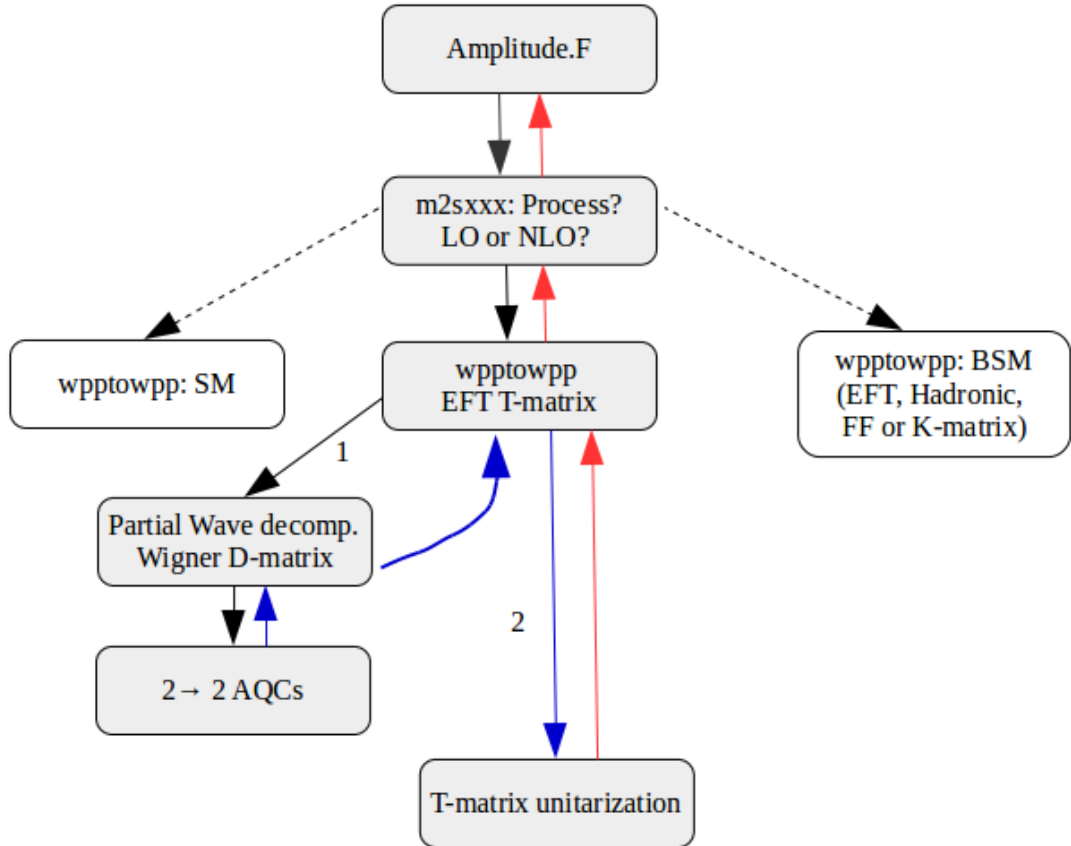


FIGURE F.1: T-matrix implementation in VBFNLO. The subroutine `Amplitude.F` will decide which process is going to be calculated, in agreement with the input given. If the T-matrix unitarization is done, the subroutine `wpptowpp` will do the Partial Wave decomposition and calculate all the quantities needed to unitarize (matrices, eigenvalues, etc.). Then, the output will be given to the `wpptowpp` subroutine after unitarizing and the respective cross section will be given.

Bibliography

- [1] Enrico Fermi. An attempt of a theory of beta radiation. 1. *Z. Phys.*, 88 (UCRL-TRANS-726):161–177, 1934.
- [2] I. S. Hughes. *Elementary Particles*. Cambridge University Press, third edition edition, 1991.
- [3] Wiktionary. Atom etymology. URL <https://en.wiktionary.org/wiki/atom>.
- [4] Gordon L. Kane. *Modern Elementary Particle Physics*. Westview Press, second edition edition, April 1993.
- [5] Sheldon L Glashow. Partial-symmetries of weak interactions. *Nuclear Physics*, 22 (4):579–588, 1961.
- [6] Steven Weinberg. A model of leptons. *Physical review letters*, 19(21):1264, 1967.
- [7] Abdus Salam. p. 367 of *Elementary Particle Theory*, ed. N. Svartholm (Almquist and Wiksells, Stockholm, 1969); SL Glashow, J. Iliopoulos, and L. Maiani. *Phys. Rev. D*, 2:1285, 1970.
- [8] J. Baglio et al. *VBFNLO: A parton level Monte Carlo for processes with electroweak bosons - Manual*, 2015. URL <http://arxiv.org/>. VBFNLO manual for version 2.7.1.
- [9] John David Jackson. *Classical electrodynamics*. John Wiley & Sons, 2007.
- [10] John F Cornwell. *Group theory in physics: An introduction*, volume 1. Academic press, 1997.
- [11] Peter W Higgs. Broken symmetries and the masses of gauge bosons. *Physical Review Letters*, 13(16):508, 1964.
- [12] François Englert and Robert Brout. Broken symmetry and the mass of gauge vector mesons. *Physical Review Letters*, 13(9):321, 1964.
- [13] Abdelhak Djouadi. The anatomy of electroweak symmetry breaking: Tome I: The Higgs boson in the Standard Model. *Physics reports*, 457(1):1–216, 2008.

- [14] M Banner, R Battiston, Ph Bloch, F Bonaudi, K Borer, M Borghini, J-C Chollet, AG Clark, C Conta, P Darriulat, et al. Observation of single isolated electrons of high transverse momentum in events with missing transverse energy at the CERN pp collider. *Physics Letters B*, 122(5-6):476–485, 1983.
- [15] Georges Aad, T Abajyan, B Abbott, J Abdallah, S Abdel Khalek, AA Abdelalim, O Abdinov, R Aben, B Abi, M Abolins, et al. Observation of a new particle in the search for the Standard Model Higgs boson with the ATLAS detector at the LHC. *Physics Letters B*, 716(1):1–29, 2012.
- [16] Serguei Chatrchyan, Vardan Khachatryan, Albert M Sirunyan, Armen Tumasyan, Wolfgang Adam, Ernest Aguilo, T Bergauer, M Dragicevic, J Erö, C Fabjan, et al. Observation of a new boson at a mass of 125 GeV with the CMS experiment at the LHC. *Physics Letters B*, 716(1):30–61, 2012.
- [17] S. Rao C. N. Leung, S. T. Love. Low energy manifestations of a new interaction scale: Operator analysis. *Fermi National Accelerator Laboratory*, 1984.
- [18] I. W. Stewart. Effective Field Theory: Course 8.851, lecture notes, 2014. URL <http://courses.edx.org/c4x/MITx/8.EFTx/asset/notesEFT.pdf>.
- [19] Limits on anomalous triple and quartic gauge couplings at CMS. URL <https://twiki.cern.ch/twiki/bin/view/CMSPublic/PhysicsResultsSMPaTGC>.
- [20] M. Misiak J. Rosiek B. Grzadkowski, M. Iskrzyski. Dimension-six terms in the Standard Model Lagrangian. *arXiv:1008.4884*, 2010.
- [21] Oscar JP Éboli, MC Gonzalez-Garcia, and JK Mizukoshi. $pp \rightarrow jje^\pm\mu^\pm\nu\nu$ and $jje^\pm\mu^\mp\nu\nu$ at $O(\alpha_{em}^6)$ and $O(\alpha_{em}^4\alpha_s^2)$ for the study of the quartic electroweak gauge boson vertex at CERN LHC. *Physical Review D*, 74(7):073005, 2006.
- [22] LEP TGC Working Group et al. A combination of preliminary results on gauge boson couplings measured by the LEP experiments. Technical report, LEPEWWG/TGC/2003-01, 2004.
- [23] Georges Aad, Tatevik Abajyan, Brad Abbott, Jalal Abdallah, S Abdel Khalek, AA Abdelalim, O Abdinov, R Aben, B Abi, M Abolins, et al. Measurement of $W+W^-$ production in pp collisions at $\sqrt{s}=7$ TeV with the ATLAS detector and limits on anomalous WWZ and $WW\gamma$ couplings. *Physical Review D*, 87(11):112001, 2013.
- [24] Georges Aad, Tatevik Abajyan, B Abbott, Jalal Abdallah, S Abdel Khalek, AA Abdelalim, O Abdinov, R Aben, B Abi, M Abolins, et al. Measurement of $W\pm Z$ production in proton-proton collisions at $\sqrt{s}=7$ TeV with the ATLAS detector. *The European Physical Journal C*, 72(10):2173, 2012.

- [25] Georges Aad, Tatevik Abajyan, Brad Abbott, Jalal Abdallah, S Abdel Khalek, AA Abdelalim, O Abdinov, R Aben, B Abi, M Abolins, et al. Measurements of $W\gamma$ and $Z\gamma$ production in pp collisions at $\sqrt{s}=7$ TeV with the ATLAS detector at the LHC. *Physical Review D*, 87(11):112003, 2013.
- [26] CMS collaboration et al. Measurement of the W^+W^- cross section in pp collisions at $\sqrt{s}=8$ TeV and limits on anomalous gauge couplings. *arXiv preprint arXiv:1507.03268*, 2015.
- [27] Serguei Chatrchyan, V Khachatryan, AM Sirunyan, Armen Tumasyan, W Adam, E Aguilo, Thomas Bergauer, M Dragicevic, J Erö, C Fabjan, et al. Measurement of the sum of WW and WZ production with W+ dijet events in pp collisions at $\sqrt{s}=7$ TeV. *The European Physical Journal C*, 73(2):2283, 2013.
- [28] Celine Degrande, Oscar Eboli, Bastian Feigl, Barbara Jäger, Wolfgang Kilian, Olivier Mattelaer, Michael Rauch, Jürgen Reuter, Marco Sekulla, and Doreen Wackerroth. Monte Carlo tools for studies of non-standard electroweak gauge boson interactions in multi-boson processes: A Snowmass White Paper. *arXiv preprint arXiv:1309.7890*, 2013.
- [29] OJP Éboli and MC Gonzalez-Garcia. Mapping the genuine bosonic quartic couplings. *arXiv preprint arXiv:1604.03555*, 2016.
- [30] D Zeppenfeld. Collider physics, lectures given at TASI98. *arXiv preprint hep-ph/9902307*.
- [31] Claude Itzykson and Jean-Bernard Zuber. *Quantum field theory*. Courier Corporation, 2006.
- [32] Michael Edward Peskin. *An introduction to quantum field theory*. Westview press, 1995.
- [33] Martina Laura Ojeda, Tamara Vázquez Schröder, and François Corriveau. Study of the associated production of tt and Higgs with the ATLAS detector. 2015.
- [34] C Patrignani, Particle Data Group, et al. *Review of particle physics*, volume 40. IOP Publishing, 2016.
- [35] Robin Roth. *Precise Predictions for LHC Cross Sections and Phenomenology beyond NLO*. PhD thesis, KIT, 2017.
- [36] K. Hagiwara H. Murayama, I. Watanabe. HELAS: HELicity Amplitude Subroutines for Feynman diagram evaluations. *Tech. Rep. KEK-91-11*, 1992.

- [37] J. Alwall et al. MadGraph/MadEvent v4: The new web generation. *JHEP*, 0709 (028), 2007. URL <http://arxiv.org/abs/0706.2334>.
- [38] M Jacob and Gr C Wick. On the general theory of collisions for particles with spin. *Annals of Physics*, 281(1-2):774–799, 2000.
- [39] Sally Dawson. Higgs physics: MITP summer school, lecture notes, 2016.
- [40] Ta-You Wu and Takashi Ohmura. Quantum theory of scattering. 1962.
- [41] Marco Sekulla. *Anomalous couplings, resonances and unitarity in vector boson scattering*. PhD thesis, Universität Siegen, 2015.
- [42] Wolfgang Kilian, Marco Sekulla, Thorsten Ohl, and Jürgen Reuter. High-energy vector boson scattering after the Higgs boson discovery. *Physical Review D*, 91(9):096007, 2015.
- [43] Bastian Feigl. Anomale Vier-Vektorboson-Kopplungen bei der Produktion von drei Vektorbosonen am LHC. Master’s thesis, KIT, 2010.
- [44] Maximilian Löschner. Unitarisation of anomalous couplings in vector boson scattering. Master’s thesis, KIT, 2014.
- [45] CMS collaboration et al. Observation of electroweak production of same-sign W boson pairs in the two jet and two same-sign lepton final state in proton-proton collisions at $\sqrt{s}=13$ TeV. *arXiv preprint arXiv:1709.05822*, 2017.
- [46] M Baranger, B Giraud, SK Mukhopadhyay, and PU Sauer. Off-energy-shell continuation of the two-nucleon transition matrix. *Nuclear Physics A*, 138(1):1–12, 1969.
- [47] DJ Kouri and FS Levin. K matrix and unitarity constraints on off-shell T matrix elements. *Physical Review C*, 10(5):2096, 1974.
- [48] Neil D Christensen and Claude Duhr. FeynRules–Feynman rules made easy. *Computer Physics Communications*, 180(9):1614–1641, 2009.
- [49] K Arnold, J Bellm, M Brieg, M Worek, M Kubocz, G Bozzi, F Geyer, C Englert, B Feigl, S Plätzer, et al. VBFNLO: A parton level Monte Carlo for processes with electroweak bosons–Manual for version 2.7. 0. Technical report, 2011.
- [50] John D. Cook. Don’t invert that matrix, 2010. URL <https://www.johndcook.com/blog/2010/01/19/dont-invert-that-matrix/>.
- [51] Hannes Thiel. The QR algorithm (and other methods to compute the eigenvalues of complex matrices). *University of Potsdam*, 2005.

- [52] The Eigen project. Linear algebra and decompositions. URL https://eigen.tuxfamily.org/dox/group__TutorialLinearAlgebra.html.
- [53] Pablo Tarazaga. Eigenvalue estimates for symmetric matrices. *Linear Algebra and its Applications*, 135:171–179, 1990.
- [54] Ridzalski B. Izyumin I. QR factorization method for finding eigenvalues.
- [55] KJF Gaemers and George J Gounaris. Polarization amplitudes for $e^+e^- \rightarrow W^+W^-$ and $e^+e^- \rightarrow ZZ$. *Zeitschrift für Physik C Particles and Fields*, 1(3):259–268, 1979.
- [56] Kaoru Hagiwara, RD Peccei, D Zeppenfeld, and K Hikasa. Probing the weak boson sector in $e^+e^- \rightarrow W^+W^-$. *Nuclear Physics B*, 282:253–307, 1987.
- [57] Roberto Contino, Adam Falkowski, Florian Goertz, Christophe Grojean, and Francesco Riva. On the validity of the effective field theory approach to SM precision tests. *Journal of High Energy Physics*, 2016(7):144, 2016.
- [58] Vardan Khachatryan, AM Sirunyan, Armen Tumasyan, W Adam, T Bergauer, M Dragicevic, J Erö, M Friedl, R Frühwirth, VM Ghete, et al. Study of vector boson scattering and search for new physics in events with two same-sign leptons and two jets. *Physical review letters*, 114(5):051801, 2015.
- [59] Morad Aaboud, G Aad, B Abbott, J Abdallah, O Abdinov, B Abeloos, R Aben, OS AbouZeid, NL Abraham, H Abramowicz, et al. Measurement of $W^\pm W^\pm$ vector-boson scattering and limits on anomalous quartic gauge couplings with the ATLAS detector. *Physical Review D*, 96(1):012007, 2017.
- [60] Wikipedia. Weak hypercharge. URL en.wikipedia.org/wiki/Weak_hypercharge.
- [61] Joshua P Ellis. Tikz-feynman: Feynman diagrams with tikz. *Computer Physics Communications*, 210:103–123, 2017.
- [62] Ruth Pöttgen. *Search for Dark Matter with ATLAS: Using Events with a Highly Energetic Jet and Missing Transverse Momentum in Proton-Proton Collisions at $\sqrt{s} = 8$ TeV*. Springer, 2016.
- [63] M. Peskin. Higgs and EWSB: ICTP summer school on particle physics, lecture notes, 2015.
- [64] Jorge de Blas. Electroweak limits on physics beyond the Standard Model. In *EPJ Web of Conferences*, volume 60, page 19008. EDP Sciences, 2013. URL <arXiv:1307.6173>.
- [65] David Bailin and Alexander Love. *Introduction to Gauge Field Theory Revised Edition*. CRC Press, 1993.

-
- [66] James D Bjorken and Sidney David Drell. Relativistic quantum mechanics. 1964.
- [67] Jacob Groth-Jensen. *Luminosity determination and simulation of the LUCID detector at the ATLAS experiment*. PhD thesis, Lund University, 2010.
- [68] Bastian Feigl. *Electroweak Processes in the Standard Model and Beyond: Backgrounds to Higgs Physics and Semileptonic Decay Modes*. PhD thesis, KIR, 2013.
- [69] D. Wyler W. Buchmüller. Effective Lagrangian analysis of new interactions and flavour conservation. *Nuclear Physics*, B(268):621–653, 1986.

Acknowledgements

I am heartily grateful to my supervisor, Prof. Dr. Dieter Zeppenfeld, who gave me the opportunity to work with him the last years. I thank him for trusting my abilities since the first day.

I owe a sincere and earnest thankfulness to Dr. Robin Roth, who was always there to help me with VBFNLO, Git and in general any IT problem, even the day before his own Ph.D. exam. I also would like to thank Dr. Michael Rauch for helping me always with my programming issues and being there every time I had questions about VBFNLO.

I would like to thank KSETA and the ITP, who financed my project. Without them, I would not be here doing this research. Thanks for welcoming me and giving me the chance to be part of this excellence group.

I also would like to thank Prof. Dr. Margarete Mühlleitner who gave me a helpful feedback and took the time to discuss this work. As well, I would like to show my gratitude to Dr. Francisco Campanario, M.Sc. Maximilian Löschner and Dr. Marco Sekulla for their suggestions.

Nada de esto habría sido posible sin el apoyo incondicional de mi familia, quienes ha estado conmigo en cada paso y alentado todas y cada una de mis decisiones. Muchas gracias por todo su apoyo y paciencia, por estar siempre a mi lado y ser mi base.

I also need to thank Radek Podskubka, who held my shoulders in every struggle and helped me to find the strength within me when I felt hopeless. You showed me grace and peace through the mountains. Thanks for spending all those hours listening to ideas and presentations, thanks for sharing climbing and life stories with me.

Quiero agradecer a Gustavo Guerrero, quien ha sido mi hermano durante los últimos años. Sin su ayuda y apoyo este proyecto tampoco habría sido posible.

Finally, I am obliged to many of my friends in France, Venezuela, United States, and Germany, who help me in one or another way. To my colleagues from the 12th, 11th, and 9th floor throughout these years, who were not only co-workers but friends. To my former supervisors and professors, for their help and advice, and every one of those persons who has been walking by my side all these years.

Thank you all for your support.

“So long, and thanks for all the fish.”